TECHNISCHE UNIVERSITÄT MÜNCHEN

Lehrstuhl für Technische Chemie II

Understanding elementary steps in methanol-to-olefins chemistry

Sebastian Müller

Vollständiger Abdruck der von der Fakultät für Chemie der Technischen Universität München zur Erlangung des akademischen Grades eines

Doktors der Naturwissenschaften (Dr. rer. nat.)

genehmigten Dissertation.

Vorsitzender: Univ.-Prof. Dr.-Ing. K.-O. Hinrichsen

Prüfer der Dissertation:

    1. Univ.-Prof. Dr. J.A. Lercher

    2. Univ.-Prof. Dr. K. Köhler

Die Dissertation wurde am 15.12.2015 bei der Technischen Universität München eingereicht und durch die Fakultät für Chemie am 25.01.2016 angenommen.

Für meine Eltern

und Elisabeth

Acknowledgements

The success of this thesis is closely related to the help of many people to whom I want to express my deepest gratitude.

First of all, I would like to thank Prof. Dr. Johannes A. Lercher for giving me the opportunity to work on this stimulating topic, for excellent scientific discussions and the guidance throughout the thesis. I enjoyed the freedom of research that I had and the lessons and anecdotes which Johannes shared with me.

I am very grateful to Dr. Maricruz Sanchez-Sanchez for the excellent collaboration during the last years. Her support, guidance and trust throughout my PhD thesis as well as numerous stimulating discussions and all corrections are gratefully acknowledged.

I am also very grateful to my co-worker, Dr. Yue Liu, for being such a great partner. I appreciated the collaboration a lot and wish him all the best for the future.

I would also like to thank Prof. Dr. André C. van Veen for the smooth collaboration we had at the beginning of my PhD.

Furthermore, I would like to thank the BU Catalysts, Clariant Produkte (Deutschland) GmbH (former Süd-Chemie AG) for financial support and interesting discussions in the framework of MuniCat. In particular, I am very thankful to Prof. Dr. Richard Fischer and Dr. Markus Tonigold for their help.

I am particularly indebted to my predecessor, Dr. Xianyong Sun, who helped me a lot at the beginning of my PhD and introduced me into the secrets of the 10-fold unit. I also thank my successor, Jürgen Hajdo, who joined me in the last months of my PhD, giving me new views on our topic. Moreover, I thank Dr. Muthusamy Vishnuvarthan for help with catalyst characterization at the beginning of my PhD.

I am very grateful to our technical staff in this group for their strong support. Xaver Hecht helped me a lot with my setups and technical problems. I also would like to thank our current and former secretaries, Ulrike Sanwald, Bettina Federmann, Stefanie Seibold, Karen Schulz and Helen Lemmermöhle. Andreas Marx and Martin Neukamm are gratefully acknowledged as well.

I have to thank several students for their good work: Andreas Schiff, Benedikt Keller, Felix Reiter, Johanna Wiethaler, Kathrin Arzt, Lorenz Schiegerl, Martin Riedl, Michael Sauer,

Abbreviations

AHFS	Ammonium hexafluorosilicate
BAS	Brønsted acid site
CBU	Composite building unit
CHA	Chabazite
CSTR	Continuously operated stirred tank reactor
DICP	Dalian Institute of Chemical Physics
DME	Dimethyl ether
DMM	Dimethoxymethane
DMTO	Dimethyl ether or methanol-to-olefin
DSC	Differential scanning calorimetry
EFAL	Extra-framework aluminum
EPR	Electron paramagnetic resonance
FAU	Faujasite
FCC	Fluid catalytic cracking
HT	Hydrogen transfer
I.D.	Inner diameter
IR	Infrared
IZA	International Zeolite Association
LAS	Lewis acid site
LDI	Laser desorption/ionization
LPG	Liquefied petroleum gas
MALDI	Matrix-assisted laser desorption/ionization
MFI	Mordenite Framework Inverted
MIHT	Methanol-induced hydrogen transfer
MOGD	Mobil olefins to gasoline and distillate process
MS	Mass spectrometry
MTG	Methanol to gasoline, methanol-to-gasoline
MTH	Methanol to hydrocarbons, methanol-to-hydrocarbons
MTO	Methanol to olefins, methanol-to-olefins

MTP	Methanol to propene, methanol-to-propene
NMR	Nuclear magnetic resonance
No.	Number
OCP	Olefin cracking process
OIHT	Olefin-induced hydrogen transfer
PFR	Plug-flow reactor
RO	Reaction order
SAPO	Silicoaluminophosphate
STF	Syngas to fuels
TGA	Thermogravimetric analysis
TIGAS	Topsøe integrated gasoline synthesis
TOF	Turnover frequency, time of flight
TOS	Time on stream, time-on-stream
TPD	Temperature-programmed desorption
TPO	Temperature-programmed oxidation
TPSR	Temperature-programmed surface reaction

Abstract

High local methanol concentrations induce the formation of strongly adsorbed oxygen-containing species on Brønsted acid sites of H-ZSM-5 catalysts in methanol-to-olefins conversion. These oxygenates cause fast deactivation and are transformed with time on stream into aromatics remaining attached to Brønsted acid sites. The major pathway leading to aromatics and paraffins involves the hydrogen transfer reaction from methanol to olefins at Lewis acid sites, forming formaldehyde and paraffins. Furthermore, formaldehyde is key compound for first C-C bond and olefins formation, as well as in deactivation.

Hohe lokale Methanolkonzentrationen führen in der Methanol-zu-Olefin-Umsetzung zur Bildung stark adsorbierter sauerstoffhaltiger Spezies an Brønsted-Säurezentren von H-ZSM-5 Katalysatoren. Diese sauerstoffhaltigen Verbindungen bewirken eine schnelle Deaktivierung und werden mit der Zeit in Aromaten umgewandelt, die an Brønsted-Säurezentren adsorbiert bleiben. Der wesentliche Pfad zu Aromaten und Paraffinen schließt die Hydrogentransferreaktion von Methanol zu Olefinen an Lewis-Säurezentren ein, wodurch sich Formaldehyd und Paraffine bilden. Zudem ist Formaldehyd Schlüsselkomponente für die Bildung der ersten C-C-Bindung und von Olefinen, ebenso wie in der Deaktivierung.

Table of Contents

Chapter 1

1.   Introduction

1.1   General introduction

Olefins are valuable building blocks for the chemical and petrochemical industries. In particular, ethene and propene are key compounds for the production of a multitude of chemicals. The majority of olefins consumption is driven by polymers production (polyethylene [1] and polypropylene [2]). Furthermore, ethene is used to synthesize, for instance, styrene, ethene oxide, vinyl chloride and vinyl acetate monomers and functionalized hydrocarbons (dichloroethane, ethylbenzene, acetaldehyde and ethanol) [1]. Important propene derivatives are acrylonitrile, oxoalcohols, propylene oxide and cumene [2].

Currently, ethene is mainly produced by steam cracking [2, 3]. In this process (Figure 1.1) the feed (naphtha, ethane, LPG), diluted with steam, is briefly heated in a furnace. To achieve high ethene yields and prevent further reactions, the product gas is quenched in a heat exchanger. Subsequently, cooling is continued by the injection of quench oil. This part of a steam cracking plant is called "hot section". Afterwards, the product stream is separated by fractional distillation in the "cold section" [4, 5]. Propene is obtained as a by-product in a steam cracking unit which accounts for 66% of global propene production at present [2]. In addition, propene is produced by fluid catalytic cracking (FCC), which contributes to 32% of propene fed to petrochemical processes, and propane dehydrogenation or metathesis reactions (2%) [2].

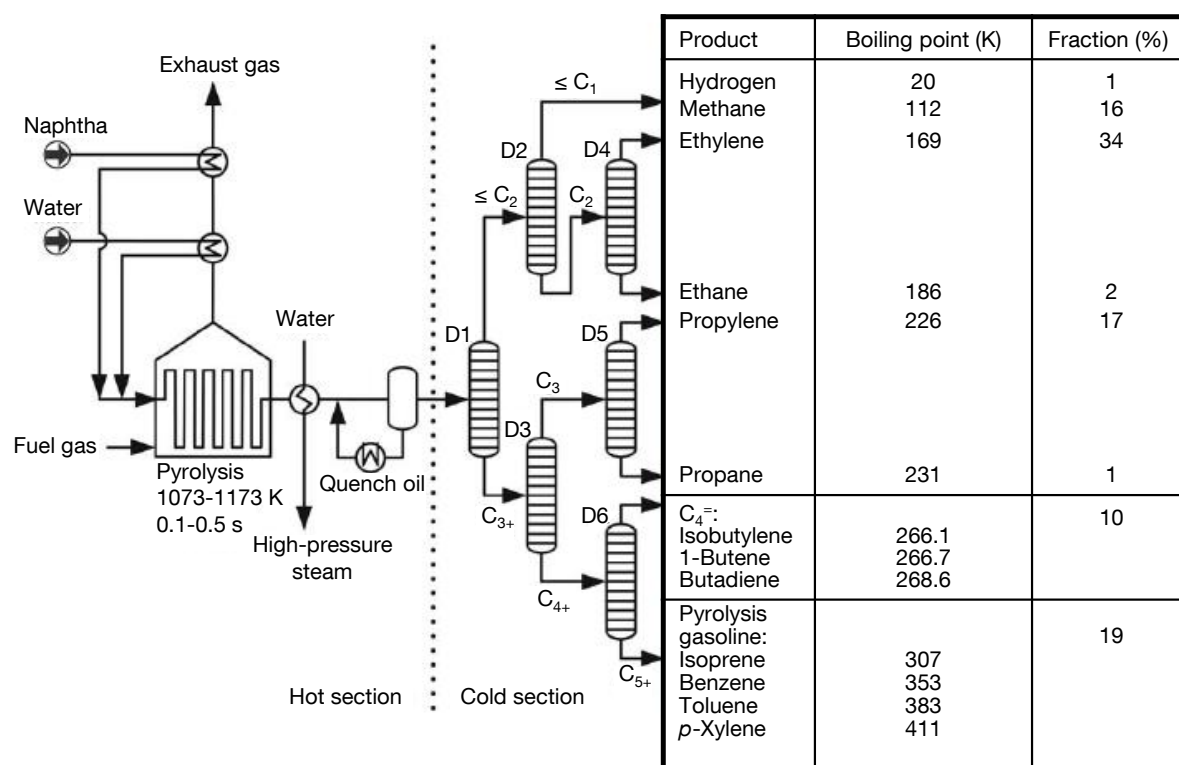| Product	Boiling point (K)	Fraction (%)
Hydrogen	20	1
Methane	112	16
Ethylene	169	34
Ethane	186	2
Propylene	226	17
Propane	231	1
$C_4^=$: Isobutylene 1-Butene Butadiene	266.1 266.7 268.6	10
Pyrolysis gasoline: Isoprene Benzene Toluene *p*-Xylene	307 353 383 411	19

Figure 1.1. Sketch of a steam cracking reaction configuration (D1-D6: distillation columns) [4].

The demand for ethene and propene is forecasted to increase over the next decade. The ethene production is projected to grow to 160 million tons per year by 2015 at a rate of 4 to 6%, while the propene production is projected to grow to 105 million tons per year by 2015 at a rate of 6 to 8% [2]. Due to the differently predicted growth rates of propene and ethene production, steam crackers cannot satisfy the demand because low propene/ethene ratios are obtained from steam cracking [6]. Moreover, steam cracking exhibits some major disadvantages. This process has to be operated at high temperatures (~1073-1173 K) because the reaction is highly endothermic. Furthermore, the deposition of coke, the regeneration of the furnace and insufficient heat transfer to the heating medium are serious problems [1, 7]. Thus, alternative processes have to be found to overcome these drawbacks.

The conversion of methanol to hydrocarbons (MTH) is a promising alternative for hydrocarbons production because methanol can be produced from various carbon-based feedstocks [8-11] and the product spectrum of MTH can be flexibly adjusted by process conditions [9].

1.2   Catalysts in methanol-to-hydrocarbons (MTH) conversion

Different types of zeolites and zeotype materials have been reported in literature as catalysts for MTH reactions. They are classified according to different topologies (channels and cavities dimensions and interconnections), compositions (concentration and distribution of acidic sites, defects) and morphologies (crystal dimensions, micro- and mesoporosity). The zeolite H-ZSM-5 with MFI topology and the zeotype H-SAPO-34 with CHA topology are, however, the only two catalysts applied in industrial MTH processes. Both materials have a three-dimensional structure, but with very different pore and cavity sizes. The surface of H-ZSM-5 can be described by interconnected tubes, whereas H-SAPO-34 consists of larger cavities with narrow connections [9]. For H-SAPO-34, the highest selectivity was observed for lights olefins such as ethene and propene, and no aromatics were detected. In contrast, aromatics were detected on H-ZSM-5 besides high selectivities toward ethene and propene [12]. This can be assigned to the prominent product shape selectivity for the narrow-pore catalyst H-SAPO-34 (8-ring channel structure) in comparison to the medium-pore zeolite H-ZSM-5 (10-ring channel structure). It is, however, important to note that H-SAPO-34 deactivates significantly faster than H-ZSM-5 [9]. Several authors attributed this to the formation of polycyclic arenes in the

spacious cavities of H-SAPO-34, while only monocyclic arenes are generated in H-ZSM-5 [9, 13-16]. This thesis is focused on the use of the MFI zeolite H-ZSM-5. Therefore, some theoretical background on zeolites and then in particular on the MFI topology is given in the following sections.

1.2.1 Zeolites

1.2.1.1 General background

One of the most important reasons for using zeolites in catalysis is their acidity and the fact that the strength, location and accessibility of these sites changes with the zeolite structure and the composition (Si/Al). In general, the acidity of zeolites is difficult to define because both Brønsted and Lewis acid sites are present in zeolites [17]. Typically, Brønsted acid sites (BAS) and Lewis acid sites (LAS) are presented as shown in Scheme 1.1. LAS may be formed by dehydroxylation of the zeolite surface in H-form. Since framework dealumination may follow as next step, cationic extra-framework species, such as AlO^+ and $Al(OH)_2^+$, might form that can act as LAS [18-22].
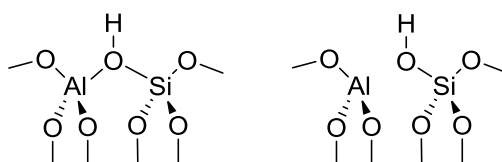
Scheme 1.1. Common representation of Brønsted (left) and Lewis acid site (right) in zeolites [23].

Another important feature of zeolites is that the shape, or topology, of the internal pore structure affects the selectivity toward formation of certain products in reactions catalyzed by zeolites. In the case of reactant shape selectivity (Figure 1.2 (a)), merely those molecules of a multi-component feed may be converted which diffuse sufficiently fast to the active site and are adsorbed by the zeolite. However, the feed molecules also need to be converted and the product molecules need to desorb and diffuse away. The shape of the zeolite may play a role in each of these steps. If the product formation step is responsible for a change in product distribution, this effect is called transition state selectivity (Figure 1.2 (c)). For instance, the shape of the zeolite pore prevents the formation of a bulky molecule which does not fit inside. On the other hand, a bulky molecule may be stabilized and formed preferentially over other

products, if it fits optimally to the zeolite pore. In the case of product shape selectivity, diffusion limitations inhibit desorption of too large product molecules (Figure 1.2 (b)) [24].
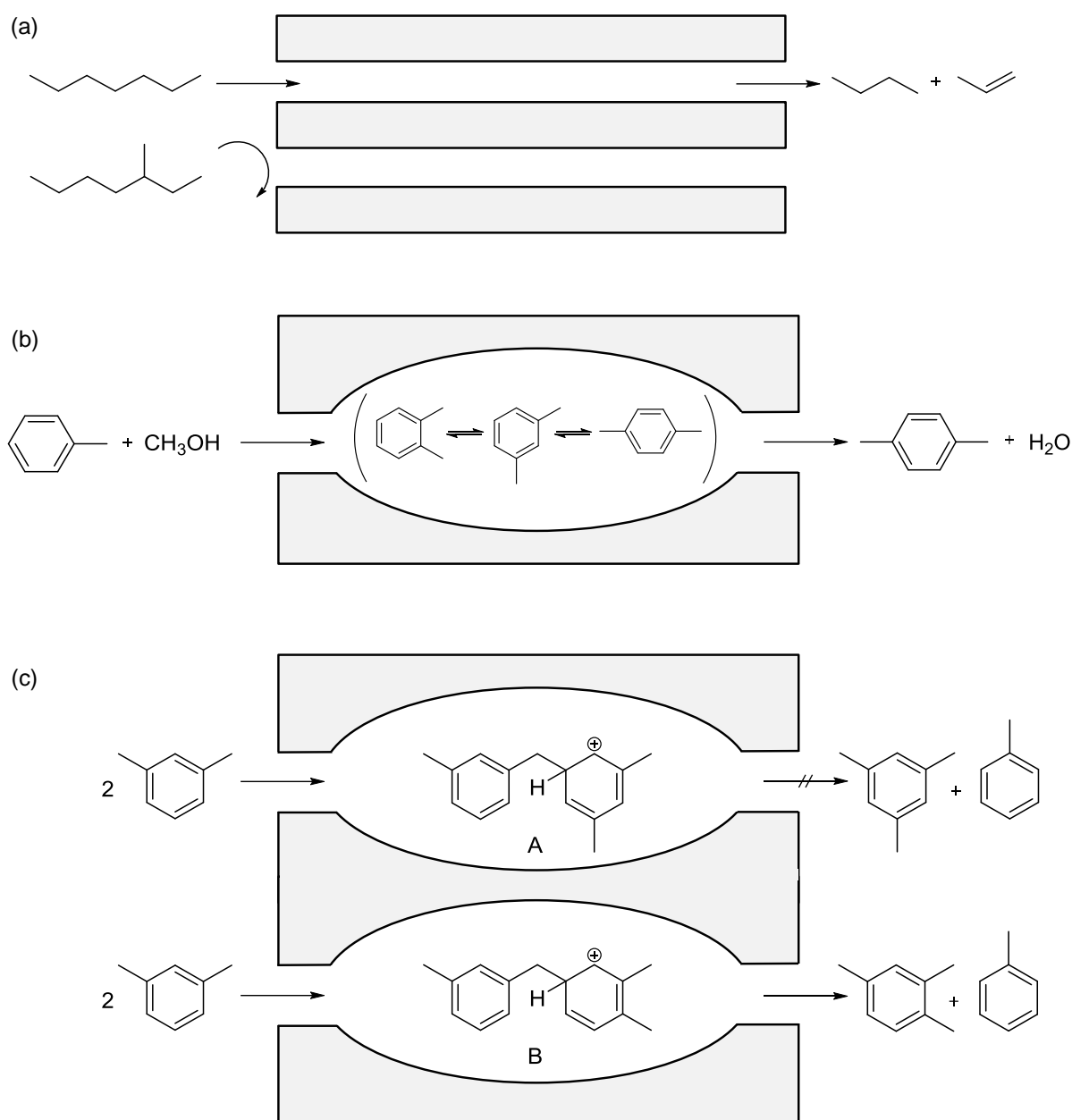
Figure 1.2. Basic mechanisms giving rise to shape selectivity: Reactant shape selectivity in the case of hydrocarbons cracking (a), product shape selectivity in the case of toluene methylation (b) and transition state shape selectivity in the case of *m*-xylene disproportionation (c) [24, 25].

Smit and Maesen [24] extended the concept of shape selectivity, considering also thermodynamic effects. According to their proposal, the formation of molecules with the lowest free energy of formation in the adsorbed phase is favored over other possible products (transition state selectivity). Further, molecules with the highest free energy of adsorption will

preferentially desorb as products (product shape selectivity). Likewise, reactants with the lowest free energy of adsorption are preferentially adsorbed and undergo reaction (reactant shape selectivity).

1.2.1.2   Methods for adjusting the chemical properties of zeolites

To modify the chemical properties of zeolites, different approaches can be taken. One method is to replace tetrahedral framework atoms with other atom types [26]. Cations that can be incorporated are gallium, iron and boron. By this procedure the strength of acid sites in zeolites may be tailored as well [27]. Another way to modify zeolite properties is by changing the nature of the non-framework cations through cation exchange [28, 29]. Since (hydro)thermal treatment of H-ZSM-5 generates extra-framework aluminum (EFAl) [30], a multitude of dealumination techniques has been used to control the concentration of acid sites. Furthermore, dealumination is frequently applied for investigating the role of EFAL in H-ZSM-5-catalyzed reactions. Reported dealumination methods include treatment with steam or $SiCl_4$ vapor at elevated temperature or treatment with ammonium hexafluorosilicate (AHFS). Furthermore, treatments with acids and chelating agents have been reported [31-36].

1.2.1.3   Structure type Mordenite Framework Inverted (MFI)

A special framework type which is one of the most important ones for methanol-to-olefins (MTO) conversion is **M**ordenite **F**ramework **I**nverted (MFI) [9]. Its structure is described in more detail in this section because all samples used in this study are H-ZSM-5 catalysts and belong to this framework type.

The MFI structure can be understood as an assembly of five-rings. For the buildup of one composite building unit (CBU), these five-rings are linked together in the way it is illustrated on the left side of Figure 1.3. The common descriptor of this structure unit is $[5^4 5^4]$ which stands for two units of four equal five-rings linked together to one CBU [26, 37, 38]. These units are connected via edges to form chains as shown on the right side of Figure 1.3. These so-called pentasil chains are ordered side-by-side in x- as well as in y-direction, creating straight ten-ring channels (5.3 Å x 5.6 Å) parallel to the [010]-direction and sinusoidal ten-ring channels (5.1 Å x 5.5 Å) parallel to the [100]-direction [38, 39]. The channel structure is shown in Figure 1.4.
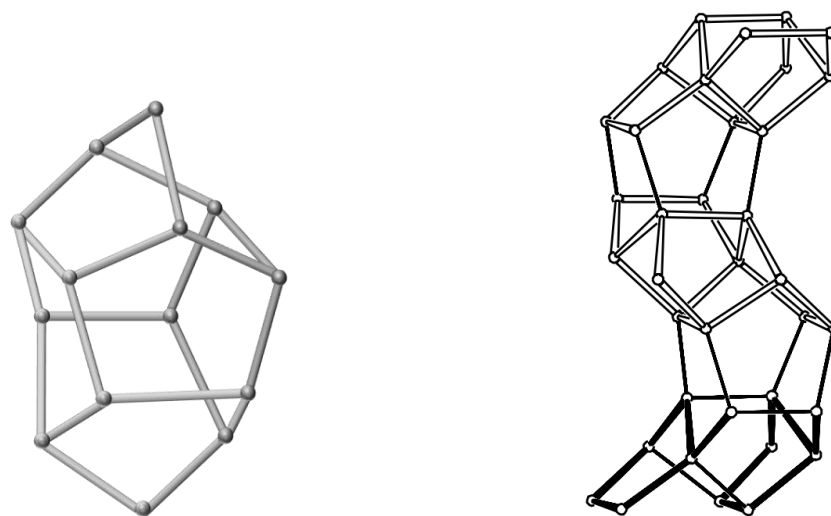
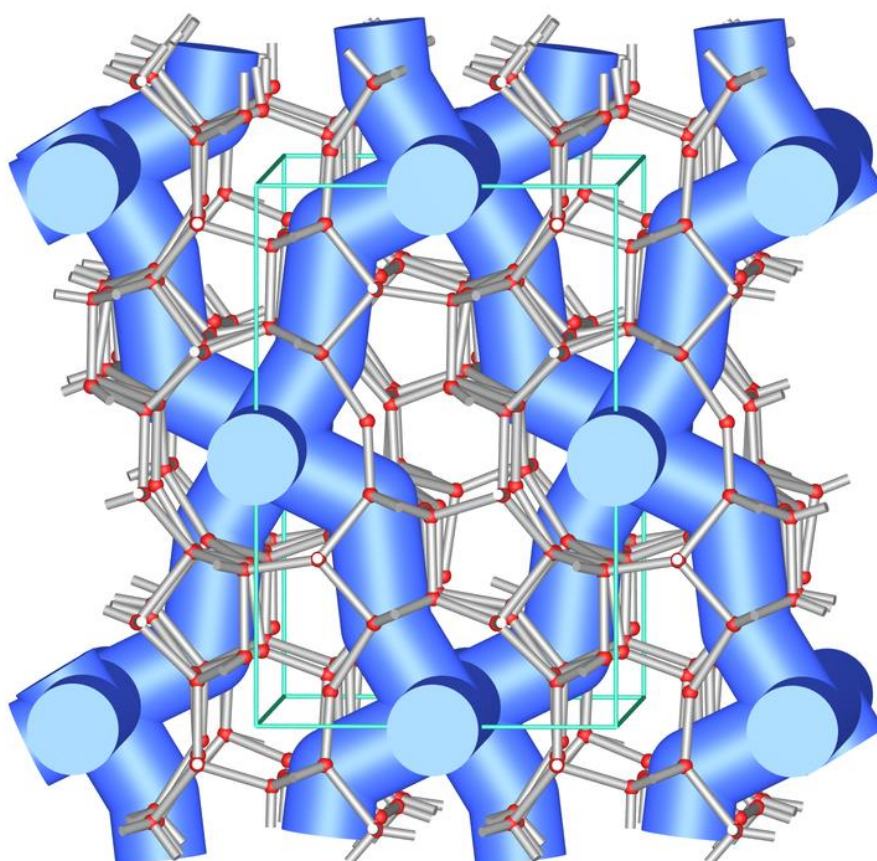**Figure 1.3.** Pentasil unit of MFI framework (left) and T-T linkage scheme of a pentasil chain (right) [37, 40].

Figure 1.4. Illustration of channel system in H-ZSM-5 [41].

It has to be emphasized that the rings are not in a "steady state". They are flexible and can be distorted to varying degrees in real materials. Additionally, temperature and thermal vibration can affect the apertures. As a consequence, the apparent size changes with temperature. Moreover, guest species may reduce the apparent apertures of zeolites [26].

1.3   Mechanistic aspects in MTH reaction

Intensive mechanistic studies of the conversion of methanol to hydrocarbons have been conducted for more than thirty years [2, 9, 10]. It is very challenging to obtain information on the elementary steps of the reaction mechanism due to the complex reaction network and the fact that information on gas-phase products and intermediates confined within the pores or cavities of the catalyst to varying degrees should be obtained simultaneously. Furthermore, it is important to consider adsorption/desorption and diffusion phenomena as a consequence of the porous nature of the zeolites and zeotype materials and the kinetic diameter of hypothetical intermediates before deriving kinetic parameters from experimental results [9].

1.3.1   Reaction network

The simplified reaction sequence in MTH conversion was proposed at first by Chang and Silvestri, analyzing the effect of contact time on product distribution [42]. According to that (Figure 1.5), the overall reaction can be divided into three steps [10, 42-44]. In the first step, methanol is dehydrated to dimethyl ether. Olefins are then formed from the equilibrium mixture of methanol, dimethyl ether and water. These olefins can be further converted to higher olefins via methylation/oligomerization and to naphthenes, aromatics and paraffins via cyclization and hydrogen transfer reactions. This reaction sequence is summarized in Scheme 1.2.
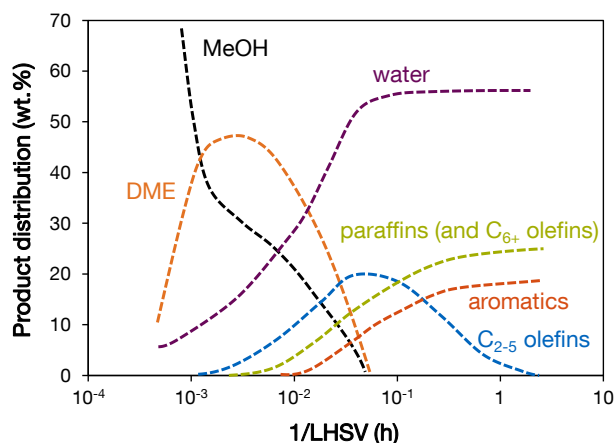
Figure 1.5. Reaction pathway of MTH reaction as originally presented by Chang and Silvestri [42].
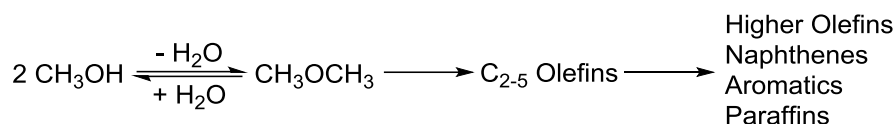
Scheme 1.2. Simplified MTO reaction pathway [10, 42-44].

1.3.2   Generation of first hydrocarbon species from methanol/DME

The early years of MTH research were dedicated to understanding the formation of the first C-C bond. Over 20 mechanisms for direct C-C coupling have been proposed, despite lacking experimental evidence [9]. In these routes, species such as carbocations (Scheme 1.3 (a)), carbenes (Scheme 1.3 (b)), alkoxy groups (Scheme 1.3 (c)), free radicals (Scheme 1.3 (d)) and oxonium ylides (Scheme 1.3 (e)) are involved [9, 45]. Lestaeghe et al. investigated a large set of direct mechanisms theoretically, determining both rate coefficients and reaction barriers. According to their results, direct C-C coupling fails due to unstable intermediates and high activation barriers [46]. On the other hand, Song et al. used highly purified reagents and showed that the initial rate of methanol conversion was reduced by orders of magnitude. They further concluded that for normal feedstocks the direct C-C coupling reaction is probably much slower than reactions of methanol with trace impurities, which indeed initiate the reaction [9, 47]. Since no or little conversion is observed at short contact time, the direct C-C bond formation from methanol or DME is concluded to be relevant only until sufficient hydrocarbons are present and the rate of methylation reactions overcomes the rate of direct C-C bond formation from C1 units. Overall, a S-shaped curve for the hydrocarbon yield as a function of contact time is

observed, which is typical for autocatalytic reactions as outlined in detail in the following section. Under realistic industrial conditions with recycling of undesired products, direct mechanisms are also of little importance [9]. However, understanding first C-C bond formation from methanol is still fascinating und subject of numerous research activities.
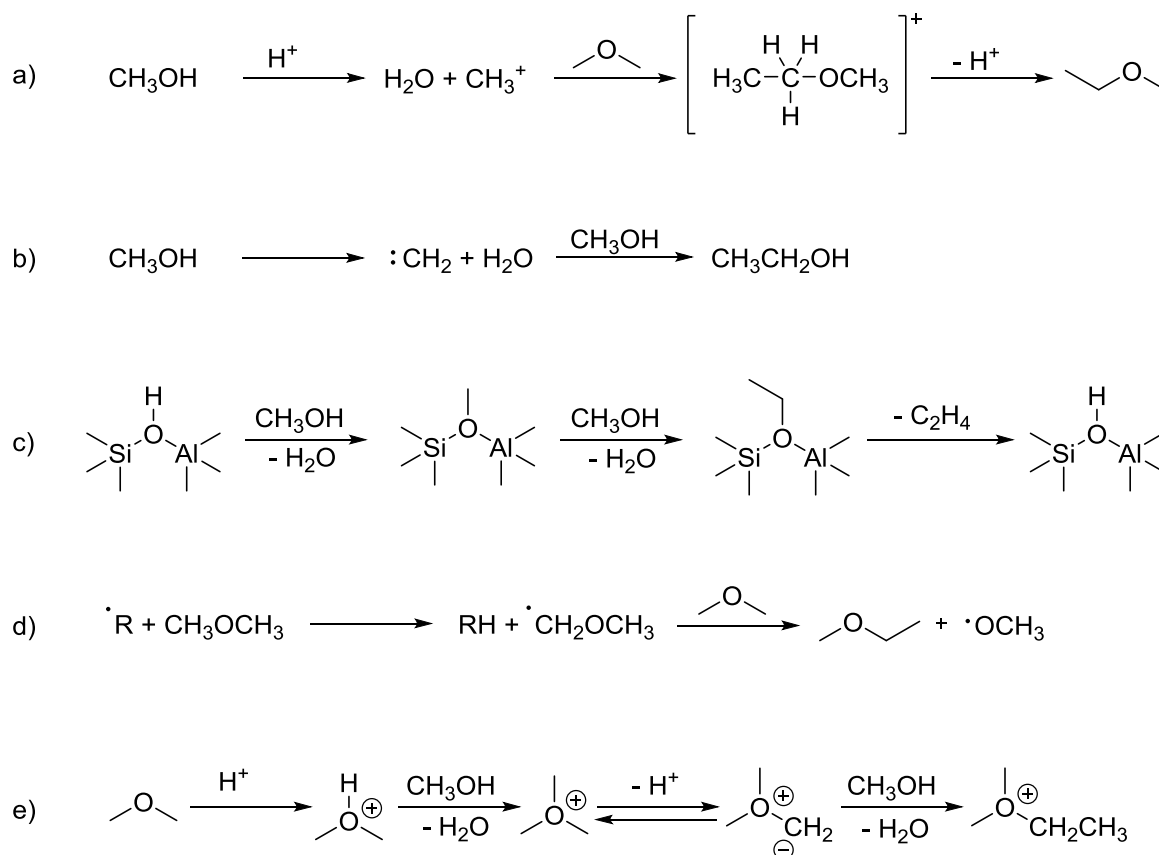
Scheme 1.3. Proposed "direct" mechanisms for methanol/dimethyl ether conversion to olefins (or olefin precursors): Pathway showing a carbenium ion alkylating dimethyl ether to form a carbonium ion (a), one of several proposed carbene pathways (b), an alkoxy chain growth process occurring on a framework site (c), an abbreviation of one of several free radical routes with 'R as an unspecified surface radical species (d) and an oxonium-ylide route (e) [45].

1.3.3   Autocatalysis and hydrocarbon pool mechanism

As already discussed in the last section, the formation of light olefins under steady-state operation is usually explained with indirect mechanisms. In 1979, Chen and Reagan gave evidence of autocatalytic reactions as important steps for methanol conversion on zeolites [48]. After the equilibration of methanol and dimethyl ether, olefins can form from these oxygenates:

$$A \xrightarrow{k_1} B \qquad (1.1)$$

where A represents the oxygenates and B represents the olefins.

Subsequently, the olefins react with the oxygenates again, producing a mixture of olefinic species with different chain length. This step can be considered as an autocatalytic step:

$$A + B \xrightarrow{k_2} B \qquad (1.2)$$

In a final step, the olefins may react to paraffins and aromatics in secondary reactions. Latter compounds are represented by C:

$$B \xrightarrow{k_3} C \qquad (1.3)$$

If the conversion of methanol is low, reaction path (1.3) can be neglected and the reaction can be kinetically described with equation (1.4):

$$-\frac{d[A]}{dt} = k_1[A] + k_2[A][B] \qquad (1.4)$$

where [A] represents the oxygenates concentration and [B] the concentration of olefins.

Importantly, Chen and Reagan noted that k_1 is very small compared to k_2, from which they deduced an initial phase where the first olefins are formed rather slowly. After this step, the formation rate of further olefins is enhanced in the autocatalytic region [48]. This is in line with the observation that methanol conversion follows a characteristic S-shape as a function of contact time [49]. In accordance with that, Langner observed a remarkable shortening of the induction period by co-feeding of cyclohexanol [50].

Dessau and co-workers described the autocatalytic effect by an olefin homologation/cracking mechanism (Scheme 1.4) [51, 52]. Olefins formed in the induction period react via methylation and cracking to C_{2-4} olefins. Aromatics and paraffins form as end products by aromatization [9]. Lesthaeghe et al. conducted theoretical calculations and showed that the olefin methylation/cracking cycle is a viable pathway both for ethene and propene production [53].

$$CH_3OH \xrightarrow{H^+} CH_3^+ + H_2O$$
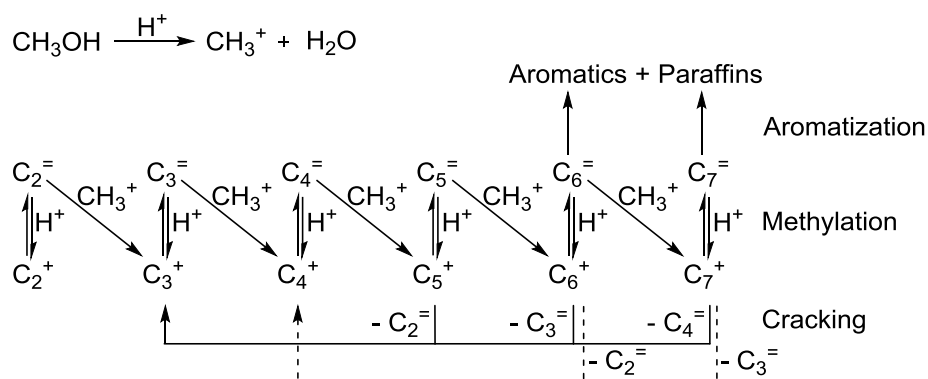
Scheme 1.4. Mechanism for methanol reaction on H-ZSM-5, based on classical carbenium ion chemistry, proposed by Dessau and co-workers [51, 52]

On the other hand, the important role of aromatics and unsaturated cyclic species was noted in parallel with the olefin-based mechanistic proposal [9]. In 1982, Mole and co-workers and Langner discussed in independent papers the impact of aromatics on methanol conversion [45]. Mole et al. observed an acceleration of zeolite-catalyzed methanol conversion by aromatics co-feeding and proposed a methylbenzene side-chain alkylation mechanism [54] which is presented in Scheme 1.5 (a). This effect was called aromatic co-catalysis [9]. Langner investigated the role of small amounts of higher alcohols on the duration of the induction period [50]. He found a significant reduction of induction period when he cofed 36 ppm cyclohexanol and speculated that C_{3-5} hydrocarbons are formed by the paring reaction of methylated cyclics (Scheme 1.5 (b)) [45].
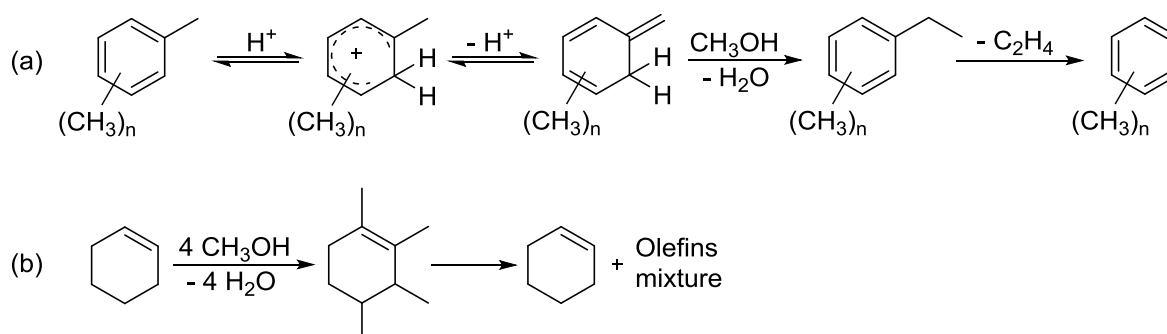
Scheme 1.5. Mole's mechanism of methylbenzene side-chain alkylation [54] (a) and an abbreviated version of Langner's explanation for the pronounced effect of cyclohexanol and other co-feeds on reducing the kinetic induction period (b) [45, 50].

Inspired by the findings on the role of olefins and aromatics in MTH conversion, Dahl and Kolboe reacted isotopically labelled methanol with ethanol/ethene and propene over H-SAPO-

34 in the 90s. Since ethene and propene exhibited little reactivity and most of the products were formed exclusively from methanol, they proposed a hydrocarbon pool mechanism [9, 55-57] which is depicted in Scheme 1.6. The hydrocarbon pool with stoichiometry $(CH_2)_n$ was proposed to represent an adsorbate which may have many characteristics in common with ordinary coke and probably contains less hydrogen than indicated in Scheme 1.6 [55]. It is important to note that the chemical structure of the pool was not further specified [9].
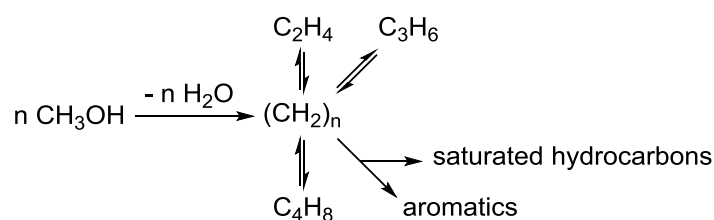

Scheme 1.6. Hydrocarbon pool mechanism according to Dahl and Kolboe [55-57].

1.3.4   Paring and side-chain reaction concepts

To further investigate the hydrocarbon pool mechanism, Mikkelsen et al. studied methylation of toluene with ^{13}C-methanol [58]. They observed isotopic scrambling for ethene and propene. On the basis of these results they concluded that a major part of propene is formed under involvement of arenes or arene derivatives. All their results were in accordance with a carbon pool mechanism. With the aim of gaining further insight into the composition of the carbon pool, Arstad and Kolboe made use of the specific structure of H-SAPO-34 and probed "trapped" carbon intermediate species [13, 59]. In these studies, methylbenzenes were identified as key compounds of the hydrocarbon pool. Parallel studies of Haw and co-workers further supported the role of aromatics as the organic reaction centers [14, 15, 60, 61]. The active site for MTO was defined as supramolecular inorganic-organic hybrid (zeolite-hydrocarbon species), which acts as a scaffold for light olefins formation [45, 49, 62]. Haw and Marcus proposed a mechanism in which methylbenzene is methylated by methanol to the more active hexamethylbenzene. By side-chain alkylation, hexamethylbenzene is further methylated to either an ethylbenzene or isopropylbenzene derivative. In the critical step for selectivity control, the former one loses ethene, the latter one loses propene. The catalytic cycle is finally completed by formation of hexamethylbenzene via methylation [62]. The importance of aromatics for the reaction mechanism could also be shown for H-beta [63]. Further studies over

the large pore zeolite H-beta by Bjørgen et al. led to the conclusion that the heptamethylbenzenium cation is a key intermediate [64-67]. Haw et al. investigated the MTH reaction on an H-ZSM-5, utilizing solid-state NMR spectroscopy. They found methylated cyclopentenyl cations and hypothesized that these species might be reactive for alkene formation [45].

Two models were invoked to rationalize these observations (Scheme 1.7). In the paring reaction concept (Scheme 1.7 (left)) which was first proposed by Sullivan et al. [68], ring contraction and ring expansion are key reaction steps. Olefins are cleaved off after ring contraction. Studies on the unimolecular decomposition of protonated methylbenzenes gave evidence of paring-type reactions [69]. Conversely, a side-chain methylation mechanism was proposed [54, 63, 70] which is shown in Scheme 1.7 (right). After methylation of hexamethylbenzene, a proton is transferred back to the zeolite conjugate base (Z^-) to form an exo-cyclic olefin. Then, the latter species undergoes a series of methylation and deprotonation steps. Finally, an olefin is cleaved off and the catalytic cycle is completed [45]. Conducting *in situ* NMR studies, Seiler et al. obtained spectroscopic evidence supporting the side-chain methylation mechanism [71].
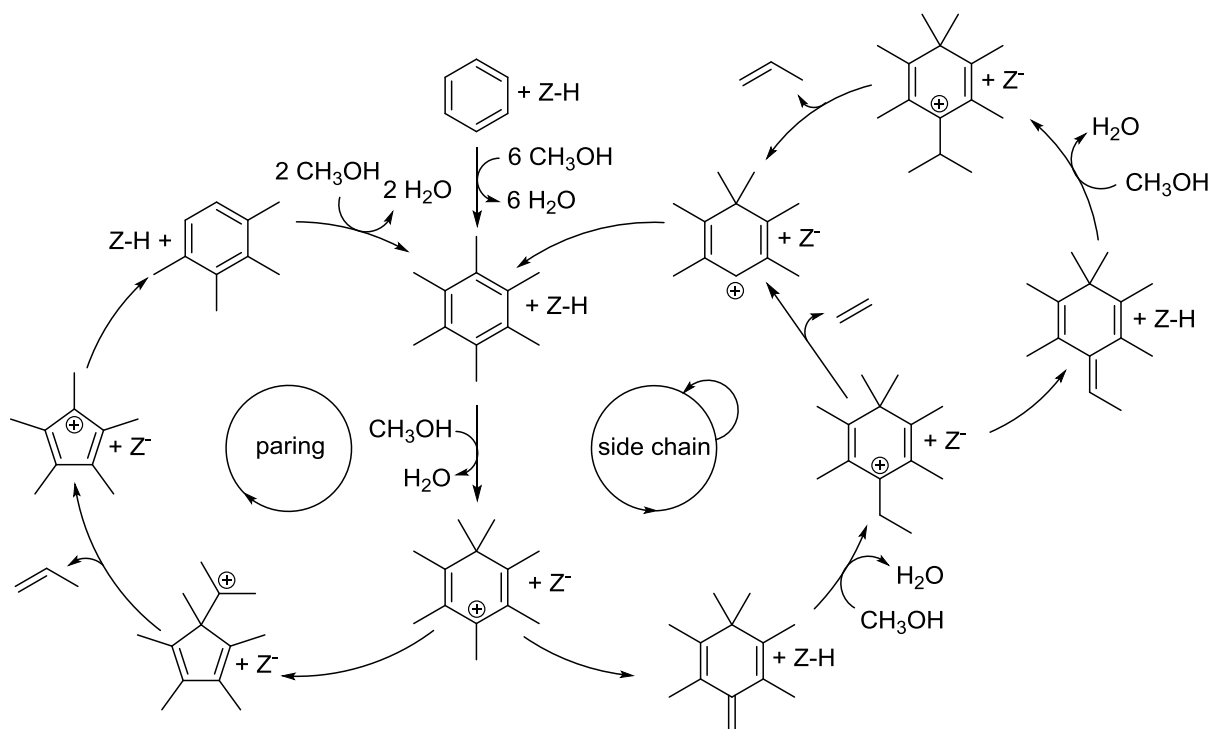
Scheme 1.7. Illustration of the paring and side-chain reaction concepts in MTH catalysis according to ref. [72].

1.3.5   Dual cycle concept

Apart from the role of aromatics as active hydrocarbon pool species in MTH conversion, it was observed that the isotopic distribution pattern of ethene was different from other olefins, when ^{14}C-methanol was co-processed with [12]C_{3+} alcohols on H-ZSM-5. From those results it was deduced that the mechanism of ethene formation is different from formation of higher olefins [73]. In accordance with that observation, [12]C-/^{13}C-MeOH switching experiments over H-ZSM-5 showed that ^{13}C-incorporation of ethene closely matched that of methylbenzene, indicating that both products stem from a common reaction pathway. Conversely, the rapid ^{13}C incorporation in C_{3+} alkenes was proposed to be related with their formation via rapid alkene methylation and cracking [8, 16, 74]. On the basis of these results, a mechanism was proposed involving two cycles running simultaneously (Scheme 1.8): One cycle that involves methylbenzene and ethene, and an alkene methylation/cracking cycle involving C_{3+} olefins. Hydrogen transfer reactions between olefins, forming aromatics and paraffins, link the two cycles [8, 9].
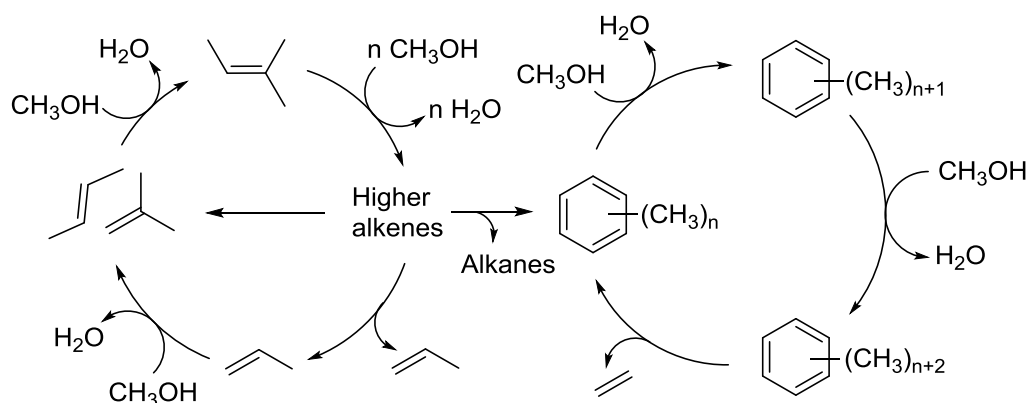
Scheme 1.8. Suggested dual-cycle concept in MTH conversion over H-ZSM-5 [9].

Since both aromatics and olefins are present in the zeolite pores, olefins- and aromatics-mediated routes operate on a competing basis. Product distribution was therefore thought to be optimized by selectively promoting or inhibiting the olefins- or aromatics-based cycle because both cycles contribute differently to ethene and propene formation. Several strategies have been taken into consideration for controlling product selectivity [11]. One approach is to adjust the pores by choosing suitable zeolite topologies [12, 75-78] as already indicated above. Considering that the active site is comprised of a hydrocarbon species (organic part) and a proximate Brønsted acid site (inorganic part), product selectivity can also by adjusted by

influencing the organic or inorganic part. Brønsted acidity can be tuned by zeolite synthesis or post-synthetic anion or cation modifications [10]. The organic part can be influenced by the concentration of olefinic or aromatic species present in the zeolite. This was shown to be achievable by co-feeding different species [11].

1.3.6   Recent insight into the autocatalysis and hydrocarbon pool concept

Recently, Sun et al. explored the effect of repeated variations of the methanol contact time on the catalytic performance. The complete reversibility of contact time variation contrasts the strictest formulation of a hydrocarbon pool mechanism. It indicates that the carbon species are unstable, decomposing or desorbing rapidly after switching back to a higher residence time. The dynamic course of interactions of zeolite (acid sites), hydrocarbon species and methanol is therefore better described by an autocatalysis mechanism than by the original hydrocarbon pool proposal as presented in Scheme 1.6. A generalized hydrocarbon pool mechanism, unifying the autocatalysis and hydrocarbon pool concept, should define the entrained hydrocarbons in the zeolite pores, other than the surface carbon species, as the working hydrocarbon pool species [49].

1.3.7   Deactivation

Deactivation of H-ZSM-5 catalysts is a major issue to be solved in the industrial application of MTH conversion. Catalyst deactivation by carbon deposition is often only discussed with regard to graphitic species blocking active sites or channels. However, any molecule which is too large to diffuse through the microporous channels or has too high proton affinity may block the access to the active sites in the catalysts. These species are often denominated as hydrocarbon residues [9].

The significance of hydrocarbon residues or graphitic coke for catalyst deactivation is not only linked to catalyst topology, but also to temperature. Schulz reported that alkylated benzene molecules are responsible for severe deactivation of an H-ZSM-5 during MTH conversion at 543 K and 563 K by pore filling. Since these molecules were dealkylated at temperatures above 623 K, as deduced from temperature-programmed desorption (TPD) of the spent catalyst, it was

concluded that the alkylation-dealkylation equilibrium was shifted to the alkene-forming side at higher temperature and that deactivation occurred by external coking. Furthermore, longer catalyst lifetimes and lower amounts of hydrocarbons retained on the catalyst were found at temperatures above 623 K [9, 79]. A similar effect of temperature on the nature and amount of hydrocarbon residues was observed for H-SAPO-34 and its topological analogue H-SSZ-13 [80]. These studies give an interesting view on MTH conversion because compounds which are recognized as reaction intermediates in one combination of reaction conditions and catalyst topology may have a deactivating effect in other cases [9].

For MTH reactions in fixed bed reactors, a S-shaped curve is observed for conversion versus time-on-stream (TOS) plots. A period of full conversion is followed by fast deactivation (Figure 1.6). At low conversion levels, the deactivation rate decreases again [9, 81]. This progress can be explained by a reverse W/F curve assuming that the effective contact time decreases by deactivation.
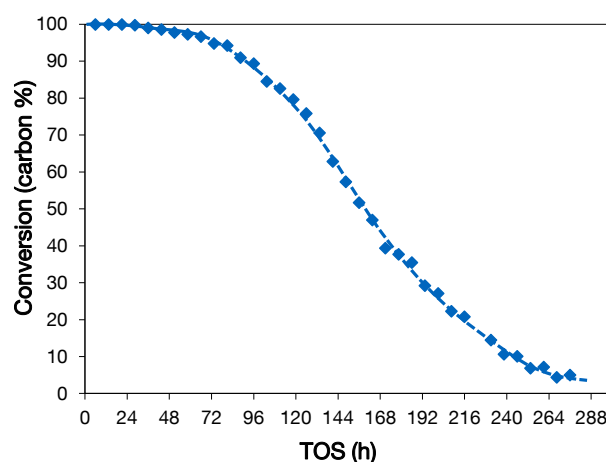

Figure 1.6. Typical conversion versus time on stream curve for the MTH reaction, here shown as an example for the MTO reaction over H-ZSM-5.

Deactivation studies in MTH conversion have often been conducted on catalysts having different topologies with the aim of identifying the best catalyst. Direct comparisons are, however, often complicated because in most studies more than one parameter affecting catalyst deactivation was varied. This includes crystal size, acid strength and acid site density. Furthermore, catalysts are often compared under full conversion. The time on stream at which deactivation will be observed (as appearance of methanol in the outlet) depends on the initial amount of sites, the particular TOF of the sites and the rate of deactivation of those sites.

However, these variables cannot be estimated quantitatively at full conversion and therefore their individual contribution to the observed lifetime is unclear.

Bleken et al. carried out a single-parameter variation study, comparing four 10-ring topologies [82]. They linked deactivation with the formation of heavier polycyclic arenes in larger intersections of certain topologies. Similar conclusions were drawn by Park et al. for topologies with 8-ring windows and different cavity sizes [83]. Deactivation has, however, not only been linked to polycyclic arene formation. Hereijgers et al. found an onset of deactivation before the formation of such polycycles [76]. Taking these results into consideration, they suggested that the initial deactivation was caused by (gaseous) product molecules which were too bulky for leaving the catalyst cavities. Hence, such bulky molecules in the cavities are believed to prevent the diffusion of smaller reactant and product molecules which would then react further to polycyclic arenes and alkanes.

A further important issue which has to be addressed for understanding deactivation is acid strength and acid site density of zeolites. Several authors reported faster catalyst deactivation with a higher acid strength and higher acid sites density [10, 84-86]. Guisnet et al. explained the faster coking rate with stronger acidic sites by faster chemical steps and the more pronounced retention of coke precursors and coke molecules [87]. The increase in coking rate with a higher density of acid sites was associated with the larger number of successive chemical steps undergone by reactant molecules along the diffusion path within the zeolite crystallites and the more favorable condensation reactions. In addition, some authors suggested that coke formation in catalysts with high acid strength is further increased by a high selectivity towards intermolecular hydride transfer [88]. Since intramolecular hydride transfer reactions are involved as reaction steps in the alkene-forming cycle from polymethylated arene molecules (Scheme 1.7), it is difficult to deduce whether higher selectivity toward light olefins could be obtained with lower acid strength. Further, it is important to compare isotopological samples with sufficiently large pore sizes, so that the influence of shape selectivity is reduced and the role of acid strength for coke formation selectivity is elucidated [9].

Due to the fact that catalysts of MFI and CHA topology are the most important catalysts in MTH conversion, numerous studies have been conducted to understand the deactivation of these distinct catalysts. On the basis of the different response of product formation to deactivation, conclusions were drawn on the relative importance of internal and external coke formation for MFI and CHA topologies during deactivation. In MFI, mainly external coke was proposed to be responsible for catalyst deactivation. In the case of internal coke formation, the channels or channel intersections should be completely filled by penta- or hexamethylbenzene

molecules. As a consequence, coke formation should block the access to any active site in the coked channel. In the CHA topology, internal coke is reported to be of major relevance for catalyst deactivation. Its large cavities are spacious enough so that alkene molecules have access to active sites at the interior of a coked cavity even if bi- or polycyclic aromatic compounds/coke precursors are present [9].

1.4   Industrial implementation of MTH processes

Liquid hydrocarbon fuels are of major importance in the global energy chain due to their high energy density and easy transportability. Olefins play a similar role in the production of consumer goods. The MTH process is relevant for both routes since proper choice of catalysts and reaction conditions allows tuning the production of gasoline-range (methanol to gasoline; MTG) or olefin-range (methanol to olefins; MTO) products [9].

In two independent studies of Mobil scientists in the early 1970s, methanol-to-hydrocarbons conversion was discovered by accident. One group was trying to convert methanol to ethylene oxide over the synthetic zeolite H-ZSM-5 [89], but received only hydrocarbons [10]. The other Mobil group was attempting to methylate isobutane with methanol in the presence of ZSM-5 [89]. Surprisingly, they obtained a mixture of aromatics and paraffins formed from methanol and found isobutane to be unreactive [10].

The oil crisis in 1973 and the second oil crisis in 1978 stimulated the development of a commercial MTG process [89] which was first commercialized in New Zealand in 1985. Methanol was produced from natural gas via intermediate synthesis gas formation [9]. In the MTG process (Figure 1.7), methanol is dehydrated in the first reactor over a slightly acidic alumina-based catalyst at a reactor inlet temperature of 583-593 K and about 26 bar pressure [89], giving an equilibrium mixture of methanol, dimethyl ether and water [9]. This mixture is fed into the gasoline reactor at an inlet temperature of 623 K and is converted to C_{1-11} hydrocarbons with high C_{5+} selectivity. Since the reaction is highly exothermic, undesired products (light hydrocarbons, hydrogen, and carbon oxides) are recycled to dilute the feed and control the temperature [9]. Due to depleting crude oil prices, the production of gasoline from methanol in the MTG plant in New Zealand was stopped in the mid-nineties, but methanol was still produced [9].
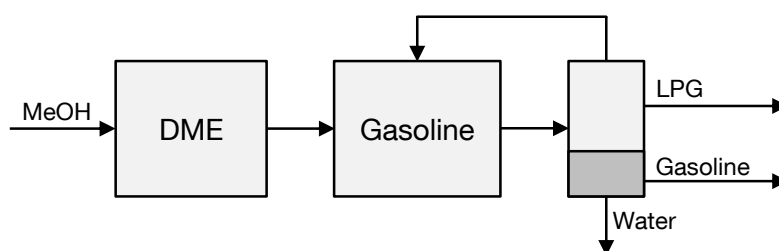
Figure 1.7. Simplified presentation of the Methanol-to-gasoline (MTG) process with adiabatic dehydration reactor for DME synthesis and parallel adiabatic gasoline reactors (DME = Dimethyl ether, LPG = liquefied petroleum gas) [9].

Another possible way to produce gasoline is via the Topsøe integrated gasoline synthesis (TIGAS) process which was demonstrated on an one tonne per day scale in the 1980s [90]. The process outline is illustrated in Figure 1.8. In this process, methanol, dimethyl ether and gasoline syntheses are integrated into one loop. By that, the process is more efficient due to reduced recycle rates and prevention of methanol condensation and re-evaporation [9, 89].
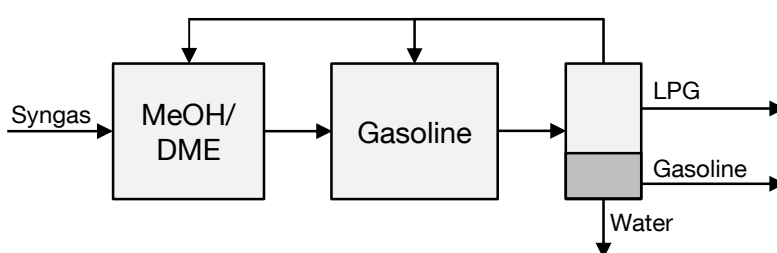

Figure 1.8. Simplified process outline for the Topsøe integrated gasoline synthesis (TIGAS), a syngas-to-gasoline process: Cooled, boiling-water MeOH/DME reactor and parallel adiabatic gasoline reactors [9].

Further variants of the MTG process which are under investigation are the STF process (syngas-to-fuels; via methanol) from CAC Chemnitz and a MTG process from the Shanxi Coal Institute in China.

Chang and Silvestri described in 1977 the reaction of C_{2-5} olefins to paraffins, aromatics, cycloparaffins and C_{6+} as final step in the reaction path [42]. Further, olefins selectivity was shown to increase by low pressure (kinetic effect) and high temperature (partly thermodynamic) [9, 10, 44]. This was utilized in the development of MTO conversion processes.

Mobil developed a fluid-bed process for production of mainly propene and butene on H-ZSM-5. High octane gasoline is formed as side product. In the Mobil olefins to gasoline and distillate (MOGD) process, outlined in Figure 1.9, the olefin production is combined with

another ZSM-5 based process [9, 10, 91]. Light olefins, from either refinery streams or MTO, are oligomerized into high-molecular-weight olefins in the gasoline, distillate and lubricant range [10].
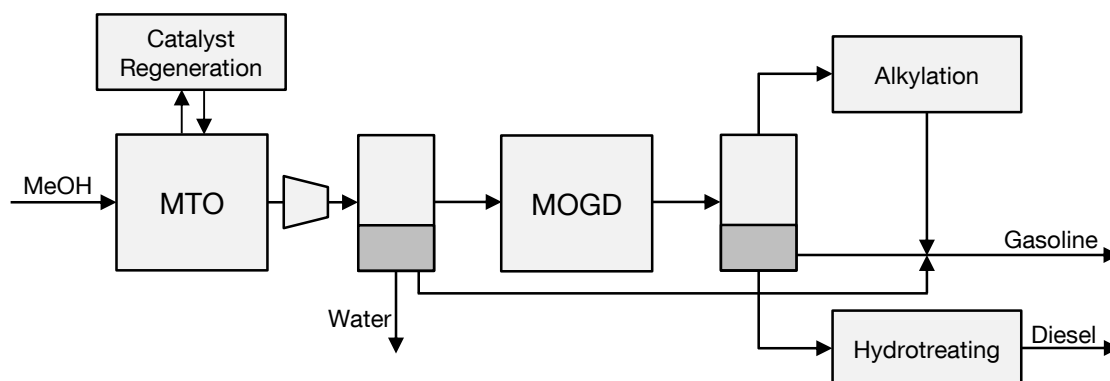

Figure 1.9. Fluidized-bed MTO reactor (H-ZSM-5) with continuous regeneration and parallel fixed-bed reactors for gasoline and diesel synthesis in the Mobil olefins to gasoline and distillate process (MOGD) [9].

UOP in collaboration with Norsk Hydro (now INEOS) developed another MTO process. The reaction is conducted in a low-pressure fluidized-bed reactor design for efficient temperature control and continuous regeneration [9, 89]. In this process, an H-SAPO-34 catalyst is used which was originally discovered by Union Carbide (now UOP). Its chabazite topology of large cavities connected by 8-rings favors olefins formation, but causes rapid coking, so that frequent regeneration is required. In order to further increase propene and ethene selectivity, Total Petrochemicals and UOP developed an olefin cracking process (OCP) to combine it with the UOP/INEOS MTO process (Figure 1.10) [9].
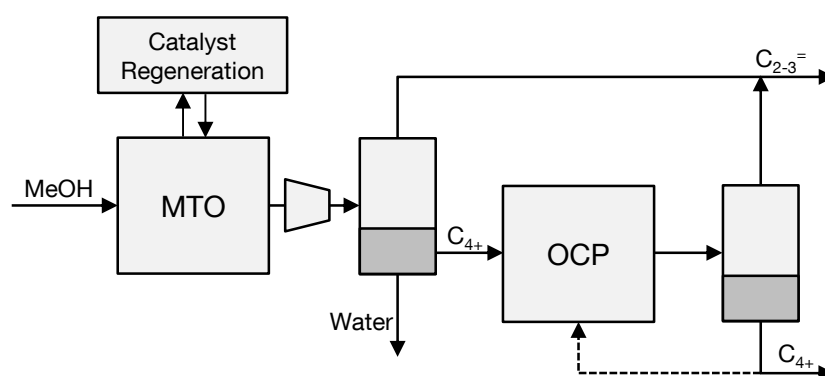

Figure 1.10. Schematic diagram of the INEOS MTO fluidized-bed process using SAPO-34 in combination with the UOP/Total OCP olefin cracking process [9].

The Dalian Institute of Chemical Physics (DICP) developed another MTO technology, using an H-SAPO-34 in a fluidized-bed process. The first plant was successfully put into operation in 2010 [92]. Unlike the UOP process, the C_{4+} stream is recycled to increase the overall ethene and propene selectivity (Figure 1.11) [9]
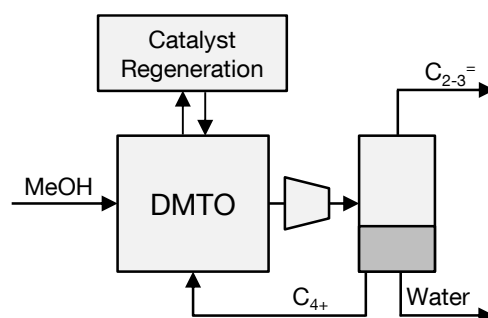

Figure 1.11. Simplified scheme of dimethyl ether- or methanol-to-olefins (DMTO) fluidized-bed process using H-SAPO-34 with recycle of C_{4+}.

Lurgi (now Air Liquide) developed a process to maximize propene yield, using a highly siliceous H-ZSM-5 catalyst at atmospheric pressure and temperatures of 733-753 K. The process is run with parallel fixed-bed reactors, thereby enabling intermittent regeneration. Furthermore, the MeOH/DME feed is injected between the beds to control temperature. After fractionation of the product stream, undesired by-products (ethene, butenes, and higher aliphatic products) are recycled to be converted in the MTP reactor again (Figure 1.12) and to provide a heat sink for the exothermic reaction. In addition, olefins selectivity is increased by recycling of process condensate water, acting as diluting agent [9, 93].
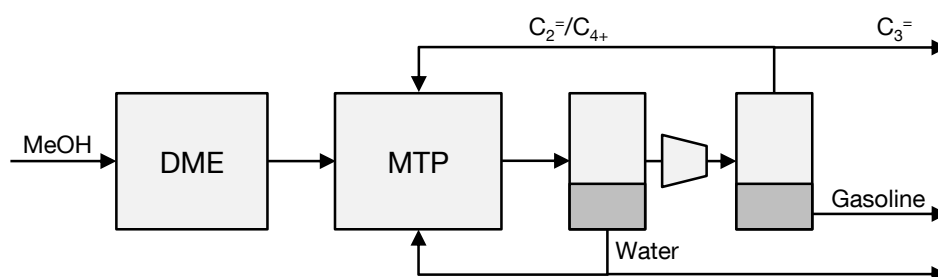

Figure 1.12. Simplified scheme of Lurgi´s MTP process with an adiabatic reactor for DME synthesis and parallel adiabatic reactors with interstage feed (quench) addition and recycle of process condensate, $C_2^=$ and C_{4+} aliphatics.

1.5 Motivation and scope of the thesis

The conversion of methanol to olefins is an industrial process with great potential to increase the production of light olefins. Despite considerable experimental and theoretical efforts within the last thirty years [9, 11], there are still plenty of limitations that need to be resolved for achieving adequate catalyst lifetime and selectivity control. Therefore, the scope of this thesis is to understand elementary reaction steps in methanol-to-olefins conversion.

After having given a broad introduction about zeolites/zeotype materials and the state of the art in methanol-to-hydrocarbons (MTH) conversion in Chapter 1, Chapter 2 deals with coke formation and deactivation pathways in the conversion of methanol to olefins. The catalysis in plug-flow (PFR) and fully back-mixed reactors (CSTR) is compared to draw conclusions on the location and type of deactivating species. Furthermore, the dependence of deactivation on local methanol concentration is elucidated. Mechanisms leading to the formation of highly deactivating oxygen-containing species and localized aromatics are proposed, involving CO and formaldehyde as intermediates.

Aside from understanding catalyst deactivation, it is of major importance to know how to tune product selectivity and how to prevent hydrogen transfer. In a former contribution [49] indications of a methanol-related hydrogen transfer pathway were found which would be the major contributor to aromatics and paraffins formation. This mechanism is investigated at a molecular level in Chapter 3. The specific role of Lewis and Brønsted acid sites is shown both for methanol-related and olefin-related hydrogen transfer reactions. It is shown that the methanol-related hydrogen transfer comprises the reaction of methanol and olefins at LAS and the reaction of olefins and formaldehyde at BAS.

Since formaldehyde was shown to be generated at LAS and to act as a linking species in the methanol-induced hydrogen transfer (Chapter 3), the impact of present formaldehyde on methanol conversion over H-ZSM-5 is discussed in detail in Chapter 4. At first, the formation of formaldehyde via different pathways under MTO conditions is presented. By conducting temperature-programmed surface reactions, the importance of formaldehyde in first C-C bond and subsequent olefins formation is demonstrated. Because formaldehyde is proposed to be involved in the formation of highly deactivating carbon deposits in Chapter 2, the deactivation under a pure methanol feed is compared with mixed methanol/formaldehyde and methanol/toluene feeds. The obtained results support the mechanistic proposal given in Chapter 2.

1.6 References

[1] C.A. Gärtner, A.C. van Veen, J.A. Lercher, ChemCatChem 5 (2013) 3196.

[2] T. Mokrani, M. Scurrell, Catal. Rev.-Sci. Eng. 51 (2009) 1.

[3] B. Tope, Y. Zhu, J.A. Lercher, Catal. Today 123 (2007) 113.

[4] A. Behr, D.W. Agar, J. Jörissen, Einführung in die Technische Chemie, Spektrum Akademischer Verlag, Heidelberg, 2010, p. 179.

[5] A. Behr, A. Kleyensteiber, U. Hartge, Chem. Ing. Tech. 82 (2010) 201.

[6] J.Q. Chen, A. Bozzano, B. Glover, T. Fuglerud, S. Kvisle, Catal. Today 106 (2005) 103.

[7] A.S. Bodke, D.A. Olschki, L.D. Schmidt, E. Ranzi, Science 285 (1999) 712.

[8] S. Ilias, A. Bhan, ACS Catal. 3 (2013) 18.

[9] U. Olsbye, S. Svelle, M. Bjørgen, P. Beato, T.V.W. Janssens, F. Joensen, S. Bordiga, K.P. Lillerud, Angew. Chem. Int. Ed. 51 (2012) 5810.

[10] M. Stöcker, Microporous Mesoporous Mater. 29 (1999) 3.

[11] X. Sun, S. Mueller, H. Shi, G.L. Haller, M. Sanchez-Sanchez, A.C. van Veen, J.A. Lercher, J. Catal. 314 (2014) 21.

[12] J. Li, Y. Wei, G. Liu, Y. Qi, P. Tian, B. Li, Y. He, Z. Liu, Catal. Today 171 (2011) 221.

[13] B. Arstad, S. Kolboe, Catal. Lett. 71 (2001) 209.

[14] W. Song, H. Fu, J.F. Haw, J. Phys. Chem. B 105 (2001) 12839.

[15] H. Fu, W. Song, J. Haw, Catal. Lett. 76 (2001) 89.

[16] M. Bjørgen, S. Svelle, F. Joensen, J. Nerlov, S. Kolboe, F. Bonino, L. Palumbo, S. Bordiga, U. Olsbye, J. Catal. 249 (2007) 195.

[17] S.A. Bradley, R.W. Broach, T.M. Mezza, S. Prabhakar, W. Sinkler, Zeolite Characterization, in: S. Kulprathipanja (Ed.), Zeolites in Industrial Separation and Catalysis, Wiley-VCH, Weinheim, 2010, p. 85.

[18] M. Elanany, M. Koyama, M. Kubo, E. Broclawik, A. Miyamoto, Appl. Surf. Sci. 246 (2005) 96.

[19] T. Chen, A. Men, P. Sun, J. Zhou, Z. Yuan, Z. Guo, J. Wang, D. Ding, H. Li, Catal. Today 30 (1996) 189.

[20] M.H.W. Sonnemans, C. Den Heijer, M. Crocker, J. Phys. Chem. 97 (1993) 440.

[21] N.O. Gonzales, A.T. Bell, A.K. Chakraborty, J. Phys. Chem. B 101 (1997) 10058.

[22] H. Abrevaya, Unique Aspects of Mechanisms and Requirements for Zeolite Catalysis in Refining and Petrochemicals, in: S. Kulprathipanja (Ed.), Zeolites in Industrial Separation and Catalysis, Wiley-VCH, Weinheim, 2010, p. 403.

[23] G.L. Woolery, G.H. Kuehl, H.C. Timken, A.W. Chester, J.C. Vartuli, Zeolites 19 (1997) 288.

[24] B. Smit, T.L.M. Maesen, Nature 451 (2008) 671.

[25] O. Deutschmann, H. Knözinger, K. Kochloefl, T. Turek, Heterogeneous Catalysis and Solid Catalysts, in: G. Bellussi (Ed.), Ullmann's Encyclopedia of Industrial Chemistry, Wiley-VCH, Weinheim, 2000.

[26] R.W. Broach, Zeolite Types and Structures, in: S. Kulprathipanja (Ed.), Zeolites in Industrial Separation and Catalysis, Wiley-VCH, Weinheim, 2010, p. 27.

[27] C.T.W. Chu, C.D. Chang, J. Phys. Chem. 89 (1985) 1569.

[28] D. Barthomeuf, Catal. Rev.-Sci. Eng. 38 (1996) 521.

[29] J.W. Ward, J. Catal. 10 (1968) 34.

[30] C.S. Triantafillidis, A.G. Vlessidis, L. Nalbandian, N.P. Evmiridis, Microporous Mesoporous Mater. 47 (2001) 369.

[31] F. Lónyi, J.H. Lunsford, J. Catal. 136 (1992) 566.

[32] A.I. Biaglow, D.J. Parrillo, G.T. Kokotailo, R.J. Gorte, J. Catal. 148 (1994) 213.

[33] C.S. Triantafillidis, N.P. Evmiridis, Ind. Eng. Chem. Res. 39 (2000) 3233.

[34] L. Kubelková, S. Beran, A. Malecka, V.M. Mastikhin, Zeolites 9 (1989) 12.

[35] J. Sanz, V. Fornes, A. Corma, J. Chem. Soc., Faraday Trans. 1 84 (1988) 3113.

[36] C.S. Triantafillidis, A.G. Vlessidis, N.P. Evmiridis, Ind. Eng. Chem. Res. 39 (2000) 307.

[37] http://www.iza-structure.org/, accessed 09.06.2015.

[38] G.T. Kokotailo, S.L. Lawton, D.H. Olson, W.M. Meier, Nature 272 (1978) 437.

[39] C. Baerlocher, L.B. McCusker, D.H. Olson, ATLAS OF ZEOLITE FRAMEWORK TYPES, Elsevier, Amsterdam, 2007, p. 212

[40] L.B. McCusker, F. Liebau, G. Engelhardt, Pure Appl. Chem. 73 (2001) 381.

[41] http://ruby.chemie.uni-freiburg.de/Vorlesung/silicate_8_9.html, accessed 16.06.2015.

[42] C.D. Chang, A.J. Silvestri, J. Catal. 47 (1977) 249.

[43] C.D. Chang, Catal. Rev.-Sci. Eng. 26 (1984) 323.

[44] C.D. Chang, C.T.W. Chu, R.F. Socha, J. Catal. 86 (1984) 289.

[45] J.F. Haw, W. Song, D.M. Marcus, J.B. Nicholas, Acc. Chem. Res. 36 (2003) 317.

[46] D. Lesthaeghe, V. Van Speybroeck, G.B. Marin, M. Waroquier, Ind. Eng. Chem. Res. 46 (2007) 8832.

[47] W. Song, D.M. Marcus, H. Fu, J.O. Ehresmann, J.F. Haw, J. Am. Chem. Soc. 124 (2002) 3844.

[48] N.Y. Chen, W.J. Reagan, J. Catal. 59 (1979) 123.

[49] X. Sun, S. Mueller, Y. Liu, H. Shi, G.L. Haller, M. Sanchez-Sanchez, A.C. van Veen, J.A. Lercher, J. Catal. 317 (2014) 185.

[50] B.E. Langner, Appl. Catal. 2 (1982) 289.

[51] R.M. Dessau, R.B. LaPierre, J. Catal. 78 (1982) 136.

[52] R.M. Dessau, J. Catal. 99 (1986) 111.

[53] D. Lesthaeghe, J. Van der Mynsbrugge, M. Vandichel, M. Waroquier, V. Van Speybroeck, ChemCatChem 3 (2011) 208.

[54] T. Mole, G. Bett, D. Seddon, J. Catal. 84 (1983) 435.

[55] I.M. Dahl, S. Kolboe, Catal. Lett. 20 (1993) 329.

[56] I.M. Dahl, S. Kolboe, J. Catal. 149 (1994) 458.

[57] I.M. Dahl, S. Kolboe, J. Catal. 161 (1996) 304.

[58] Ø. Mikkelsen, P.O. Rønning, S. Kolboe, Microporous Mesoporous Mater. 40 (2000) 95.

[59] B. Arstad, S. Kolboe, J. Am. Chem. Soc. 123 (2001) 8137.

[60] W. Song, J.F. Haw, J.B. Nicholas, C.S. Heneghan, J. Am. Chem. Soc. 122 (2000) 10726.

[61] W. Song, H. Fu, J.F. Haw, J. Am. Chem. Soc. 123 (2001) 4749.

[62] J.F. Haw, D.M. Marcus, Top. Catal. 34 (2005) 41.

[63] A. Sassi, M.A. Wildman, H.J. Ahn, P. Prasad, J.B. Nicholas, J.F. Haw, J. Phys. Chem. B 106 (2002) 2294.

[64] M. Bjørgen, U. Olsbye, S. Kolboe, J. Catal. 215 (2003) 30.

[65] M. Bjørgen, U. Olsbye, D. Petersen, S. Kolboe, J. Catal. 221 (2004) 1.

[66] M. Bjørgen, U. Olsbye, S. Svelle, S. Kolboe, Catal. Lett. 93 (2004) 37.

[67] M. Bjørgen, F. Bonino, S. Kolboe, K.-P. Lillerud, A. Zecchina, S. Bordiga, J. Am. Chem. Soc. 125 (2003) 15863.

[68] R.F. Sullivan, C.J. Egan, G.E. Langlois, R.P. Sieg, J. Am. Chem. Soc. 83 (1961) 1156.

[69] S. Svelle, M. Bjørgen, S. Kolboe, D. Kuck, M. Letzel, U. Olsbye, O. Sekiguchi, E. Uggerud, Catal. Lett. 109 (2006) 25.

[70] T. Mole, J.A. Whiteside, D. Seddon, J. Catal. 82 (1983) 261.

[71] M. Seiler, W. Wang, A. Buchholz, M. Hunger, Catal. Lett. 88 (2003) 187.

[72] D. Lesthaeghe, A. Horré, M. Waroquier, G.B. Marin, V. Van Speybroeck, Chem. Eur. J. 15 (2009) 10803.

[73] L.-M. Tau, A.W. Fort, S. Bao, B.H. Davis, Fuel Process. Technol. 26 (1990) 209.

[74] S. Svelle, F. Joensen, J. Nerlov, U. Olsbye, K.-P. Lillerud, S. Kolboe, M. Bjørgen, J. Am. Chem. Soc. 128 (2006) 14770.

[75] S. Teketel, U. Olsbye, K.-P. Lillerud, P. Beato, S. Svelle, Microporous Mesoporous Mater. 136 (2010) 33.

[76] B.P.C. Hereijgers, F. Bleken, M.H. Nilsen, S. Svelle, K.-P. Lillerud, M. Bjørgen, B.M. Weckhuysen, U. Olsbye, J. Catal. 264 (2009) 77.

[77] M. Bjørgen, F. Joensen, K.-P. Lillerud, U. Olsbye, S. Svelle, Catal. Today 142 (2009) 90.

[78] S. Svelle, U. Olsbye, F. Joensen, M. Bjørgen, J. Phys. Chem. C 111 (2007) 17981.

[79] H. Schulz, Catal. Today 154 (2010) 183.

[80] F. Bleken, M. Bjørgen, L. Palumbo, S. Bordiga, S. Svelle, K.-P. Lillerud, U. Olsbye, Top. Catal. 52 (2009) 218.

[81] G.F. Froment, Catal. Rev.-Sci. Eng. 50 (2008) 1.

[82] F. Bleken, W. Skistad, K. Barbera, M. Kustova, S. Bordiga, P. Beato, K.P. Lillerud, S. Svelle, U. Olsbye, PCCP 13 (2011) 2539.

[83] J.W. Park, J.Y. Lee, K.S. Kim, S.B. Hong, G. Seo, Appl. Catal. A: Gen. 339 (2008) 36.

[84] S. Wilson, P. Barger, Microporous Mesoporous Mater. 29 (1999) 117.

[85] Q. Zhu, J.N. Kondo, R. Ohnuma, Y. Kubota, M. Yamaguchi, T. Tatsumi, Microporous Mesoporous Mater. 112 (2008) 153.

[86] I.M. Dahl, H. Mostad, D. Akporiaye, R. Wendelbo, Microporous Mesoporous Mater. 29 (1999) 185.

[87] M. Guisnet, L. Costa, F.R. Ribeiro, J. Mol. Catal. A: Chem. 305 (2009) 69.

[88] L.-T. Yuen, S.I. Zones, T.V. Harris, E.J. Gallegos, A. Auroux, Microporous Mater. 2 (1994) 105.

[89] F.J. Keil, Microporous Mesoporous Mater. 29 (1999) 49.

[90] J. Topp-Jørgensen, Topsøe Integrated Gasoline Synthesis – The Tigas Process, in: D.M. Bibby, C.D. Chang, R.F. Howe, S. Yurchak (Eds.), Stud. Surf. Sci. Catal., Elsevier, Amsterdam, 1988, p. 293.

[91] A.A. Avidan, Gasoline and Distillate Fuels From Methanol, in: D.M. Bibby, C.D. Chang, R.F. Howe, S. Yurchak (Eds.), Stud. Surf. Sci. Catal., Elsevier, Amsterdam, 1988, p. 307.

[92] P. Tian, Y. Wei, M. Ye, Z. Liu, ACS Catal. 5 (2015) 1922.

[93] H. Koempel, W. Liebner, Lurgi's Methanol To Propylene (MTP®) Report on a successful commercialisation, in: M.S. Fábio Bellot Noronha, S.-A. Eduardo Falabella (Eds.), Stud. Surf. Sci. Catal., Elsevier, Amsterdam, 2007, p. 261.

Chapter 2

2. Coke formation and deactivation pathways on H-ZSM-5 in the conversion of methanol to olefins

The role of parallel and sequential reactions in Brønsted acid-catalyzed conversion of methanol to olefins (MTO) on H-ZSM-5 was explored by comparing the catalysis in plug-flow (PFR) and fully back-mixed reactors (CSTR). Catalysts deactivated under homogeneous gas phase in the back-mixed reactor show unequivocally that in the early stages of the reaction the zeolite deactivates via blocking of individual Brønsted acid sites and not by coke-induced impeding access to pores. While the two reactors led only to slight differences in product distribution, catalyst deactivation rates were drastically lower in the CSTR. H-ZSM-5 deactivated in the CSTR first rapidly and then at a much slower rate. During the initial phase, the rate was directly proportional to the methanol partial pressure and was caused by oxygen-containing surface species. These species were transformed to aromatic compounds with time on stream and the deactivation proceeded then via methylation of aromatic compounds, forming the typical coke species for MTO processes. The outer surface of the polycrystalline particles is virtually carbon free under these conditions. Formation of condensed aromatic species throughout the deactivation in voids between crystalline domains occurs as parallel reaction without affecting the deactivation kinetics.

2.1 Introduction

Propene is an important building block for the production of a multitude of chemicals. Currently, it is mainly produced by steam cracking [1, 2]. Due to the increasing gap between propene demand and production [3], alternative processes have been intensely explored. Especially, the methanol-to-hydrocarbons (MTH) route has been developed in a series of variants [4-6]. The popularity of this exothermic process [7] is associated with a well-established route to produce methanol from synthesis gas, which can be in turn generated from carbon-based feedstocks [8]. Also, the flexible adjustment of the product spectrum through process conditions and catalyst modifications explains why a large number of processes have been installed over the last decade.

As a particular example, the methanol-to-propene (MTP) process by Lurgi has focused on maximizing the propene yield, carrying out the reaction at near atmosphere pressure and at temperatures of 733-753 K [7]. The reaction is performed in a fixed-bed reactor over an H-ZSM-5 catalyst [9]. Recycling of process condensate and olefins has been reported to be required to achieve economic yields of propene [7].

To enhance the single-pass yield of propene, different approaches have been previously considered. Early on Chang [10] reported that a high Si/Al ratio of MFI reduced the rate of aromatization compared to that of olefin formation, consequently leading to higher propene yields. However, higher contact times were required to achieve full conversion. Higher propene yields have also been associated with reduced methanol partial pressure, which causes, however, the necessity of separating propene from dilute streams [10]. The third approach to increase the propene yield is associated with high reaction temperatures [10, 11] which in turn is accompanied by faster catalyst deactivation [12]. Thus, all approaches have clear limitations and the quest for an intrinsically higher selectivity of catalytic materials is intense.

In general, however, materials and operating conditions favoring propene selectivity tend to induce faster deactivation than conventional catalysts and operating conditions. Deactivation is attributed to the formation of carbonaceous deposits, which strongly adsorb on Brønsted and Lewis acid sites and block pore entrances [13]. Guisnet and Magnoux [14, 15] showed, for example, that coking and consequent deactivation depended equally on zeolite pore structures and on operating conditions. At low temperatures, coke formation involved mainly condensation and rearrangement steps, while at temperatures above 623 K hydrogen transfer began to influence the coke formation. Deactivation rates in various zeolite topologies are

strongly influenced by crystal size, acid site strength and concentration [7]. Two systematic studies [16, 17] have related the rate of deactivation to the formation of polycyclic aromatics.

Because of such relations, it has been suggested that coke formation occurs preferentially on the outer surface of the zeolitic crystals [13, 18-20]. However, it has also been hypothesized that external coke formation begins only after the catalyst is deactivated by intra-porous coke [21, 22]. Bjørgen et al. [23], in contrast, did not find a correlation between the concentration of organic molecules retained in the pores and the zeolite deactivation at 643 K. They concluded that external coke deposition caused activity loss with time on stream, in agreement with Schulz [24].

Whatever the detailed mechanism is, the concentration of acid sites has been identified as a key factor for reactivity and product distribution [25-27]. Topsøe et al. were the first to note the significant decrease in the concentration of acid sites during methanol conversion over H-ZSM-5, associating it with catalyst deactivation [28]. McLellan et al. [29] showed that an initial strong decrease in the acid site concentration was followed by a second slower deactivation phase. The initial deactivation regime was speculated to be associated with blocking of acid sites at channel intersections. The second deactivation stage was ascribed to external coking and/or to topological blocking of the zeolites channels.

Despite the fact that the MTO/MTP catalysis is a sequential process involving very different reactions as a function of conversion and, hence, as a function of the position in the reactor, most studies on deactivation have been carried out in plug-flow reactors. It has been observed that distinct reaction zones (and coke deposits) form along the reactor length [30, 31]. In the catalyst layer closest to the inlet, the equilibrium between methanol and dimethyl ether was concluded to be established and C-C bond formation to occur only to a minor extent. Next is a region where the core of the methanol-to-olefin (MTO) reaction takes place. Between the DME-MeOH equilibration zone and the MTO zone, a region with highly coked catalyst particles appears, which grows with time on stream as full deactivation of the particles shifts the reaction to positions downstream. In the last region of the catalyst bed, the primary products (mainly olefins) undergo further reactions, producing a lower concentration of coke deposits. As to be expected from the various chemistries involved, the deposited coke is very heterogeneous.

Characterization of a sample deactivated in a plug-flow reactor for a certain time on stream provides, therefore, little information on the chemistry of the deactivating processes, because it contains inevitably a mixture of carbonaceous deposits from different reaction regimes. Bleken et al. [6] addressed this issue, dividing the catalyst bed into several parts and characterizing the different fractions. A shift toward heavier or more condensed coke species was observed from

the top to the bottom of the catalyst bed. This suggests that the chemistry forming carbonaceous deposits changes with the composition along the catalyst bed.

In order to eliminate the influence of the changing external environment, the present contribution characterizes, therefore, the deactivation of the MFI catalysts under reaction conditions in which all catalyst particles are exposed to a homogeneous gas atmosphere, that is in an ideally back-mixed reactor, and compares it with information obtained in a plug-flow reactor. Characterization of such samples by various physicochemical techniques was combined with analysis of reaction data obtained in a back-mixed reactor as well as in a plug-flow reactor.

2.2   Experimental

2.2.1   Materials

The synthesis method of the H-ZSM-5 catalyst (Si/Al = 90) used in this study was reported in a former publication by Ong et al. [32]. The catalyst was steamed at 753 K for 24 h with WHSV = 1 h^{-1} prior to reaction. Methanol ($\geq$99.9%), 4-Hydroxy-TEMPO benzoate (97%), MgO (99.99%), trifluoroacetic acid (99%), acetonitrile (99.8%) and pyridine (99.8%) were supplied by Sigma-Aldrich. The 10% hydrofluoric acid solution was supplied by Zefa.

2.2.2   Catalyst characterization

2.2.2.1   Electron paramagnetic resonance (EPR) spectroscopy

EPR spectra were recorded on a Jeol JES FA 200 spectrometer equipped with a cylindrical mode cavity and a liquid helium cryostat operating in X-band mode. Ten milligrams of each deactivated catalyst (after cooling from reaction temperature to room temperature in N_2) was filled in quartz EPR tubes. The EPR spectra were recorded at ambient pressure (9.25 GHz, 1 mW microwave power). Different mixtures of 4-Hydroxy-TEMPO benzoate/MgO were used as reference for calculating the concentration (amount) of spins. The g values were determined by using the following formula (2.1):

$$g = 71.4484 \cdot \nu_0 \, [\text{GHz}]/B_0 \, [\text{mT}] \tag{2.1}$$

2.2.2.2   Temperature-programmed oxidation of deactivated catalysts

Coke deposits formed on the catalysts were quantitatively analyzed by thermogravimetric analysis (TGA) on a SETARAM Sensys Evo TGA-DSC connected to a MS. Typically 10-20 mg powdered sample (free of SiC) was loaded in the cell and pretreated at 473 K in 16 mL/min He flow until the weight stabilized. Then, the temperature was raised to 923 K at 5 K/min in 16 mL/min O_2/He (1/9) flow and kept for 1 h. Coke amount and its combustion heat were obtained from the total weight loss and integration of heat flow. Coke C/H/O ratios were calculated according to the quantification of consumed O_2 and generated H_2O, CO, CO_2 from MS and their comparison with coke weight from TGA.

2.2.2.3   IR spectroscopy

The concentration of acid sites was determined by IR spectroscopy using pyridine as probe molecule. Spectra were recorded on a Nicolet 5700 FT-IR spectrometer with a resolution of 4 cm^{-1}. The samples were pressed into self-supporting wafers and pretreated in vacuum ($<10^{-5}$ mbar) at 723 K for 1 h. All spectra were collected at 423 K. Pyridine adsorption was carried out at a partial pressure of 0.1 mbar at 423 K for half an hour followed by 1-h evacuation to remove physically adsorbed pyridine. The concentration of Brønsted and Lewis acid sites (referred to as BAS and LAS) was calculated from the areas of the bands at 1515–1565 cm^{-1} and 1435–1470 cm^{-1} and normalized to sample wafer weight.

2.2.2.4   LDI-TOF MS

For laser desorption/ionization (LDI)-TOF MS measurements, the samples were prepared in two ways. In the first mode, the deactivated samples were studied directly with LDI-TOF MS. In this way, information was only obtained about the coke species formed on the outer surface of the catalyst [33]. For analyzing the deactivated samples, a solution of 1% trifluoroacetic acid in acetonitrile was prepared, and 10 mg of the deactivated catalyst was suspended in 200 µL of this solution. A sample of 0.9 µL of the resulting suspension was deposited on the sample holder. After air-drying the drop, the sample holder was introduced into the ion source of the mass spectrometer. The LDI-TOF mass spectra were recorded using

a Bruker Ultraflex TOF/TOF MALDI-TOF mass spectrometer equipped with a N_2 laser ($v =$ 337 nm). The ions were accelerated with pulsed ion extraction after a delay of 50 ns by a voltage of 28.5 kV. The analyzer was operated in reflectron mode, and the ions were detected using a micro-channel plate detector. The mass spectrometer was calibrated prior to measurement with a peptide calibration standard.

In addition, deactivated catalysts were treated in aqueous HF in order to dissolve the silica fraction and liberate the coke deposits. With this procedure, the mass spectra included contributions of all coke compounds, independently of their location in the matrix. This was done by complete dissolution of 10 mg deactivated zeolite with 2 mL 10% hydrofluoric acid solution (procedure repeated twice). Unreacted HF was evaporated and the remainder was mixed with a solution of 1% trifluoroacetic acid in acetonitrile. For analyzing the free deposits with LDI-TOF MS after evaporation of unreacted HF and mixing with trifluoroacetic acid, the same procedure and the same instrument settings as for the intact deactivated catalyst were applied.

2.2.2.5　　Nitrogen physisorption

The micropore volume of the materials was obtained by nitrogen adsorption using a PMI automated BET sorptometer. The micropore volume was calculated utilizing the t-plot method. Before N_2 adsorption, the sample was activated in vacuum at 523 K for 2 h. After activation, the weight of the dried sample was determined. Subsequently, the sample was cooled to 77 K and liquid nitrogen was adsorbed at increasing partial pressures.

2.2.3　　Catalytic measurements

Activity tests were performed on a homemade plug-flow reaction unit and a CSTR (Micro-Berty reactor of Autoclave Engineers).

Catalytic testing in the PFR with an internal diameter of 6 mm was carried out at ambient pressure and a reaction temperature of 723 K. The catalyst H-ZSM-5-S (where S = steaming for 24 h at 753 K with WHSV (water) = 1 h^{-1}) was pelletized, crushed and sieved into fractions ranging from 200 to 280 μm. The zeolite was 1:20 (wt.) diluted in 355-500 μm silicon carbide beads (ESK-SiC) to ensure isothermal conditions. Catalyst activation prior to methanol

conversion involved heating at 723 K for 1 h under 50 mL/min N_2 flow. Methanol was fed by passing 50 mL/min N_2 through a methanol evaporator kept at 299 K. Weight hourly space times were adjusted by charging varying amounts of catalyst (every single data point was taken after 10 min on stream). To investigate the deactivation, 0.090 g of the catalyst H-ZSM-5-S was deactivated at a contact time of W/F (h · g_{cat} / mol_{MeOH}) = 3.4.

Reaction studies in the CSTR were conducted at a constant pressure of 6.5 bar to achieve good back-mixing of the gas phase (realized by adding inert N_2 at MeOH partial pressure corresponding to p = 178 mbar, which is identical with the pressure used in the PFR) and temperatures of 723 K, 748 K and 773 K. By using enhanced pressures and high impeller speeds (4000 rpm), homogeneous concentration and temperature profiles were achieved [34]. The catalyst H-ZSM-5-S was pressed and sieved to obtain particles between 500 and 710 μm. The zeolite was 1:10 (wt.) diluted in 710-900 μm silicon carbide beads (ESK-SiC). The catalyst was activated at the respective reaction temperatures for 1 h under a flow of 203 mL/min N_2 before switching to the feed. The contact time was varied by varying the catalyst loading (every single data point was taken after 10 min on stream). To investigate the deactivation during MTO reaction, 50 mg of the catalyst H-ZSM-5-S was deactivated for 5 h, 15 h, 22 h, 47 h, 78 h and 92 h (samples denoted as H-ZSM-5-S-X where X = 5, 15, 22, 47, 78 and 92 h). For the determination of the coke combustion heat, the coke composition and the change of acid sites concentration, a sample was deactivated for 2 h. To determine the change of acid sites concentration at very short time on stream, a sample was also deactivated for 0.8 h. For the determination of the deactivation reaction order, reactant flow velocities were varied at constant catalyst loading of 50 mg, so that contact times of W / F (h · g_{cat} / mol_{MeOH}) = 2.3, 3.6 and 7.1 were obtained. In each case, the reaction was stopped after 23 h.

If a positive reaction order with respect to methanol is assumed for the reactions generating coke, the deactivation rate can be expressed by equation (2.2).

$$r_d = -\frac{\Delta r}{\Delta t} = k_d \cdot (\dot{n}_0(MeOH))^n \tag{2.2}$$

where r_d: deactivation rate, r: reaction rate, defined as $r = X \cdot \frac{F}{W}$, t: time, $\dot{n}_0(MeOH)$: molar flow rate of methanol, n: reaction order of deactivation and k_d: deactivation rate constant.

The reactor effluents from both reactors were analyzed by gas chromatographs equipped with a HP-PLOTQ capillary column (30 m, 0.32 mm i.d.) and a flame ionization detector.

Due to the rapid interconversion, both oxygenates, that is, methanol and dimethyl ether, were considered together as "reactant". Conversion and yields were calculated on a carbon

basis. The comparison of the CSTR with the PFR was done by means of varying the contact time for both reactors.

2.3   Results

2.3.1   Methanol-to-olefins (MTO) reaction in a plug flow reactor and in a back-mixed reactor

2.3.1.1   Reaction pathway of methanol-to-olefins conversion

The methanol conversion and the product yields obtained in the plug-flow reactor are shown as a function of contact time in Figure 2.1. The conversion curve followed a sigmoidal shape, resembling autocatalytic reactions [35]. An initial phase with no conversion was observed at very short contact times (0-2 h $\cdot$ g_{cat} / mol_{MeOH}), until the concentration of products sufficed to enable faster reaction pathways. The yields of propene, butenes and C_5 aliphatics reached the maximum when the methanol conversion attained 100%. A simplified MTO reaction pathway [36, 37], depicted in Scheme 2.1, suggests that these C_{3-5} hydrocarbons are formed by consecutive methylations. The ethene yield, however, increased continuously with contact time. The same trend was observed for the yield of aromatics, suggesting that both products were kinetically linked [38, 39]. The similar yields of C_{1-4} paraffins and aromatics are concluded to be the consequence of the stoichiometry of the hydrogen transfer reaction, which has been proposed to take place from the cyclic hydrocarbon to a light olefin to produce alkanes and an aromatic molecule [40]. The C_{6+} aliphatics yield reached its maximum at a conversion of 80% (contact time = 3.8 h $\cdot$ g_{cat} / mol_{MeOH}) and decreased at higher contact times. This suggests that C_{6+} aliphatics were cracked to shorter olefins at longer residence times [31].

The product distribution and conversion of methanol in the back-mixed reactor are compiled in Figure 2.2. The initial phase without conversion at short contact times was not observed. This is attributed to the homogeneous distribution of reaction products in the back-mixed reactor, which in turn leads to a more rapid accumulation of surface species, enabling the fast reaction pathways almost instantly. On the other hand, at very long contact times, only MeOH/DME conversions of around 90% were reached, given the very modest volume (19 cm^3) of the Micro-Berty reactor used [41].

The selectivity towards C_2-C_5 olefins, aromatics and paraffins in the CSTR was similar to the selectivities achieved in the PFR at 10-80% of methanol conversion. Important differences were only observed for C_{6+} aliphatic molecules (Figures 2.1 (b) and 2.2 (b)). In the back-mixed

reactor (Figure 2.2 (b)), the C_{6+} yield gradually increased to a final yield and remained constant at longer residence times, while in the case of the plug-flow reactor (Figure 2.1 (b)) a pronounced maximum in the yield was observed as a function of contact time. As reactants are homogeneously distributed in the CSTR, all catalyst particles convert methanol under the same concentrations of methanol and intermediates, without establishing sequential reaction zones as in the PFR. In the latter case, the first layers of catalyst face a very high MeOH concentration, leading to a high coverage of BAS and a higher rate of methylation generating heavier olefins. Only at conversions above 80%, the rate along this reaction pathway started to decrease, because under such conditions the lower methanol concentration in the final layers of the catalytic bed would allow C_{6+} aliphatics to crack to lower hydrocarbons at BAS. In contrast, in the back-mixed reactor, all catalyst particles were exposed to a methanol pressure which was significantly lower than the values in the initial zone of the plug-flow reactor. Depending on the methanol conversion, BAS were available for C_{6+} aliphatics to adsorb and to crack to lower hydrocarbons. A steady state between olefin methylation and olefin cracking was established, leading to the observed product distribution.
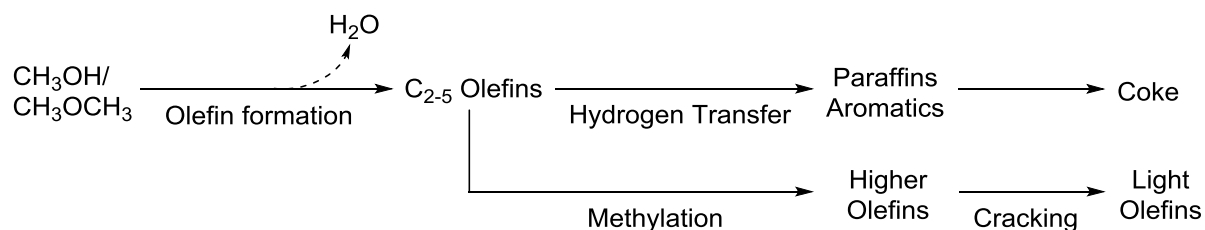
Scheme 2.1. Simplified MTO reaction pathway [36, 37].
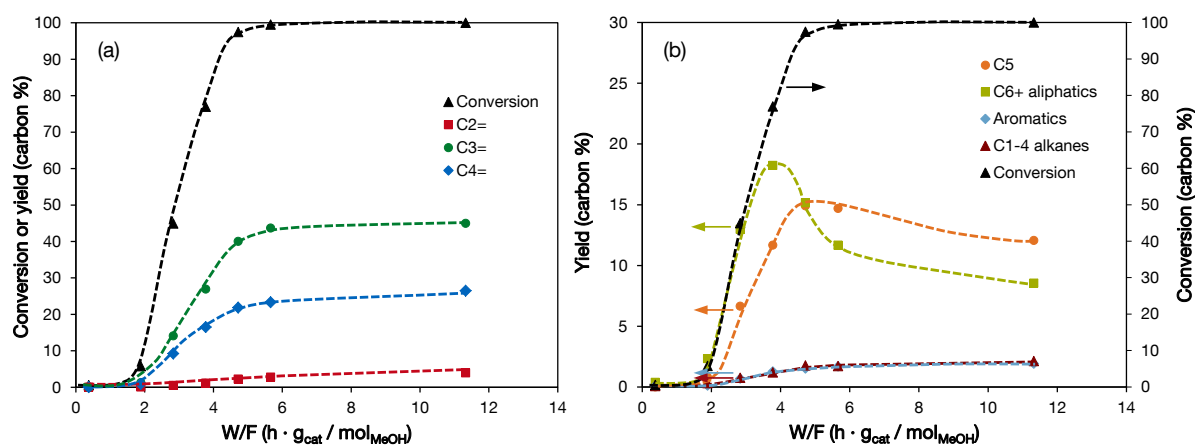
Figure 2.1. Conversion and product yields in PFR as a function of contact time on H-ZSM-5-S at p_{MeOH} = 178 mbar and 723 K: MeOH/DME conversion, $C_2^=$, $C_3^=$ and $C_4^=$ yield (a); and MeOH/DME conversion, C_5, C_{6+}, aromatics and C_{1-4} paraffins yield (b).
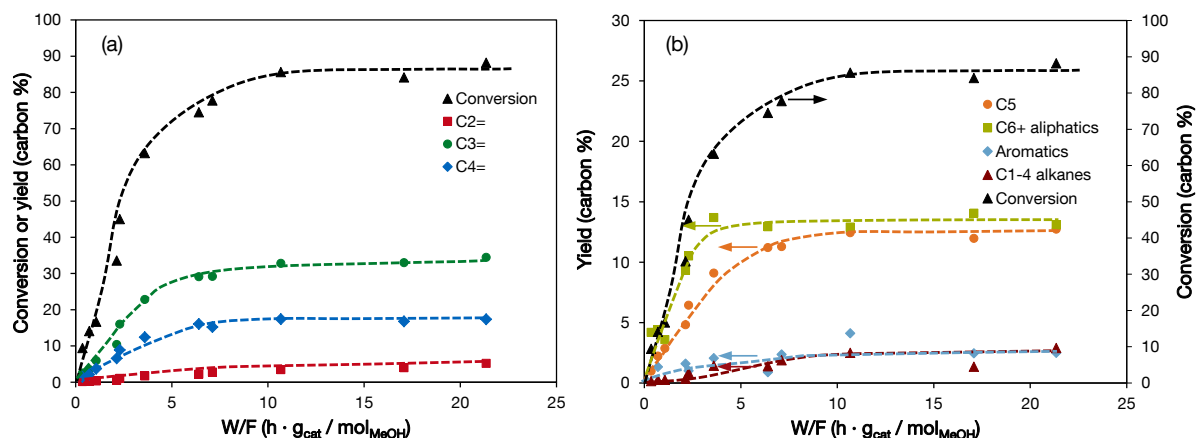
Figure 2.2. Conversion and product yields in CSTR as a function of contact time on H-ZSM-5-S at p_{MeOH} = 178 mbar and 723 K: MeOH/DME conversion, $C_2^=$, $C_3^=$ and $C_4^=$ yield (a); and MeOH/DME conversion, C_5, C_{6+}, aromatics and C_{1-4} paraffins yield (b).

Conversion and product selectivities as a function of contact time are presented for both reactors in Figure 2.3 and Figure 2.4.

Interestingly, high methane selectivity was observed at very short contact time for the PFR in agreement with, for example, Ref. [42].
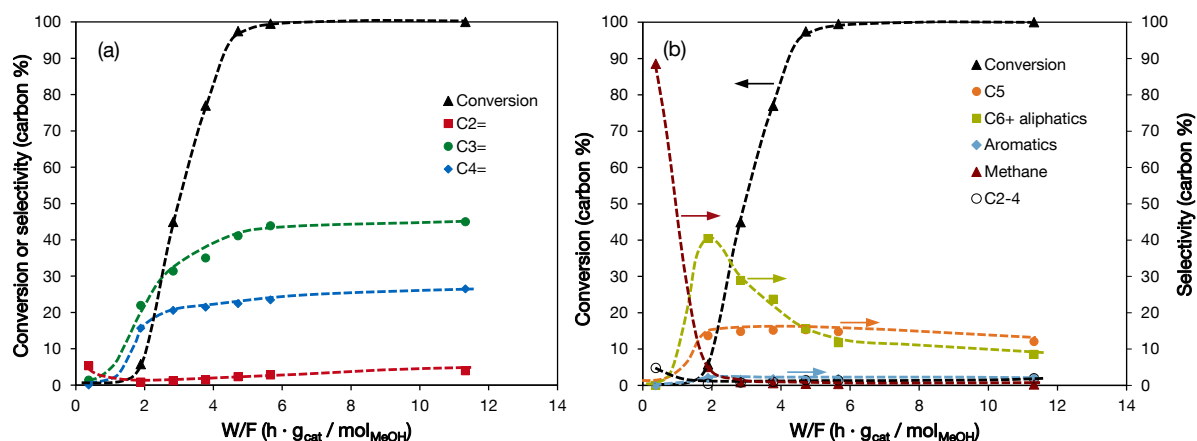
Figure 2.3. Conversion and product selectivities (in hydrocarbons) in PFR as a function of contact time on H-ZSM-5-S at p_{MeOH} = 178 mbar and 723 K: MeOH/DME conversion, $C_2^=$, $C_3^=$ and $C_4^=$ selectivity (a); and MeOH/DME conversion, C_5, C_{6+}, aromatics, methane and C_{2-4} paraffins selectivity (b).
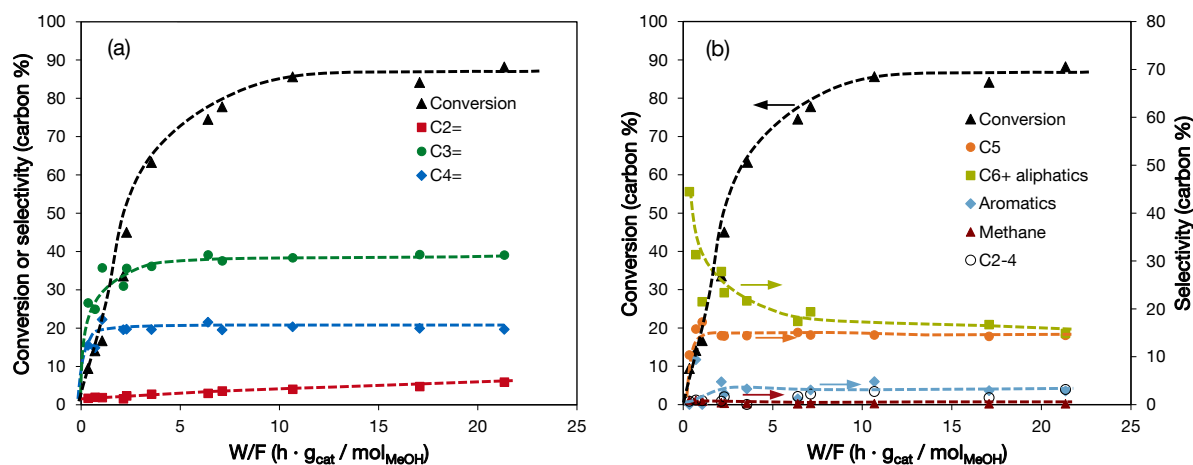
Figure 2.4. Conversion and product selectivities (in hydrocarbons) in CSTR as a function of contact time on H-ZSM-5-S at p_{MeOH} = 178 mbar and 723 K: MeOH/DME conversion, $C_2^=$, $C_3^=$ and $C_4^=$ selectivity (a); and MeOH/DME conversion, C_5, C_{6+}, aromatics, methane and C_{2-4} paraffins selectivity (b).

2.3.1.2   Deactivation of the catalyst

The time-dependent deactivation of H-ZSM-5 catalysts in the PFR and CSTR at 723 K is shown in Figure 2.5. Different catalyst amounts were used in the reactors (90 mg in PFR and 50 mg in CSTR) to ensure similar initial conversion levels and comparable contact times. In the PFR, the conversion dropped rapidly within the first 1.5 h of time on stream (TOS). Afterward, it decreased at a slightly slower rate with reaction time, but only ca. 10% of methanol was converted after 30 h on stream. In contrast, the conversion declined considerably slower in the CSTR. Between 0 h and 5 h TOS, the decrease in conversion was slightly more pronounced than at longer reaction times. But the catalyst was able to retain most of its activity for more than 90 h, leading to a final conversion of about 54%. The dramatically different deactivation behavior suggests contributions of different reaction pathways to deactivation and coke formation.

Under these reaction conditions and in good agreement with other published reports [43-46] deactivation of H-ZSM-5 did not affect the product selectivity for a given level of conversion. Hence, similar selectivities were observed at the same conversion levels, independent of the reactor type. Along the PFR reactor, marginal differences were observed in the yields of C_{6+} and propene and, to a lesser extent for ethylene and aromatics. It was found that ca. 3.3% more C_{6+} aliphatics and 2.6% less propene were formed in the plug-flow reactor

(see Figure 2.6) at a conversion of 56.5%. This suggests that more cracking of higher aliphatics to lower hydrocarbons and less methylation of propene occur in the CSTR.

The local differences in methanol concentration are identified as the apparent cause for the markedly different deactivation. The hypothesis is that the higher initial methanol concentration in the plug-flow reactor favors the formation of a catalyst poison, which in turn causes fast deactivation. In the CSTR, the local methanol concentration was insufficient to enhance the formation of such poisoning species and, therefore, a different and slower deactivation mechanism dominated.
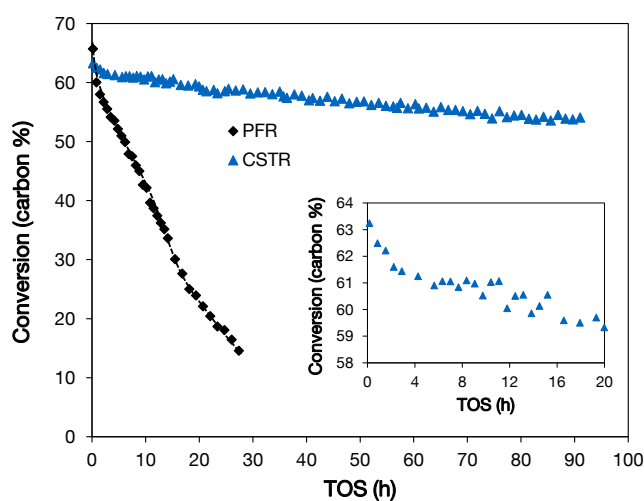
Figure 2.5. Methanol/DME conversion during MTO reaction of 90 mg catalyst H-ZSM-5-S in the PFR at ambient pressure and 50 mg catalyst H-ZSM-5-S in the CSTR at 6.5 bar, T = 723 K and p_{MeOH} = 178 mbar (enlargement of the conversion change in the CSTR from 0 h to 20 h).
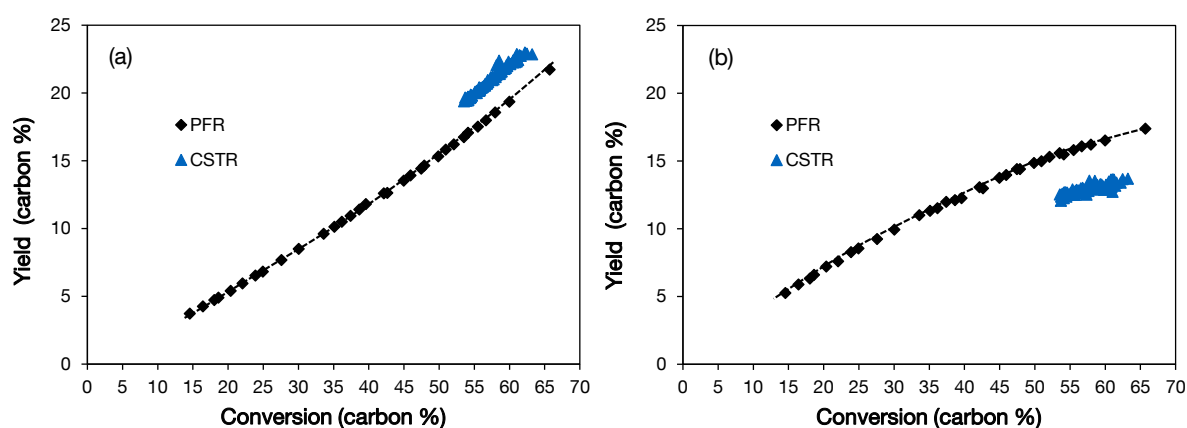
Figure 2.6. Propene yield (a) and C_{6+} aliphatics yield (b) during MTO reaction of 90 mg catalyst H-ZSM-5-S in the PFR at ambient pressure and 50 mg catalyst H-ZSM-5-S in the CSTR at 6.5 bar, T = 723 K and p_{MeOH} = 178 mbar.

2.3.1.3   Reaction order of deactivation

It has been noted above that high local methanol concentrations led to fast deactivation of H-ZSM-5. The specific nature of this fast poisoning is unknown at present and should be subject to further studies. The use of the CSTR allowed, however, translating the different zones in the PFR to different time regimes across the total catalyst mass. Thus, the deactivation kinetics was experimentally derived from data collected in the CSTR.

Figure 2.7 exhibits the change of conversion with reaction time for different contact times. As the products are immediately back-mixed in the CSTR, a high conversion corresponds to a low local methanol concentration. The conversion decreased faster with higher flow rate (that is, lower contact time), indicating a dependence of deactivation on the methanol partial pressure. An initial faster deactivation occurred in the first 5-h TOS. For longer TOS, a slower, but constant deactivation rate was observed. Therefore, two different kinetic regimes were taken into account, that is, one dominating from 0 to 5 h and the other from 5 to 23 h.

The observed change of reaction rate was fitted from 0 h to 5 h and from 5 h to 23 h, using Eq. (2.3), derived from Eq. (2.2).

$$\ln\left(\frac{-\Delta r}{\Delta t}\right) = \ln(k_d) + n \cdot \ln(\dot{n}_0(MeOH)) \tag{2.3}$$

The deactivation of the H-ZSM-5 catalyst was observed to have a reaction order (RO) of 1 for the TOS range 0-5 h and a RO of 1.7 for the TOS range 5-23 h (see Figure 2.8), that is, the deactivation rate is more sensitive to MeOH partial pressure in the slower deactivation regime.
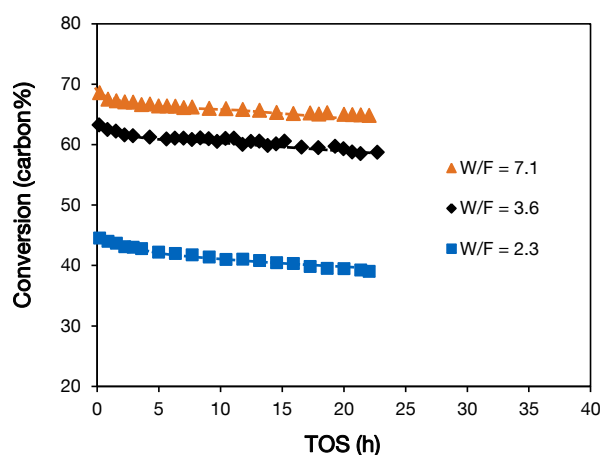
Figure 2.7. Decrease in conversion with contact times W / F (h · g_{cat} / mol_{MeOH}) = 2.3, 3.6 and 7.1 (varying feed rate).
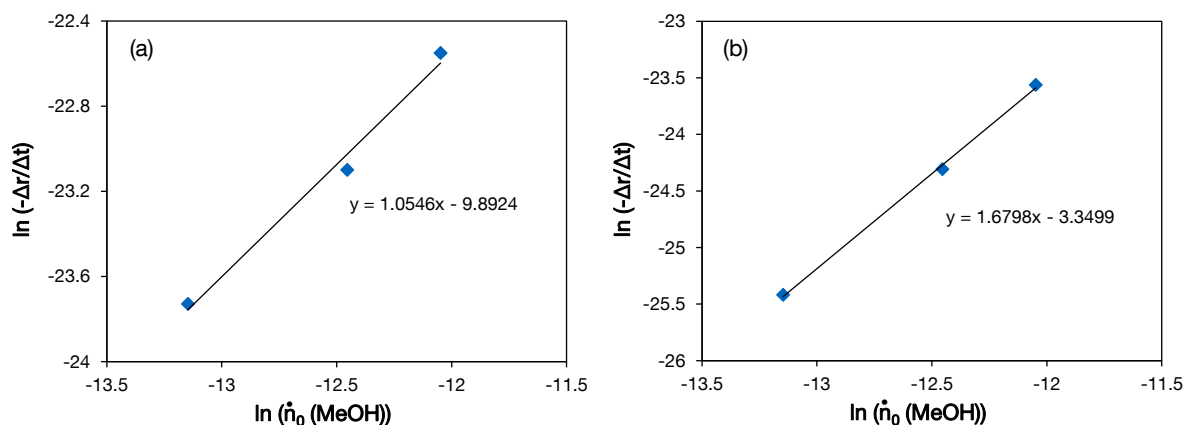
Figure 2.8. Determination of deactivation reaction order from 0-5 h (a) and 5-23 h (b) for MeOH feed rates of 0.007 mol/h, 0.014 mol/h and 0.021 mol/h.

2.3.2 Characterization of homogeneously deactivated samples

2.3.2.1 EPR spectroscopy of carbonaceous deposits

As aromatics form radical cations by protonation over acid sites of the zeolite [47-49], EPR spectroscopy was used to monitor the concentration of carbonaceous deposits. The same H-ZSM-5 catalyst was used in the MTP reaction at 723, 748 and 773 K for 5 h, 15 h, 22 h, 47 h, 78 h and 92 h. The spent catalysts were then analyzed by EPR spectroscopy. The spectra are shown in Figures 2.9, 2.10 and 2.11.
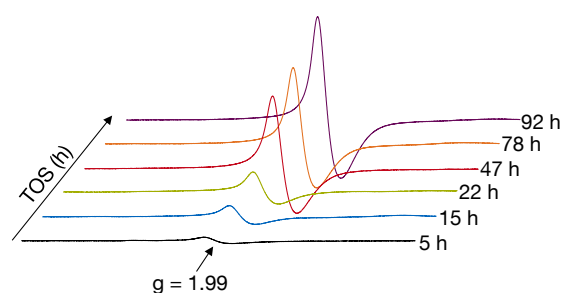
Figure 2.9. EPR spectra of samples deactivated at 723 K in a CSTR.
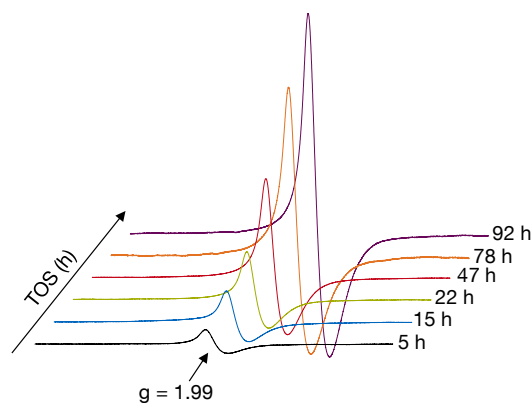
Figure 2.10. EPR spectra of samples deactivated at 748 K in a CSTR.
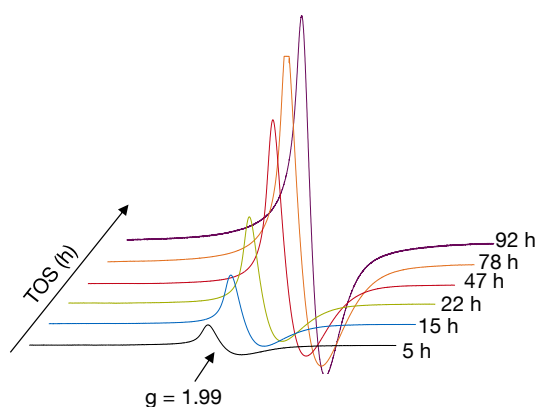
Figure 2.11. EPR spectra of samples deactivated at 773 K in a CSTR.

All samples exhibited one signal with a g-value of 1.991 ± 0.001. The EPR signals did not show hyperfine splitting because of high spin-spin interaction of the large variety of aromatic hydrocarbons in the sample used for reaction [49]. The spin density as a function of reaction time is displayed in Figure 2.12 for reactions at 723 K, 748 K and 773 K. It increased steadily at all temperatures. At the same TOS, the density of radicals was higher for higher temperatures, indicating a higher concentration of aromatic molecules at the surface. It is important to note that for all reaction temperatures the formation of carbonaceous deposits was faster in the first 5 h of reaction as deduced from the radical formation rates measured at short TOS.
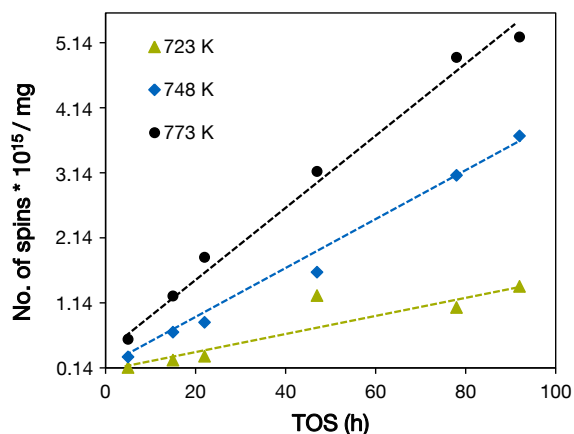
Figure 2.12. Density of radicals (spins) formed during methanol conversion over H-ZSM-5-S at 723 K, 748 K and 773 K as a function of reaction time.

By applying the analysis method adopted from Van Speybroeck et al. [50], the activation energy of this carbonaceous species was deduced from the change of spin density at reaction temperatures of 723, 748 and 773 K.

$$\ln (\text{No. of spins } [92\,h] - \text{No. of spins}) = \ln (\text{No. of spins } [92\,h]) - kt \qquad (2.4)$$

In this way, the rate constants of radical formation associated to the presence of methylated polyaromatic molecules were calculated (Figure 2.13). By plotting ln(k) as a function of 1/T (Figure 2.14), the apparent activation energy of coke formation derived from the Arrhenius relation was 85 kJ/mol.
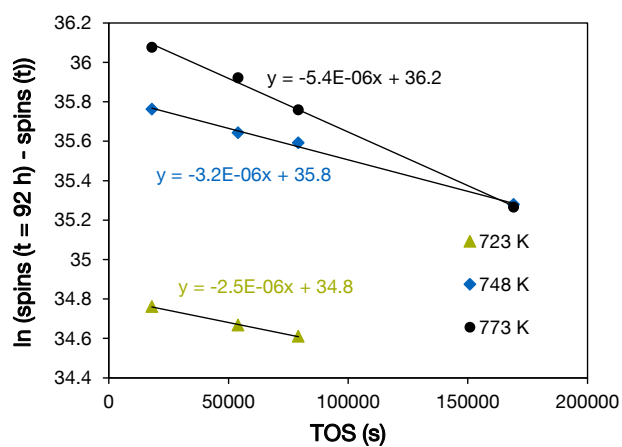
Figure 2.13. Determination of the rate constants of radical formation at 723 K, 748 K and 773 K.
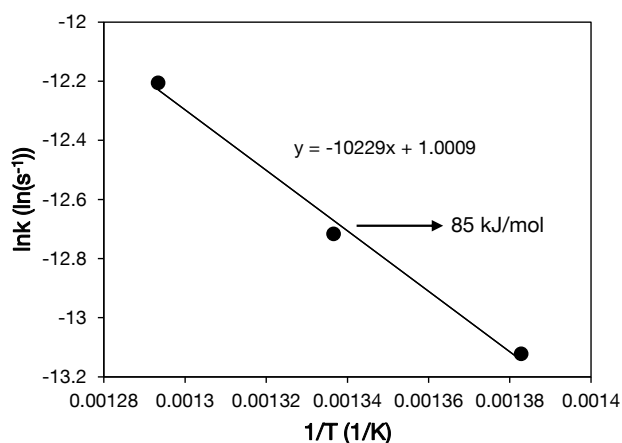
Figure 2.14. Arrhenius plot derived from the temporal evolution of the spin density at temperatures of 723 K, 748 K and 773 K.

2.3.2.2   Thermogravimetric analysis (TGA)

The coke deposits on samples reacted at 723, 748 and 773 K were analyzed by temperature-programmed oxidation. Figure 2.15 shows the linear increase of the overall amount of carbonaceous deposits with reaction time and temperature. These molecules are named here for simplicity "coke", although the composition of these deposits varies substantially and is far from graphitic carbon. Within the first five hours of reaction, ~0.4 wt.% coke was deposited at 723 K, ~0.6 wt.% at 748 K and 0.9 wt.% at 773 K. This corresponds to coke formation rates of 0.08 wt.% coke/h, 0.12 wt.% coke/h and 0.18 wt.% coke/h. The rate of coke deposition was significantly slower for longer reaction time and had a higher temperature dependence than in the initial hours on stream. From 5-h to 92-h TOS, the rate of coke formation was 0.02 wt.% coke/h for 723 K, 0.04 wt.% coke/h for 748 K and 0.07 wt.% coke/h for 773 K. This suggests that two regimes of coke formation exist during deactivation: an initial fast coke deposition pathway, followed by a slower coke formation mechanism.

For all temperatures, a linear correlation between the concentration of coke deposited as quantified by TGA and the Number of spins was found (Figure 2.16). Hence, the EPR results can be regarded as representative for the formation of most of the carbonaceous deposits that are formed beyond five-hours TOS.
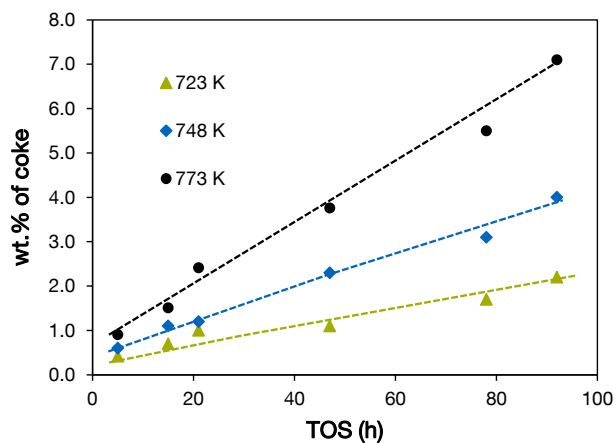
Figure 2.15. Coke deposition during methanol conversion over H-ZSM-5-S as a function of reaction temperature.
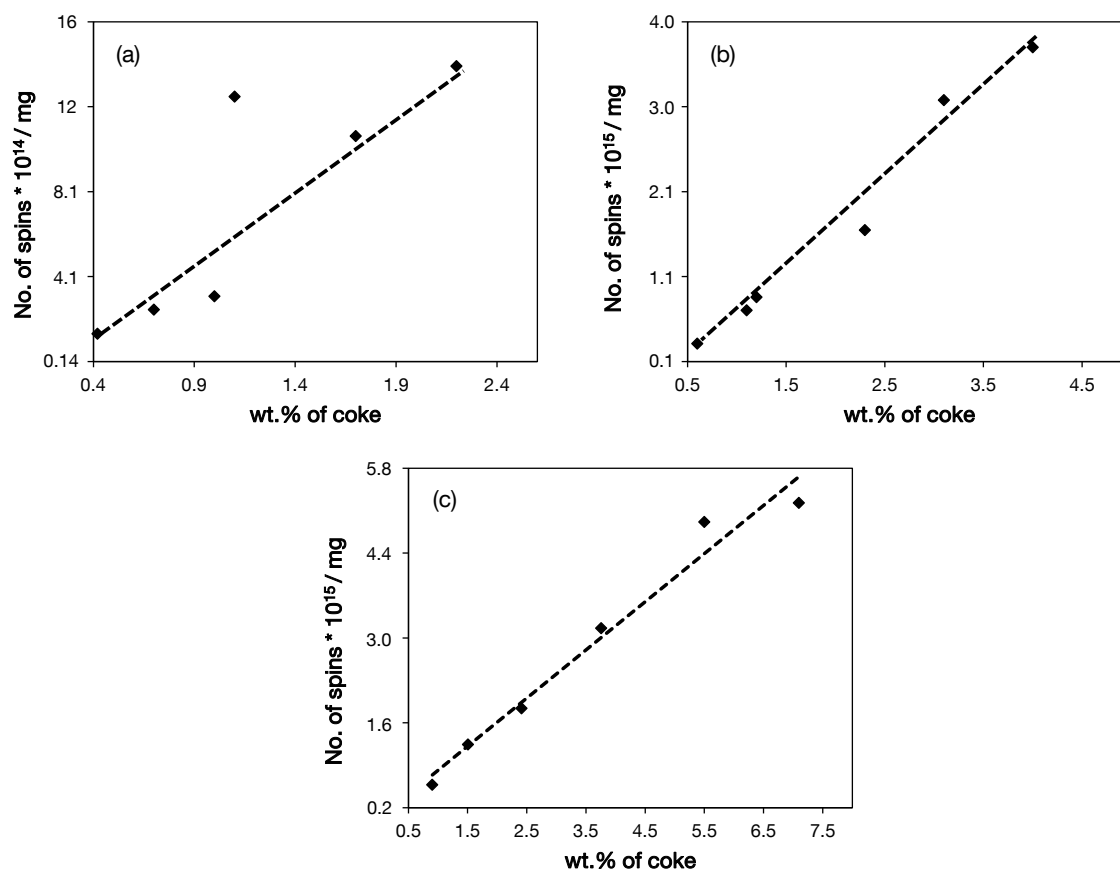
Figure 2.16. Correlation between the spin density and the amount of coke deposited during MTO reaction over H-ZSM-5-S at 723 K (a), 748 K (b) and 773 K (c).

2.3.2.3   IR spectroscopy of adsorbed pyridine

IR spectra of adsorbed pyridine were used to determine the concentration of active sites that remained accessible in the used samples. In order to remove volatile species the samples were evacuated at 723 K for one hour, before determining the concentration of pyridine interacting with acid sites at 423 K. In Figure 2.17, the concentrations of Brønsted acid sites (BAS) and Lewis acid sites (LAS) are shown as a function of reaction time. With TOS, the concentration of BAS decreased while the concentration of LAS remained fairly constant. In contrast, the used samples after oxidatively removing carbon deposits had a constant concentration of BAS (Table 2.1).

Table 2.1. Concentration of Brønsted acid sites (BAS) and Lewis acid sites (LAS) of the samples H-ZSM-5-S and H-ZSM-5-S-5/H-ZSM-5-S-47 after regeneration (determined by IR spectroscopy of adsorbed pyridine).

Sample	BAS (μmol / g)	LAS (μmol / g)
H-ZSM-5-S	67 ± 3	34 ± 2
H-ZSM-5-S-5 after regeneration	60 ± 3	34 ± 2
H-ZSM-5-S-47 after regeneration	59 ± 3	30 ± 2

Thus, it is concluded that active BAS were increasingly covered by carbonaceous deposits with increasing TOS. Blocking of BAS by reaction intermediates has been ruled out, because the samples were first treated at 723-773 K in N_2 after reaction and later outgassed at 723 K in vacuum in the IR cell, which should remove all aromatic compounds with diameters below the pore-opening size for ZSM-5, because they are light enough to desorb in this interval. The characteristic OH band of BAS ($3610 \, \text{cm}^{-1}$) disappeared after pyridine adsorption, indicating that all free BAS were accessible for pyridine. Thus, it is concluded that the carbonaceous deposits at this level of deactivation hinder the access of pyridine to BAS. The integral intensities of these bands were used to quantify the concentrations of Brønsted acid sites, because integral intensities of Brønsted acidic OH groups linearly correlated with those of pyridinium ions (Figure 2.18).
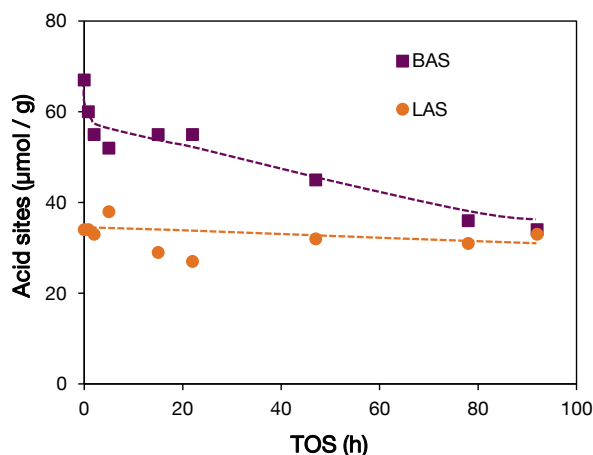
Figure 2.17. Change of the concentration of Brønsted acid sites (BAS) and Lewis acid sites (LAS) with TOS for a reaction temperature of 723 K.
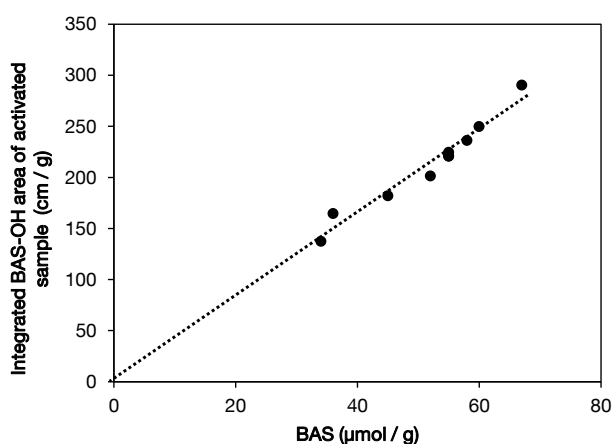
Figure 2.18. Correlation of integrated BAS-OH areas of activated samples (before pyridine adsorption) with BAS concentrations determined by pyridine adsorption.

2.3.2.4   LDI-TOF MS

LDI-TOF MS measurements were conducted to characterize the nature of carbonaceous compounds and discriminate between their locations on the zeolite. Figure 2.19 displays the mass spectra of the catalysts deactivated at 723 K. Information on the location of the carbon deposits was obtained by comparison of the two spectra, one recorded of the whole zeolite particles, and another one of the deposits freed by dissolving the zeolite in HF. While molecules detected after dissolving the catalysts by HF represent the composition of overall coke, the species detected without dissolving the zeolite are only due to deposits on the external surface of crystals that is accessible to LDI-TOF. Information on carbon deposition on the internal

inaccessible surface, that is those species present in the micropores and internal voids, can be gained by comparison of the LDI-TOF mass spectra of deactivated catalysts and free deposits.
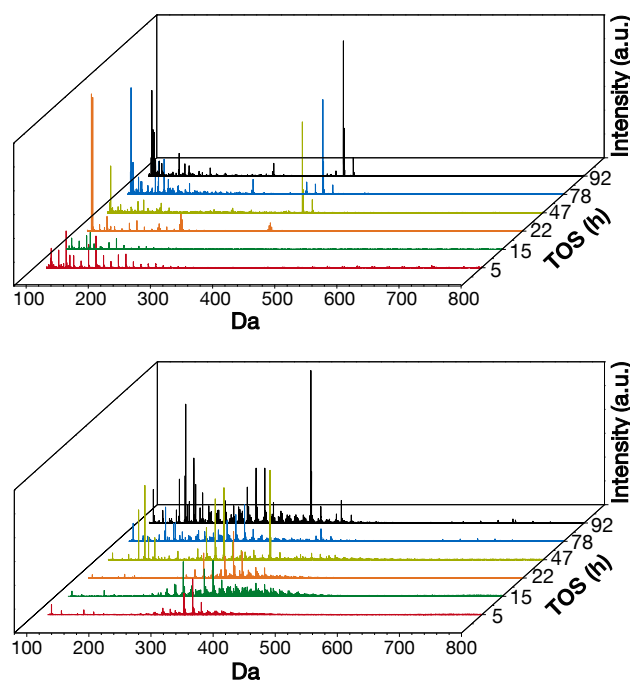
Figure 2.19. LDI-TOF mass spectra of deactivated catalysts (top) and of free deposits (bottom) after MTO reaction at 723 K.

From 5-h to 22-h TOS, coke was formed mainly within the zeolite particles and little is observed on the external surface. However, the main masses detected after HF dissolution were in the range 300-400 Da. Molecules with such size cannot be formed in the zeolite channels, which have an average diameter of 5.5 Å or in the channel intersections with a diameter of approximately 9 Å [51]. Thus, it is concluded that the first large carbonaceous deposits generated must be trapped in internal voids existing between primary zeolite single crystals domains, not exposed to the outer, externally optically accessible surface. These mesopores are speculated to be a minor fraction of the total mesopores. It is also observed that from 47- to 92-h TOS, the amount of carbonaceous deposits inside the zeolite crystals with masses in the range of 100-300 Da continuously increased. This indicates that the formation of small molecules retained in the micropores and channel intersections is still relevant at long time on stream under the conditions applied in the CSTR.

Interestingly, the LDI-TOF mass spectra of the whole catalyst particles, which represents solely the deposits on the externally optically accessible surface, had only mass signals between 100 and 300 Da at the early stages of reaction (5-h to 22-h TOS). Only with longer TOS (47-

92 h), heavier compounds with masses of 300-400 Da and compounds with masses of 401 Da, 413 Da and 429 Da were formed on the outer surface. The genesis of such external coke is exemplified in Scheme 2.2, where it is represented one of many possible specific routes for the growth of carbonaceous deposits.
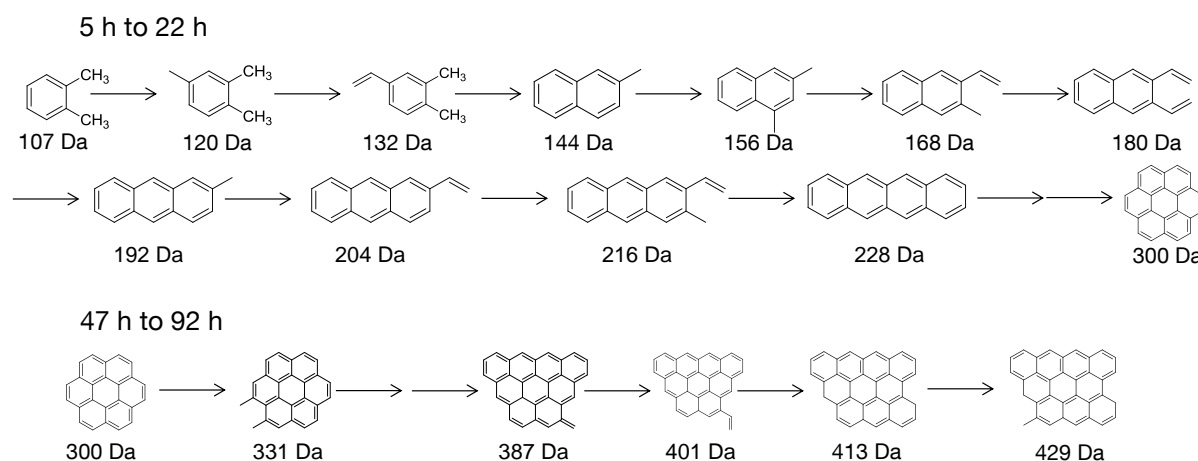
Scheme 2.2. Possible route of coke formation on the outer surface.

The mass distribution shows a pattern with mass differences of mainly 12 Da (extension of the aromatic ring system by one C atom) and, to a lesser extent, 14 Da (substitution of H by CH$_3$ group). Series of mass fragments with differences of 50 Da are not observed for the spent catalysts nor for the extracted coke after HF treatment. This is attributed to series of homologous, methylated, polycyclic aromatic compounds. Diels-Alder reactions are concluded not to play a significant role in the aromatics formation. The formation of coke deposited in the zeolite channels and optically inaccessible voids and surfaces proceeds in the time range 5- to 22-h TOS via a reaction pattern similar to the one for external coke formation, with mass differences of 12 Da and 14 Da (see examples of molecules in Schemes 2.3 and 2.4.).

5 h to 22 h

300 Da → 314 Da

306 Da → 320 Da → 334 Da → 348 Da → 370 Da → 395 Da

306 Da → 330 Da → 356 Da

348 Da → 360 Da → 376 Da → 389 Da → 401 Da
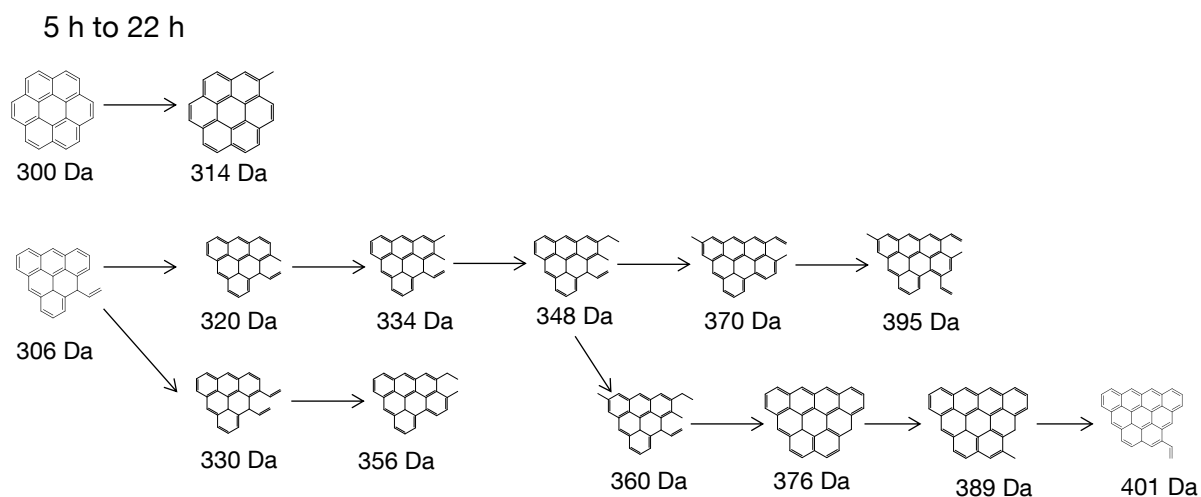
Scheme 2.3. Possible route for coke formation on the internal surface from 5 h to 22 h time on stream (only formation of main compounds is presented).

47 h to 92 h

109 Da → 122 Da → 159 Da → 175 Da

122 Da → 149 Da

109 Da → 130 Da → 155 Da → 169 Da → 183 Da → 197 Da

209 Da → 223 Da → 244 Da → 272 Da

223 Da → 250 Da

272 Da → 286 Da → 300 Da
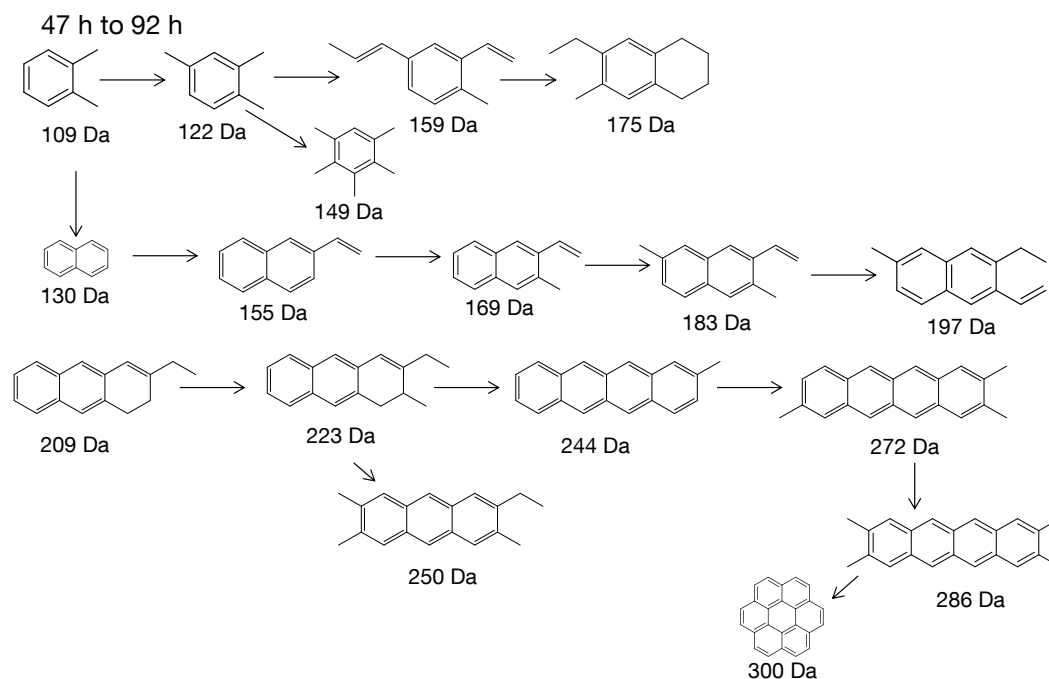
Scheme 2.4. Possible route for coke formation on the internal surface from 47 h to 92 h time on stream (only formation of main compounds is presented).

2.3.3 Temperature-programmed oxidation and elemental analysis of samples used in PFR and CSTR

The higher deactivation rate in the PFR - in comparison with the CSTR - points to different deactivation mechanisms in each reactor, as a result of the different methanol concentration

profiles. To explore whether this leads to differences in the nature of the coke, its combustion heat was determined after deactivation in a PFR and a CSTR. Figure 2.20 depicts the changes with conversion in coke combustion heat for PFR and CSTR samples.
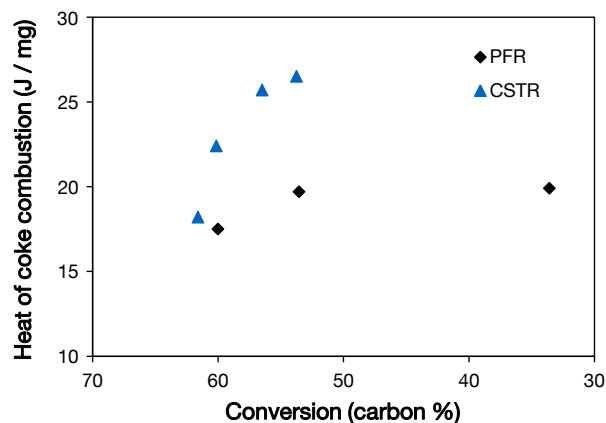
Figure 2.20. Change of coke combustion heat as a function of MeOH/DME conversion during MTO reaction on H-ZSM-5-S in the PFR and CSTR (T = 723 K and p_{MeOH} = 178 mbar).

The comparable combustion heat of the carbon deposited in the early stages of reaction indicates that in both reactors the carbonaceous species are similar. For longer TOS, the samples deactivated in the CSTR showed coke with higher combustion heat (~27 J/mg) than those deactivated in the PFR (~20 J/mg). The C/H/O ratios for the carbon deposits are calculated according to the quantification of consumed O_2 and generated products detected by MS together with coke weight from TGA. The overall composition of carbon deposits and the combustion heats for samples deactivated for different TOS are summarized in Table 2.2.

Table 2.2. Coke combustion heats and C/H/O ratios of carbonaceous deposits during MTO reaction on H-ZSM-5-S in the PFR and CSTR (T = 723 K and p_{MeOH} = 178 mbar).

Spent samples	Combustion heat (J / mg)	$C_xH_yO_z$
CSTR (2 h)	18 ± 2	$C_1H_{0.73\pm0.01}O_{0.09\pm0.04}$
CSTR (5 h)	20 ± 2	$C_1H_{0.75\pm0.01}O_{0.05\pm0.04}$
CSTR (15 h)	22 ± 2	$C_1H_{0.46\pm0.01}O_{0\pm0.03}$
CSTR (92 h)	27 ± 2	$C_1H_{0.31\pm0.01}O_{0\pm0.03}$
PFR (0.8 h)	18 ± 2	$C_1H_{1.32\pm0.01}O_{0.16\pm0.04}$
PFR (24 h)	20 ± 2	$C_1H_{0.70\pm0.01}O_{0.09\pm0.04}$

The DTG signals of zeolites used in PFR and CSTR (Figure 2.21 (a)) indicated two types of carbon deposits: type I at 500-660 K and type II at 660-900 K. The concentrations of the so-called coke-I and coke-II species were determined for several PFR and CSTR samples, and the values are depicted in Figure 2.21 (b) as a function of consumed methanol. Coke-I represents O-containing carbon deposits, which have a lower combustion temperature in TPO. The elemental analysis of carbon deposits only showed oxygen in the CSTR sample deactivated for 5-h TOS (Table 2.2). Above 0.1 mol_{MeOH} converted, coke-I was absent as judged by TPO and oxygen was not found in the carbon deposits. The degree of unsaturation increased with TOS, which is deduced from the lower hydrogen content and the increasing coke combustion heat. Thus, it is concluded that the average composition of coke-II corresponds to an aromatic hydrocarbon. For the PFR, O-containing species were still detected after 24-h TOS and the amount of coke-I was almost constant (Figure 2.21 (b)). The disappearance of O-containing carbonaceous species after a few hours TOS in the CSTR is attributed to its reaction with hydrocarbon products.
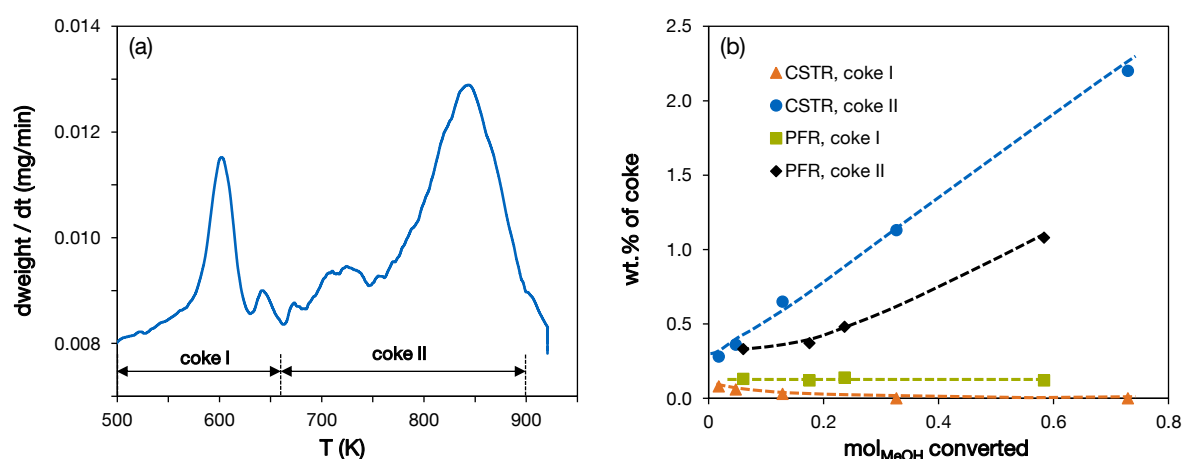
Figure 2.21. DTG curve of a PFR sample after 24 h TOS (W / F = 3.4 h · g $_{cat.}$ / mol$_{MeOH}$, 723 K, p$_{MeOH}$ = 178 mbar) (a); correlation of the amounts of coke-I and coke-II as in (a) with consumed MeOH for several PFR and CSTR spent catalysts (b).

2.4   Discussion

Coke on fully deactivated catalysts in MTO conversion has been commonly attributed to deposits consisting of large unsaturated (aromatic) hydrocarbons formed by hydride transfer and methylation [24]. This is indeed the type of carbon observed at late stages of deactivation in fixed-bed reactors, when this coke blocks pores and renders Brønsted acid sites inaccessible.

In such a configuration, the carbon deposited varies along the reactor, making it very challenging to identify its nature and location. It is unclear at which place in the zeolite crystal the carbonaceous deposits start to be formed [18, 21]. Models suggest deactivation starting from the inside (the micropores) to the outside (external surface) [21, 22] or coke formation at the surface blocking access to the domains of the crystal [13, 18-20]. Monitoring coke formation in a CSTR allows addressing this question more rigorously.

Because the overall rate of conversion decreased linearly with TOS (Figures 2.5 and 2.7), pore blocking is excluded as main reason for the activity decay. Carbonaceous species which block domains of the zeolite form only once higher concentrations of aromatic hydrocarbons are accumulated, but will then cause a fast decay in activity. The absence of large aromatic molecules on the external surface at short TOS (Figure 2.19, top) shows, therefore, that the observed initial deactivation is not related to blocking of crystal domains.

Quantification of acid sites in spent catalysts (Figure 2.17) showed a significantly higher decrease in the concentration of BAS in comparison with the decrease in the concentration of LAS. The specificity to cover BAS argues additionally against blocking of domains, which would be non-discriminating between hindering access to Brønsted or Lewis acid sites. The minor decrease in micropore volume after 92-h TOS (Table 2.3) suggests that the majority of the pores is accessible, while the zeolite deactivates.

Table 2.3. Micropore volume of fresh and 92 h deactivated sample (T = 723 K), determined by nitrogen physisorption.

Sample	Micropore volume (cm^3 / g)
H-ZSM-5-S	0.17
H-ZSM-5-S-92	0.16

Removal of Brønsted acid sites by dealumination during the reaction is ruled out, because the deactivated material can be largely restored to its original activity by combustion of the carbon deposits. Thus, it is concluded that the first steps in deactivation of ZSM-5 are caused by blocking of active sites within the micropores. This is further supported by the excellent correlation between the concentration of inaccessible BAS in spent catalysts and the coke weight for TOS >5 h (Figure 2.22).
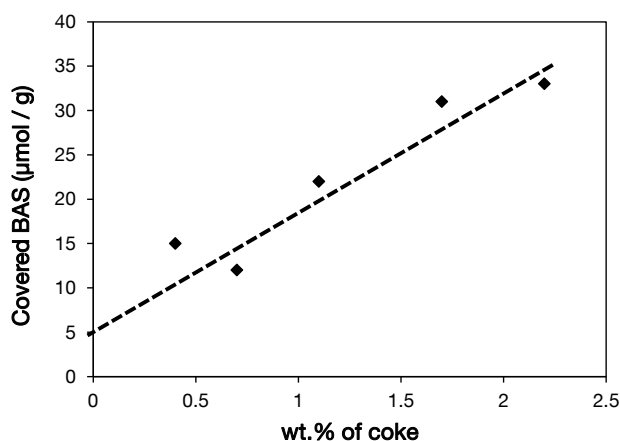
Figure 2.22. Correlation of occupied BAS with the carbon deposition at 723 K.

The analysis of carbon deposits together with the deactivation curves enabled to identify two different types of coke species responsible for such site blocking. Coke-I was formed only in significant concentrations at early stages of reaction (TOS <5 h) in the CSTR, when the catalyst was in contact with high methanol concentrations. It was able to efficiently (a lower concentration of C per BAS is needed) and rapidly deactivate H-ZSM-5 by binding to BAS. This process showed low temperature dependence (Figure 2.15). Because of the high concentration of oxygen in coke-I, its formation is hypothesized to occur via a reaction sequence illustrated in Scheme 2.5 (a) and (b). The first step involves reaction of methoxy groups with CO, which is present during MTO conversion, as communicated previously [52, 53]. In the next steps, the acetyl species reacts with formaldehyde to an α,β-unsaturated species (Scheme 2.5 (a)). Formaldehyde is proposed to form together with methane via a mechanism involving methanol as a hydride donor [42].

Reaction of formaldehyde with the α,β-unsaturated species, followed by ring closure and dehydration, leads to the formation of a furan species localized at BAS (Scheme 2.5 (b)). It should be emphasized that all species within the reaction sequence to furan formation can cause deactivation by strong adsorption on BAS.
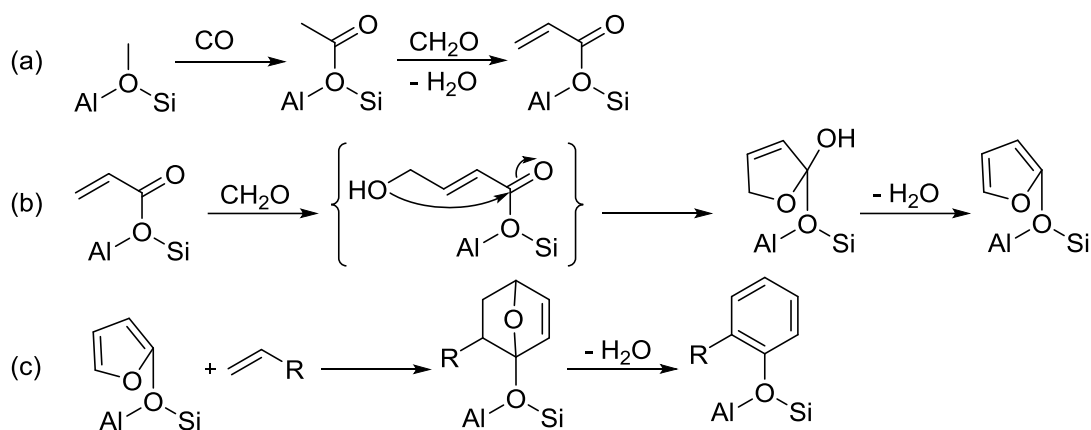
Scheme 2.5. Proposed mechanistic pathway for the formation of O-containing coke (a, b). Reaction of furan with olefins to localized aromatics (c).
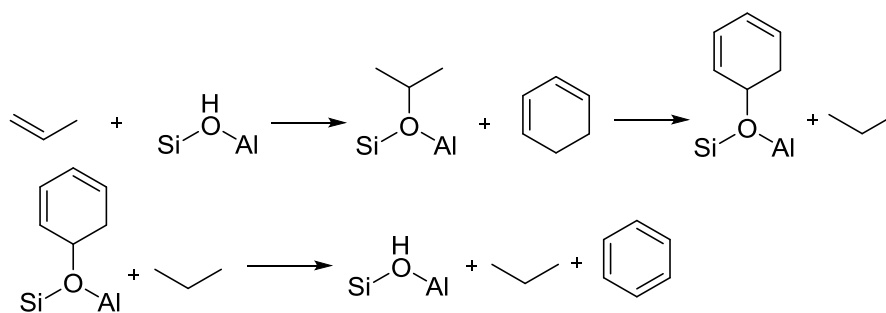
Scheme 2.6. Hydrogen transfer pathway between two olefinic species on BAS, exemplified for propene and 1,3-hexadiene.

For longer residence times (TOS >5 h), the concentration of coke-I became negligible, but overall, the carbon concentration determined by TGA correlated perfectly with the concentrations of spins (determined by EPR spectroscopy), and the concentration of BAS inaccessible for pyridine. It is therefore concluded that for TOS >5 h, deactivation is caused by coke-II. However, this deactivation is, on a carbon basis, less efficient than the deactivation by coke-I, leading to a lower deactivation rate.

The disappearance of coke-I after a few hours on stream is attributed to the reaction of furan with back-mixed olefins to form aromatics (Scheme 2.5 (c)) [54]. In such reaction, the aromatization is completed by release of one water molecule and not by transfer of a proton from the substrate to the BAS, as it occurs when aromatics are formed via typical hydrogen transfer between two olefins [7, 55, 56] (Scheme 2.6). Therefore, the release of the aromatic molecule and restoration of the BAS are not expected in the reaction shown in Scheme 2.5 (c). On the contrary, the aromatic species originated from furan remains strongly chemisorbed at BAS causing site blocking. It should be noted that such strongly chemisorbed aromatic species

are quantified and detected as coke-II by TGA and TPO analysis, and it is not possible to differentiate them from other aromatic deposits with weaker interaction with the zeolite, as it will be discussed below.

This deactivation by site blocking contrasts the description of deactivation of H-ZSM-5 reported previously, for which pore blocking by coke was identified as cause for the loss of activity [23, 24, 57]. The discrepancy may be related to the fact that these studies were performed under different reaction conditions (lower reaction temperatures and/or initial full conversion). Time on stream studies with initial full conversion start from conditions in which the early formation of compounds incorporating methanol is eclipsed by the secondary reactions of forming and cleaving C-C bonds and redistributing hydrogen between reacting molecules, that is, when the network of reactions is fully developed. Under these conditions, substantial concentrations of coke are formed at the outside of the polycrystalline zeolite particles. This masks the deactivation by localized and largely immobilized aromatic molecules at Brønsted acid sites.

It has been shown that coke-II deposits include aromatics originated via the two pathways displayed in Scheme 2.5 (c) and Scheme 2.6. Next, it is necessary to analyze their location and evolution with TOS. By LDI-TOF mass spectrometry it was shown that aromatic molecules larger than the pore diameter of H-ZSM-5 are trapped within the crystals. The formation of such large hydrocarbons occurs at early stages of the reaction in the CSTR, that is, in parallel with the formation of O-containing carbon deposits (coke-I). It is concluded that these molecules are located in voids between crystal domains, which are connected to the outside gas phase only via micropores, that is, their volume is not accounted by analysis of the N_2 adsorption/desorption isotherms. The aromatic carbonaceous deposits located in these voids can hardly block acid sites and therefore it is proposed that their impact in deactivation is negligible. Nevertheless, they account for an important part of the coke-II weight detected by TGA.

The differences in mass signals in LDI-TOF MS of 12 and 14 Da and the first-order reaction in methanol with respect to carbon deposition suggest that the growth of the aromatic species at TOS <5 h proceeds by methylation. Methanol is hypothesized to react with (polynuclear) aromatics via consecutive (Scheme 2.7 (i)) or concerted mechanisms (Scheme 2.7 (ii)) [58]. The present measurements do not differentiate whether the reactions occur via methoxy groups/methyl carbenium ions or methoxonium ions [58-60].

(i)   (ii)
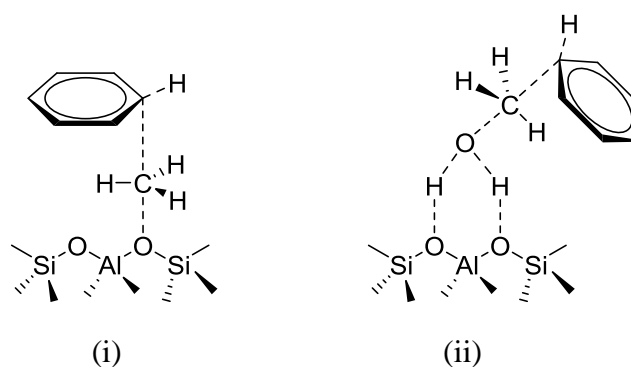
Scheme 2.7. Possible mechanisms for methylation of aromatics in the MTO reaction, exemplified with benzene: (i) Transition structure for addition of a methoxy group to benzene, that is, consecutive mechanism; (ii) transition structure for direct methylation, that is, via a coadsorption mechanism [58].

The apparent activation energy of coke-II growth between 5- and 92-h TOS was 85 kJ/mol, that is, in the range of apparent activation energies for aromatics methylation [50, 59, 61]. The buildup of molecules with higher molecular weight with time on stream is, therefore, concluded to involve the methylation of aromatic molecules as primary growth mechanism. This differs from coke accumulation in fluid catalytic cracking catalysts for which Diels-Alder type reactions have been identified as the dominating coke growth mechanism [33, 62]. The higher reaction order of 1.7 in methanol under these conditions indicates a more complex mechanism for the formation of these higher aromatics.

Having established the differences in nature and deactivating effectivity of the coke, the reasons for the very different rates of deactivation in PFR and CSTR under comparable conditions are addressed. When the stability of H-ZSM-5 was studied under MTO reaction conditions and identical initial conversions, the rate of activity decrease was significantly slower in the CSTR compared to the PFR. At first, one may argue that such a decrease in activity is due to the intrinsic characteristic response to contact time changes of the two reactors. In other words, that the slope of MeOH conversion with contact time is much steeper for the PFR than for the CSTR (Figures 2.1 and 2.2). However, if the degree of catalyst deactivation for each of the reactors is calculated based on the amount of molecules converted at a given TOS (by using the contact time curves in Figures 2.1 and 2.2), approximately 18% of the catalytic sites were deactivated in the PFR after 9 h, while only 2% were deactivated in the CSTR (Figure 2.23).
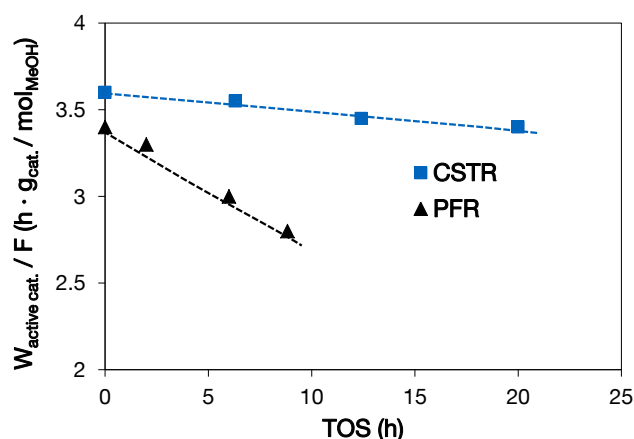
Figure 2.23. Reduction of effective contact time in CSTR and PFR by deactivation.

It is hypothesized that the differences in deactivation are associated with the different local methanol concentrations, which in turn induce different deactivation pathways. Both the local concentration of methanol and the simultaneous presence of reaction products and intermediates play a decisive role in the formation and accumulation of the highly deactivating carbon deposits. A high local concentration of methanol enables reaction pathways that are kinetically disfavored at lower MeOH partial pressures, such as the formation of oxygen-containing coke-I, which requires the presence of formaldehyde and CO. Coke-I is subsequently converted into strongly adsorbed aromatics by reaction with olefins (see Scheme 2.5).

In the CSTR, all catalyst particles face the same concentration of methanol and reaction intermediates. The localized formation of oxygenates upon contact of methanol with the fresh catalyst is concluded to cause the initial rapid deactivation (coke-I observed only at TOS <5 h). As the CSTR quickly reaches the steady state, the rate of deactivation decreased remarkably, because the multiple reactions involving back-mixed intermediates and products compete with the formation of further amounts of coke-I. Under these conditions, reactions of and between olefins dominate [63], and the carbon deposits are expected to form via typical hydride transfer (Scheme 2.6) and grow via multiple methylations.

On the other hand, the methanol concentration at the inlet of the PFR is higher than in any point of the CSTR and will lead to the formation of significant amounts of oxygenates in the first layer of the catalyst bed. This coke-I in the first layer is converted with time on stream into aromatic molecules that remained strongly adsorbed on the deactivated sites, while new coke-I species are formed downstream, leading to a slow progression of the zone of oxygen-rich coke along the reactor. Because in the PFR the concentration of oxygenates remained approximately constant throughout the reaction, it is concluded that the rate of conversion of coke-I to coke-II molecules and the rate of formation of new coke-I are nearly identical. The progressing zone of

strong deactivation and the subsequent localized aromatic molecules are concluded to deactivate the zeolite gradually, leading to a decreasing length of the active zeolite bed in the PFR.

The initial conclusions on the importance of the concentration of methanol are quantitatively supported by the kinetics of coke formation followed by TGA and EPR spectroscopy. The deactivation rate was first order in methanol at short time on stream. This starkly contrasts the model proposed by Janssens [44], which suggests that the deactivation rate is proportional to the conversion. It should be noted that the Janssens' model agrees well when describing the deactivation after long periods of full methanol conversion in a PFR. The model deviated significantly, when high partial pressures of MeOH (or short contact times) were applied [64].

2.5   Conclusions

The study of coke formation under kinetically-relevant conditions in a CSTR has allowed deducing the mechanism of the first steps of the deactivation of ZSM-5 during conversion of methanol to olefins.

The comparison between deactivation of ZSM-5 in a CSTR and in a PFR under identical reaction conditions showed that high local methanol concentrations induce the formation of oxygen-containing carbon deposits. Such deposits deactivate very effectively (on a carbon basis) the active sites by localized sorption. Accordingly, the higher local methanol concentration in the first layers of the catalytic bed in a PFR induces the formation of a larger fraction of this oxygen-containing carbon species, causing a fast deactivation of the catalyst. The back-mixing of products in the CSTR in turn causes the local methanol concentration to be moderate in the whole reactor volume. In this case, other reaction pathways such as reactions between olefins and methylation of hydrocarbons are kinetically more favored, and the formation of oxygenates is suppressed. The formation of conventional aromatic coke is expected to take place mostly by hydride transfer between olefins, and carbon growth to occur via multiple methylations of such aromatic species. The latter point has been confirmed by the kinetic analysis of coke growth on a catalyst homogeneously deactivated in a CSTR. The positive reaction order in methanol and the apparent energy of activation obtained are consistent with an extension of the polyaromatic deposits by methylation.

In the fast deactivating PFR, the evolution of the coke species depends on the position of the catalyst particle in the catalytic bed. In the first stages (at short time on stream), a large fraction of oxygen-containing carbonaceous species is formed in the first layers of the catalytic bed. Since a remarkably higher deactivation rate was realized in the PFR-type reactor without a concomitant increase in oxygen-containing deposits, it is hypothesized at present that this is due not only to the high concentration of oxygenates strongly adsorbed on BAS, but also to the transformation with time on stream of part of the oxygen-containing species into more conventional coke (aromatic molecules) that remains attached to the BAS.

Site blocking has been identified as the main deactivation mechanism operating at early stages of the reaction, well before the blocking of the pores by large amounts of external surface carbon starts. In a first step, oxygen-containing species are formed by carbonylation of methoxy groups and block the active sites. This is followed by the reaction of the oxygenates with olefins to produce a strongly adsorbed aromatic molecule. It is believed that the findings exposed here are relevant for ZSM-5 catalysts during methanol conversion to olefins, because the span of reaction conditions in the CSTR explored will have their analogy at particular points of the catalytic bed in a PFR.

It should be emphasized that methanol concentration has been found to be relevant for the deactivation of catalysts in MTO conversion. In particular, the initial reactions generated oxygenate deposits which cause fast deactivation. Such oxygen-containing surface species have not been discussed so far and explain the widely varying rates of deactivations reported in the literature.

2.6   Acknowledgements

2.7   References

[1] C. Mei, P. Wen, Z. Liu, H. Liu, Y. Wang, W. Yang, Z. Xie, W. Hua, Z. Gao, J. Catal. 258 (2008) 243.

[2] A. Corma, J. Mengual, P.J. Miguel, Appl. Catal. A: Gen. 460–461 (2013) 106.

[3] J.Q. Chen, A. Bozzano, B. Glover, T. Fuglerud, S. Kvisle, Catal. Today 106 (2005) 103.

[4] M. Bjørgen, S. Akyalcin, U. Olsbye, S. Benard, S. Kolboe, S. Svelle, J. Catal. 275 (2010) 170.

[5] U. Olsbye, M. Bjørgen, S. Svelle, K.-P. Lillerud, S. Kolboe, Catal. Today 106 (2005) 108.

[6] F.L. Bleken, K. Barbera, F. Bonino, U. Olsbye, K.P. Lillerud, S. Bordiga, P. Beato, T.V.W. Janssens, S. Svelle, J. Catal. 307 (2013) 62.

[7] U. Olsbye, S. Svelle, M. Bjørgen, P. Beato, T.V.W. Janssens, F. Joensen, S. Bordiga, K.P. Lillerud, Angew. Chem. Int. Ed. 51 (2012) 5810.

[8] I.M. Hill, S.A. Hashimi, A. Bhan, J. Catal. 285 (2012) 115.

[9] S. Hu, Y. Gong, Q. Xu, X. Liu, Q. Zhang, L. Zhang, T. Dou, Catal. Commun. 28 (2012) 95.

[10] C.D. Chang, Catal. Rev.-Sci. Eng. 26 (1984) 323.

[11] C.D. Chang, C.T.W. Chu, R.F. Socha, J. Catal. 86 (1984) 289.

[12] D. Mores, J. Kornatowski, U. Olsbye, B.M. Weckhuysen, Chem. Eur. J. 17 (2011) 2874.

[13] D. Mores, E. Stavitski, M.H.F. Kox, J. Kornatowski, U. Olsbye, B.M. Weckhuysen, Chem. Eur. J. 14 (2008) 11320.

[14] M. Guisnet, P. Magnoux, Appl. Catal. 54 (1989) 1.

[15] M. Guisnet, P. Magnoux, Appl. Catal. A: Gen. 212 (2001) 83.

[16] F. Bleken, W. Skistad, K. Barbera, M. Kustova, S. Bordiga, P. Beato, K.P. Lillerud, S. Svelle, U. Olsbye, PCCP 13 (2011) 2539.

[17] J.W. Park, J.Y. Lee, K.S. Kim, S.B. Hong, G. Seo, Appl. Catal. A: Gen. 339 (2008) 36.

[18] P. Dejaifve, A. Auroux, P.C. Gravelle, J.C. Védrine, Z. Gabelica, E.G. Derouane, J. Catal. 70 (1981) 123.

[19] B.P.C. Hereijgers, F. Bleken, M.H. Nilsen, S. Svelle, K.-P. Lillerud, M. Bjørgen, B.M. Weckhuysen, U. Olsbye, J. Catal. 264 (2009) 77.

[20] Q. Qian, J. Ruiz-Martínez, M. Mokhtar, A.M. Asiri, S.A. Al-Thabaiti, S.N. Basahel, B.M. Weckhuysen, ChemCatChem 6 (2014) 772.

[21] B.A. Sexton, A.E. Hughes, D.M. Bibby, J. Catal. 109 (1988) 126.

[22] A.T. Aguayo, A.E.S.d. Campo, A.G. Gayubo, A. Tarrío, J. Bilbao, J. Chem. Technol. Biot. 74 (1999) 315.

[23] M. Bjørgen, S. Svelle, F. Joensen, J. Nerlov, S. Kolboe, F. Bonino, L. Palumbo, S. Bordiga, U. Olsbye, J. Catal. 249 (2007) 195.

[24] H. Schulz, Catal. Today 154 (2010) 183.

[25] J.F. Haw, W. Song, D.M. Marcus, J.B. Nicholas, Acc. Chem. Res. 36 (2003) 317.

[26] J. Liu, C. Zhang, Z. Shen, W. Hua, Y. Tang, W. Shen, Y. Yue, H. Xu, Catal. Commun. 10 (2009) 1506.

[27] Y. Yang, C. Sun, J. Du, Y. Yue, W. Hua, C. Zhang, W. Shen, H. Xu, Catal. Commun. 24 (2012) 44.

[28] N.-Y. Topsøe, K. Pedersen, E.G. Derouane, J. Catal. 70 (1981) 41.

[29] G.D. McLellan, R.F. Howe, L.M. Parker, D.M. Bibby, J. Catal. 99 (1986) 486.

[30] J.F. Haw, D.M. Marcus, Top. Catal. 34 (2005) 41.

[31] M. Kaarsholm, F. Joensen, J. Nerlov, R. Cenni, J. Chaouki, G.S. Patience, Chem. Eng. Sci. 62 (2007) 5527.

[32] L.H. Ong, M. Dömök, R. Olindo, A.C. van Veen, J.A. Lercher, Microporous Mesoporous Mater. 164 (2012) 9.

[33] H.S. Cerqueira, C. Sievers, G. Joly, P. Magnoux, J.A. Lercher, Ind. Eng. Chem. Res. 44 (2005) 2069.

[34] J.M. Berty, The recycle reactor concept, in: J.M. Berty (Ed.), Stud. Surf. Sci. Catal., Elsevier, Amsterdam, 1999, p. 53.

[35] H.J. Glatzer, L.K. Doraiswamy, Chem. Eng. Sci. 55 (2000) 5149.

[36] M. Stöcker, Microporous Mesoporous Mater. 29 (1999) 3.

[37] F.J. Keil, Microporous Mesoporous Mater. 29 (1999) 49.

[38] S. Svelle, F. Joensen, J. Nerlov, U. Olsbye, K.-P. Lillerud, S. Kolboe, M. Bjørgen, J. Am. Chem. Soc. 128 (2006) 14770.

[39] M. Bjørgen, F. Joensen, K.-P. Lillerud, U. Olsbye, S. Svelle, Catal. Today 142 (2009) 90.

[40] P. Dejaifve, J.C. Védrine, V. Bolis, E.G. Derouane, J. Catal. 63 (1980) 331.

[41] J. Hagen, Chemiereaktoren: Auslegung und Simulation, Wiley-VCH, Weinheim, 2004, p. 45.

[42] G.J. Hutchings, F. Gottschalk, R. Hunter, Ind. Eng. Chem. Res. 26 (1987) 635.

[43] F.L. Bleken, T.V.W. Janssens, S. Svelle, U. Olsbye, Microporous Mesoporous Mater. 164 (2012) 190.

[44] T.V.W. Janssens, J. Catal. 264 (2009) 130.

[45] J. Abbot, B.W. Wojciechowski, Can. J. Chem. Eng. 63 (1985) 451.

[46] D. Chen, H.P. Rebo, K. Moljord, A. Holmen, Ind. Eng. Chem. Res. 36 (1997) 3473.

[47] C.J. Rhodes, C.S. Hinds, Molec. Eng. 4 (1994) 119.

[48] M. Hunger, Microporous Mesoporous Mater. 82 (2005) 241.

[49] H.-G. Jang, H.-K. Min, S.B. Hong, G. Seo, J. Catal. 299 (2013) 240.

[50] V. Van Speybroeck, K. Hemelsoet, K. De Wispelaere, Q. Qian, J. Van der Mynsbrugge, B. De Sterck, B.M. Weckhuysen, M. Waroquier, ChemCatChem 5 (2013) 173.

[51] E.G. Derouane, J.C. Vedrine, J. Mol. Catal. 8 (1980) 479.

[52] M.W. Anderson, J. Klinowski, J. Am. Chem. Soc. 112 (1990) 10.

[53] E.J. Munson, A.A. Kheir, N.D. Lazo, J.F. Haw, J. Phys. Chem. 96 (1992) 7740.

[54] A. Zheng, Z. Zhao, S. Chang, Z. Huang, K. Zhao, H. Wu, X. Wang, F. He, H. Li, Green Chem. 16 (2014) 2580.

[55] S. Ilias, A. Bhan, J. Catal. 290 (2012) 186.

[56] S. Ilias, A. Bhan, ACS Catal. 3 (2013) 18.

[57] H. Schulz, M. Wei, Top. Catal. 57 (2014) 683.

[58] S. Svelle, M. Visur, U. Olsbye, Saepurahman, M. Bjørgen, Top. Catal. 54 (2011) 897.

[59] J. Van der Mynsbrugge, M. Visur, U. Olsbye, P. Beato, M. Bjørgen, V. Van Speybroeck, S. Svelle, J. Catal. 292 (2012) 201.

[60] Saepurahman, M. Visur, U. Olsbye, M. Bjørgen, S. Svelle, Top. Catal. 54 (2011) 1293.

[61] J. Ahn, PhD thesis, 2013, p.

[62] J.O. Barth, A. Jentys, J.A. Lercher, Ind. Eng. Chem. Res. 43 (2004) 2368.

[63] X. Sun, S. Mueller, Y. Liu, H. Shi, G.L. Haller, M. Sanchez-Sanchez, A.C. van Veen, J.A. Lercher, J. Catal. 317 (2014) 185.

[64] T.V.W. Janssens, S. Svelle, U. Olsbye, J. Catal. 308 (2013) 122.

Chapter 3

3. On understanding active sites and mechanism of hydrogen transfer during methanol-to-olefins conversion on H-ZSM-5

This chapter is based on:

S. Müller, Y. Liu, M. Sanchez-Sanchez, J.A. Lercher, "On understanding active sites and mechanism of hydrogen transfer during methanol-to-olefins conversion on H-ZSM-5", in preparation.

The underlying mechanisms of hydrogen transfer pathways during conversion of methanol to olefins (MTO) on H-ZSM-5 have been elucidated. A MeOH-mediated pathway has been identified as the major hydrogen transfer pathway leading to aromatics and paraffins formation. Addition of a low concentration of formaldehyde (1 C %) to the methanol feed resulted in enhanced C_{6+} aliphatics and aromatics formation at the expense of light olefins. Experiments over a pure Lewis acid sites (LAS)-MFI unequivocally showed that methanol and propene reacted on LAS to form formaldehyde and propane. The MeOH-related HT pathway was therefore linked to the reaction of olefins and methanol to paraffins and formaldehyde at LAS and the reaction of olefins with formaldehyde to aromatics and paraffins at Brønsted acid sites (BAS). Its importance depends on the available concentrations of BAS and LAS. In agreement with that, catalysts with a low LAS concentration produce less aromatics and paraffins. Conversely, varying BAS concentrations at a high Brønsted to Lewis acid sites ratio affected hydrogen transfer only marginally. At low BAS to LAS ratios, hydrogen transfer increased due to competitive adsorption of formaldehyde on BAS, suppressing olefin methylation and cracking reactions.

3.1   Introduction

Fuels and petrochemicals play an important role in the global energy supply [1, 2]. To bypass petroleum-based routes for the production of fuels and petrochemicals, methanol-to-hydrocarbons (MTH) processes over zeolites and zeotype materials are intensively investigated [2] because methanol can be produced via synthesis gas from carbon-based feedstocks such as natural gas, biomass or coal [1-4]. In the conversion of methanol to olefins (MTO), a successfully implemented variant of the MTH process, C_{2-5} olefins form from an equilibrium mixture of methanol and dimethyl ether. These olefins are further methylated to higher olefins which easily crack down to lower olefins. Olefins also react through secondary routes to undesired paraffins and aromatics via hydrogen transfer (HT) and subsequently form coke, causing catalyst deactivation [1, 4]. Therefore, understanding hydrogen transfer reaction pathways is highly important for the design of stable MTO catalysts.

Hydrogen transfer is commonly described as a bimolecular reaction with a hydrogen atom being transferred between one adsorbed surface alkoxide and one cyclic or acyclic alkane or alkene [1]. Branched alkanes and alkenes are more reactive hydrogen donors compared to linear alkanes and alkenes because the carbocationic transition states are more stable [1, 5-8]. Furthermore, the fact that under MTO conditions mainly olefins are formed leads one to assume that hydrogen transfer reactions taking place on H-ZSM-5 occur mostly between two olefinic species on BAS [1, 2, 9] via a mechanism as illustrated in Scheme 3.1 for the reaction of propene and 1-butene.
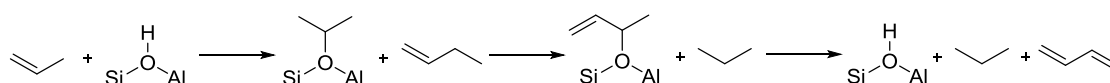
Scheme 3.1. Typical hydrogen transfer pathway between two olefinic species on BAS, exemplified for propene and 1-butene.

Insights into the mechanism and kinetics of hydrogen transfer are generally difficult to gain due to the requirements of isolating surface alkoxides on zeolites and the elimination of competing reactions such as alkylation, oligomerization and isomerization [1]. This problem was, however, overcome by conducting studies at low temperatures (~473 K) [1]. Simonetti et al. [10] investigated dimethyl ether homologation on H-BEA and measured the rates of alkene methylation, hydrogen transfer, isomerization and β-scission reactions, using mixtures of ^{13}C-labeled dimethyl ether and unlabeled alkenes. The presence of a hydride transfer co-catalyst, such as adamantane, during acid-catalyzed co-homologation of alkanes and dimethyl ether on

H-BEA provides the possibility of favoring the formation of higher value alkanes without simultaneous formation of arene side products [11]. Methanol homologation studies were also carried out on iodide based homogeneous catalysts [12-16]. Hazari et al. [16], for instance, probed the relative rates of olefin methylation to hydrogen transfer by co-feeding olefins with 1,4-cyclohexadiene. The cyclic diene was more effective in hydrogen transfer than the acyclic monoolefins.

Two possible routes for aromatics and paraffins formation from olefins must be considered in the methanol-to-olefins reaction network. One route involves dehydrogenation of olefins to form dienes and trienes which undergo cyclization to aromatics [1]. On the other hand, higher olefins can cyclize and subsequently form aromatics by hydrogen transfer, which is widely proposed to link the olefins cycle and the aromatics cycle in the so-called dual-cycle concept [2, 4, 17, 18]. In both cases, small olefins must act as hydrogen acceptors forming paraffins. Hydrogen transfer was reported to occur via sterically demanding bimolecular transition states and therefore reactions between two higher olefins should be strongly constrained in H-ZSM-5 [19]. In computational studies, olefin and diene cyclization on H-ZSM-5 through 1,5-cyclization and 1,6-cyclization pathways were investigated [20, 21]. The cyclization of physisorbed hexene to methylcyclopentane was reported to have a lower activation energy in comparison to diene cyclization [1, 20]. However, the ring expansion mechanism to cyclohexane was not studied and it is unclear if methylcyclopentane is a favorable precursor to benzene [1]. For 1,5-hexadiene, the pathway for 1,6-cyclization had a lower activation energy barrier in comparison to 1,5-cyclization [20, 21]. Thus 1,6-cyclization was concluded to occur for C_6 aliphatic precursors [21]. In a further computational study, Joshi and Thomson [22] investigated Brønsted acid-catalyzed cyclization of C_7 and C_8 dienes on H-ZSM-5 and found the activation energy barrier for cyclization of these compounds to be lower in comparison to that for C_6 diene cyclization. This was attributed by the authors to the increased stability of secondary carbenium ion transition states for C_7 or C_8 dienes over primary carbenium ion transition states for C_6 diene [22].

Lewis acid sites (LAS) in zeolites are mostly associated with extra-framework Al (EFAL) [23]. Despite detailed investigations, the nature of EFAL species is still not fully understood [23-27]. Two different modes for interaction of EFAL with BAS are mainly discussed in literature. Mirodatos proposed a direct interaction of EFAL with BAS by partial electron transfer from the OH bond (BAS) to the EFAL, which would lead to an increased acid strength [23, 28]. Conversely, in the proposal of Li et al., EFAL coordinates to an oxygen atom next to BAS, which causes an enhanced acidity [23]. Gounder et al. contradict this proposal and claim

that the rate enhancement observed is not due to an increment in acidity or due to the Lewis-acidic character of EFAL itself, but to the fact that it reduces void space in Faujasite (FAU) which results in stronger dispersive interactions [29]. In good agreement with that conclusion, Schallmoser et al. [27] located EFAL species in the direct vicinity of very active BAS by means of IR spectroscopy.

The suppression of the olefin-induced hydrogen transfer is thought to lead to higher yields of light olefins via cracking and to avoid deactivation by formation of polycondensed aromatics. Thus, several scientific studies have been devoted to understand whether the interaction of BAS and LAS plays a role in hydrogen transfer reactions of olefins over zeolite catalysts [30-33]. Bortnovsky et al. [30], for instance, observed the formation of bulky aromatics and paraffins in pentene cracking for catalysts with high concentrations of both BAS and LAS, accompanied by coke deposition. They further reported that high concentrations of strongly acidic sites favored hydrogen transfer [30]. Wichterlová et al. [31] reported that the presence of LAS in zeolites enhances Brønsted acid-catalyzed hydrogen transfer reactions and changes the product distribution in *n*-butene isomerization substantially. They proposed an intrinsic catalytic function of Lewis acid sites in *n*-butene transformation besides the possible enhancement of the strength of BAS of the zeolite [31]. Sazami et al. concluded that Al-related electron acceptor sites in H-ZSM-5 favor oligomerization and hydrogen transfer reactions in MTH conversion leading to coke formation [32, 33]. Despite this experimental evidence on the role of LAS in aromatics formation, there is no clear mechanistic explanation or description of such phenomenon in the literature.

Recently, another hydrogen transfer pathway has been identified in MTO conversion that involves directly methanol or C_1 intermediates formed from it [17]. Such pathway generates C_{1-4} paraffins and aromatics at significantly higher rate in the presence of methanol than the hydrogen transfer route between two olefinic species when only olefins are in the system (Figure 3.1, [17]). It is important to note that for this comparison a mixed methanol/olefin feed, instead of a pure methanol feed, was used to overcome the initiation phase, thereby enabling a direct comparison of hydrogen transfer rates. Upon reaching full conversion, the predominant products are C_{3-5} olefins. Therefore, a further increase of contact time under total conversion of methanol only increases the contribution of secondary reactions among olefins to the total product distribution. Thus, the slight increase in HT products yield with contact time observed under total conversion runs parallel to the increase of HT products observed for a pure olefin feed, indicating that at this point the only route for HT is the reaction between two olefinic species. The overall HT products yield comprises, however, the contribution of the methanol-

induced hydrogen transfer (MIHT) in the first part of the catalytic bed and the olefin-induced HT pathway (OIHT) in the second zone of the catalyst bed.
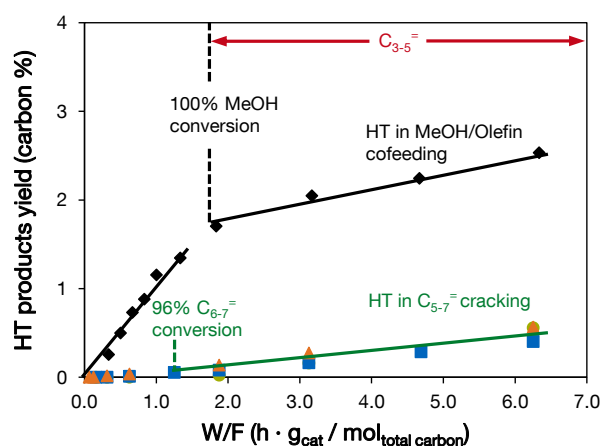
Figure 3.1. HT products yield as a function of contact time for the mixed feeds containing methanol (100 carbon %) and 1-pentene, 1-hexene and 1-heptene (20 carbon %) and for pure olefin feeds (120 carbon %) [17].

Thus, the individual role of BAS and LAS in the HT pathways existing under methanol conversion to olefins on H-ZSM-5 is explored in this contribution. The selective variation of the concentration of LAS independently from the concentration of BAS, and vice versa, allows understanding the individual contributions of each type of site to the reaction mechanism. Furthermore, the evolution of the product distribution, in particular of the hydrogen transfer products, is examined under the presence of some proposed MTO reaction intermediates such as formaldehyde. On the basis of these results, a mechanism for the MIHT is proposed.

3.2   Experimental

3.2.1   Materials

All H-ZSM-5 samples used in this study were provided by Clariant Produkte (Deutschland) GmbH and are denoted as H-ZSM-5 (B X, L Y), where "B X" and "L Y" stand for the BAS and LAS concentration of the catalysts, respectively.

The LAS-MFI catalyst was prepared by treating a silicalite sample (provided by Clariant Produkte (Deutschland) GmbH) with $Al(OC_2H_5)_3$. A certain amount of $Al(OC_2H_5)_3$ and silicalite were put into 50 mL solvent containing methanol and ethanol (1:1). Then they were

transferred to a pressure glass tube and sealed. The tube was put into an oil bath (373 K) and kept for 5 h under agitation. Subsequently, the solvent was removed by vacuum evaporation. The solid was further washed with hot ethanol for one time and hot water for two times. After that, it was dried at 373 K overnight and then calcined under air flow (100 mL/min) at 823 K for 4 h. After cooling down, the powder was stored in a bottle and ready for use.

Methanol ($\geq$99.9%), dimethoxymethane (99%), 1-hexene ($\geq$99%), 1-methoxypropane (97%), pyridine (99.8%), $Al(OC_2H_5)_3$ (97%) and ethanol (99.8%) were supplied by Sigma-Aldrich.

3.2.2   Characterization of acid sites

IR spectroscopy was used to determine the acid sites concentration of zeolites after pyridine adsorption. All spectra were collected at 423 K on a Nicolet 5700 FT-IR spectrometer. Zeolite samples were pressed into wafers and pretreated in vacuum ($<10^{-5}$ mbar) at 723 K for 1 h. Then they were exposed to 0.1 mbar pyridine at 423 K for 0.5 h. Physisorbed pyridine molecules were removed by 1-h evacuation at 423 K and the ones adsorbed on weak acid sites were removed by further outgassing at 723 K for 0.5 h. The concentrations of Brønsted and Lewis acid sites were calculated based on the band areas at 1515–1565 cm^{-1} and 1435–1470 cm^{-1} normalized to the wafer weight.

3.2.3   Catalytic testing

All catalytic tests were conducted on a bench-scale plug-flow reaction unit with an internal diameter of 6 mm of the quartz tube at ambient pressure. The catalysts were press-pelletized, crushed and used in a sieve fraction ranging from 200 to 280 µm. For the reactions, the catalyst pellets were homogeneously diluted with silicon carbide (ESK-SiC) in the range of 355-500 µm to ensure temperature uniformity. All samples were activated at 723 K with 50 mL/min N_2 for 1 h.

In order to evaluate the performance of catalysts in the MTO conversion at 723 K, 50 mL/min N_2 was passed through the methanol saturator tempered to 299 K resulting in a MeOH partial pressure of 178 mbar. Weight hourly space times were adjusted by varying the catalyst loading.

In the formaldehyde co-feeding experiments the methanol partial pressure was maintained at 100 mbar. Methanol was fed by passing dry N_2 flow through a methanol evaporator kept at 299 K. Formaldehyde was generated by introducing dimethoxymethane (DMM) which decomposes into dimethyl ether and formaldehyde. The cofed DMM vapor was adjusted by passing dry N_2 flow through a saturator containing the liquid reactant at a temperature of 273 K. Catalyst loading and reactant flow velocity were varied to achieve a wide range of contact time and methanol conversion. Here the contact time was defined as the ratio of catalyst mass to the molar flow rate of methanol.

To investigate the role of olefin-induced HT in MTO conversion, activity tests were conducted at similar reaction conditions, but with pure olefin feed. Dry N_2 was passed through a 1-hexene saturator kept at 283 K and subsequently diluted with N_2, so that experiments at a 1-hexene partial pressure of 29.7 mbar were conducted.

For the conversion of 1-methoxypropane ($CH_3OC_3H_7$) on LAS-MFI at 623 K, dry N_2 was passed through a $CH_3OC_3H_7$ saturator kept at 273 K. By further N_2 dilution a partial pressure of 178 mbar was obtained.

The reactor effluents in all reactions were analyzed by a HP 5890 gas chromatograph equipped with a HP-PLOTQ capillary column (30 m, 0.32 mm i.d.) and a flame ionization detector for on-line analysis.

Due to the rapid interconversion, both methanol and dimethyl ether were treated as reactants. Conversion and yields were calculated on a carbon basis. The C_5 fraction designates all hydrocarbons with five carbon atoms and the C_{6+} aliphatics fraction includes all other heavier hydrocarbons other than aromatics.

3.2.4 Pulse reaction with 1-methoxypropane ($CH_3OC_3H_7$) over LAS-MFI

Pulse reactions were carried out on a LAS-MFI (Al-modified silicalite) catalyst in the same reactor tube as used for the experiments in section 3.2.3 at 723 K under 25 mL/min He flow, but connected to a home-made IR cell to detect gas phase products. Each time, 0.5 µL $CH_3OC_3H_7$ was injected into the flow. IR spectra were collected every 10 s after injection.

3.3   Results

3.3.1   Hydrogen transfer in MTO conversion as a function of LAS and BAS

To investigate the role of LAS and BAS for hydrogen transfer in MTO conversion, a series of ZSM-5 catalysts with different BAS to LAS ratios was tested for this reaction at 723 K and a methanol partial pressure of 178 mbar. Under these reaction conditions, main products are C_3 and C_4 olefins and the yield of HT products is only 2-4%. However, as stated in the introduction, a major improvement of the catalyst lifetime would be achieved if the hydride transfer reactions could be suppressed, because HT products are related to deactivation by accumulation of large aromatics [17]. The LAS and BAS concentrations of the catalysts were determined by IR spectroscopy of adsorbed pyridine. The values are summarized in Table 3.1.

Table 3.1. Concentrations of Brønsted acid sites (BAS) and Lewis acid sites (LAS) of the samples H-ZSM-5 (B 113, L 22), H-ZSM-5 (B 68, L 39), H-ZSM-5 (B 67, L 38), H-ZSM-5 (B 68, L 29), H-ZSM-5 (B 68, L 23), H-ZSM-5 (B 63, L 21), H-ZSM-5 (B 63, L 20), H-ZSM-5 (B 71, L 66) and H-ZSM-5 (B 33, L 20) (determined by IR spectroscopy of adsorbed pyridine).

Sample	BAS (µmol / g)	LAS (µmol / g)
H-ZSM-5 (B 113, 22)	113 ± 6	22 ± 1
H-ZSM-5 (B 68, L 39)	68 ± 3	39 ± 2
H-ZSM-5 (B 67, L 38)	67 ± 3	38 ± 2
H-ZSM-5 (B 68, L 29)	68 ± 3	29 ± 1
H-ZSM-5 (B 68, L 23)	68 ± 3	23 ± 1
H-ZSM-5 (B 63, L 21)	63 ± 3	21 ± 1
H-ZSM-5 (B 63, L 20)	63 ± 3	20 ± 1
H-ZSM-5 (B 71, L 66)	71 ± 4	66 ± 3
H-ZSM-5 (B 33, L 20)	33 ± 2	20 ± 1

3.3.1.1   Role of LAS

Figure 3.2 shows the conversion and the yields of aromatics, C_{1-4} paraffins and C_5 aliphatics as a function of contact time for samples with same BAS concentration and varying LAS concentration.
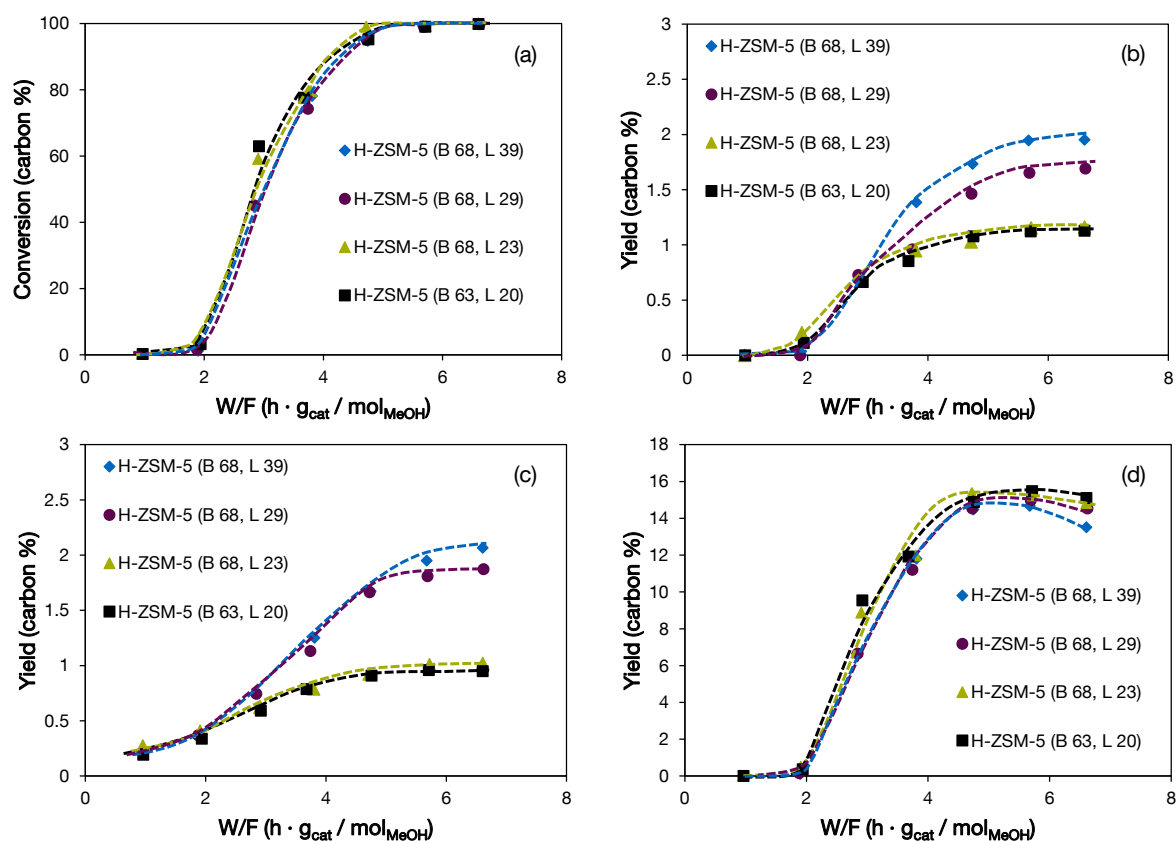
Figure 3.2. Conversion (a) and the yields of aromatics (b), C_{1-4} paraffins (c) and C_5 aliphatics (d) as a function of contact time on H-ZSM-5 (B 68, L 39), H-ZSM-5 (B 68, L 29), H-ZSM-5 (B 68, L 23) and H-ZSM-5 (B 68, L 20) at p_{MeOH} = 178 mbar and T = 723 K.

The activity of all catalysts was similar (Figure 3.2 (a)) and the reduction of the LAS concentration to low values did not show any impact on methanol conversion. This implies that catalyst activity in MTO is solely related to the concentration of available BAS, in line with reports from literature [34]. If the presence of LAS could enhance BAS activity or catalyze itself the MTO conversion, the specific increase of the BAS to LAS ratio would have increased the initiation phase, that is, the autocatalytic appearance of products would have taken place at higher W/F values. However, the yields of aromatics and paraffins declined with decreasing LAS concentration (Figure 3.2 (b) and (c)), suggesting a lower rate of hydrogen transfer when a low concentration of LAS is present. Concomitantly, a higher yield of C_5 aliphatics (Figure 3.2 (d)) was observed for low LAS concentrations. This is clearly visible at contact times above 4.7 h · g_{cat} / mol_{MeOH}. The higher yield of C_5 aliphatics is presumably due to further methylation of light olefins ($C_3^=$, $C_4^=$), because, at low LAS concentrations, this reaction pathway does not compete with hydrogen transfer which leads to aromatics and paraffins.

Having shown that the HT ability of catalysts correlates with the LAS concentration, the question arises whether the classical HT pathway (OIHT), the MIHT pathway or both pathways

are affected by LAS removal. As illustrated in the introduction, the higher rate of hydrogen transfer under partial conversion has recently been related to the contribution of the methanol-induced HT pathway [17]. Therefore, the aromatics yield for the catalysts is examined at partial and total conversion in Figure 3.3. As already evident from Figure 3.2 (b), the aromatics yield decreased with declining LAS concentration in the whole conversion range. Thus, it is hypothesized that low LAS concentrations mainly affected the contribution of the MeOH-induced HT pathway, decreasing significantly the yield of aromatics and paraffins at high BAS to LAS ratios.

Next, it is necessary to determine if low concentrations of LAS have also an impact on the olefin-induced HT pathway. For this reason, 1-hexene cracking experiments were carried out over the catalysts H-ZSM-5 (B 67, L 38) and H-ZSM-5 (B 63, L 21). Figure 3.4 depicts the obtained yields of HT products, that is, the sums of the yields of C_{1-4} alkanes and aromatics, as a function of 1-hexene conversion. Over the whole conversion range, 1-hexene cracking gave rise to only minor hydrogen transfer for both catalysts. The same selectivity toward HT products for both samples in 1-hexene cracking allows concluding that the olefin-induced HT pathway in MTO conversion was not affected by the BAS/LAS ratio and only depended on the BAS concentration.
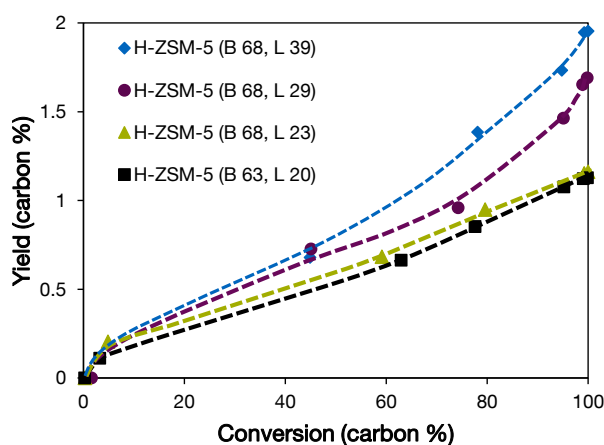
Figure 3.3. Change of aromatics yield with conversion for H-ZSM-5 samples with different LAS concentration at p_{MeOH} = 178 mbar and T = 723 K.
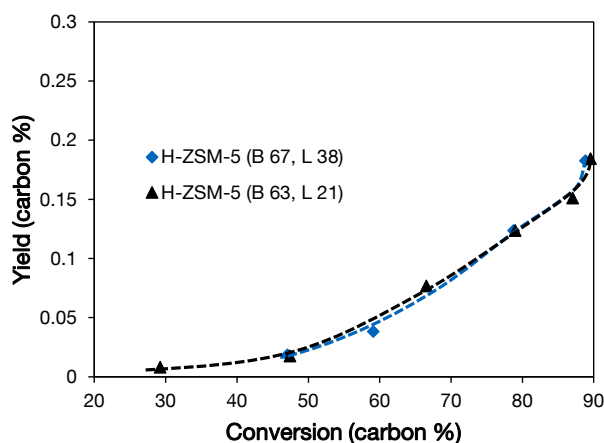
Figure 3.4. Yield of hydrogen transfer products (sum of the yields of C_{1-4} alkanes and aromatics) as a function of 1-hexene conversion for two samples with varying LAS concentration at $p_{1\text{-hexene}} = 29.7$ mbar and $T = 723$ K.

These results prove that an increase in LAS concentration induces a higher rate of MIHT but does not promote hydrogen transfer reactions between olefins as reported for MTH conversion on H-ZSM-5 [33]. It should be noted at this point that the conclusion is only drawn for Al-related LAS as those included in the samples studied here, and cannot be extended to other metal-induced LAS introduced by cation exchange. The latter LAS are reported to polarize and activate C-H bonds in alkanes, favoring hydride and hydrogen transfer [35, 36].

With the aim of gaining insight into the role of LAS for the mechanism of MIHT, a catalyst with comparable BAS and LAS concentrations, H-ZSM-5 (B 71, L 66), was tested in MTO conversion and compared with sample H-ZSM-5 (B 68, L 39). The high LAS/BAS ratio allows observing the changes induced by the presence of LAS in the product distribution of MTO at varying contact times. Figure 3.5 exhibits the obtained changes of conversion, $C_3^=$ and $C_4^=$ yields with contact time. While the catalyst activity was unaffected, the $C_3^=$ and $C_4^=$ yields decreased with the increase of LAS concentration. Interestingly, the paraffins (Figure 3.6 (a)) and aromatics (Figure 3.6 (c)) yields did not change concomitantly with residence time. At short contact times, in the region where total conversion was not yet achieved, an increase of the paraffins yield was observed for the catalyst with high concentration of LAS (66 µmol/g), (Figure 3.6 (a), red square). Conversely, the increase of aromatics yield for high LAS concentration was only verified at longer contact times, well past the threshold of total conversion (Figure 3.6 (c), red square). In the case of C_{6+} aliphatics (Figure 3.6 (b), red square), the increase in the yield with LAS concentration was detected at contact times longer than for paraffins, but shorter than for aromatics. This different evolution of products with contact time, in particular the changes of paraffins and aromatics, suggests that both LAS and BAS are

involved in MIHT. An increase in LAS concentration induces higher paraffins yield at short contact time, indicating that paraffins are a direct product of the MIHT pathway. On the other hand, a high LAS concentration favors aromatics formation with longer contact time, that is, in the region where more BAS are available for secondary steps like adsorption and reaction of C_{6+} aliphatics to aromatics.
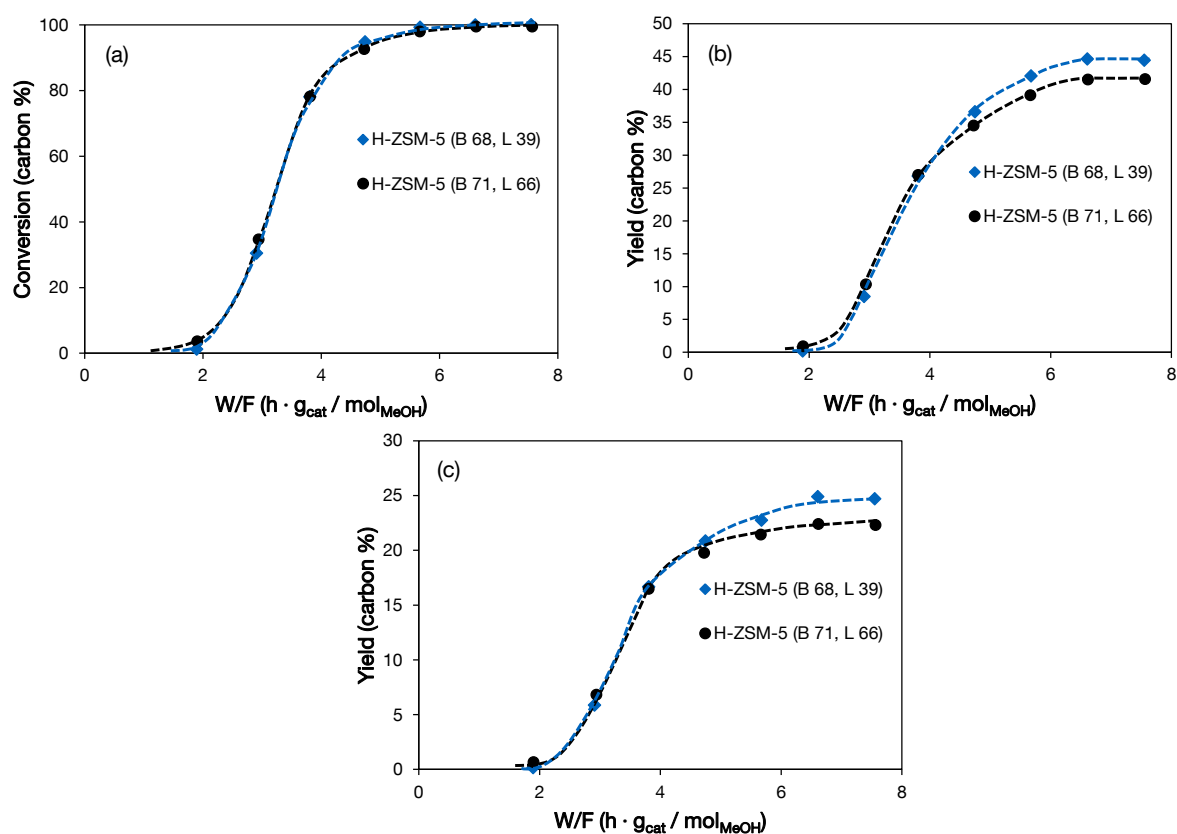
Figure 3.5. Change of conversion (a) and the yields of propene (b) and butenes (c) with contact time on H-ZSM-5 (B 68, L 39) and H-ZSM-5 (B 71, L 66) at p_{MeOH} = 178 mbar and T = 723 K.
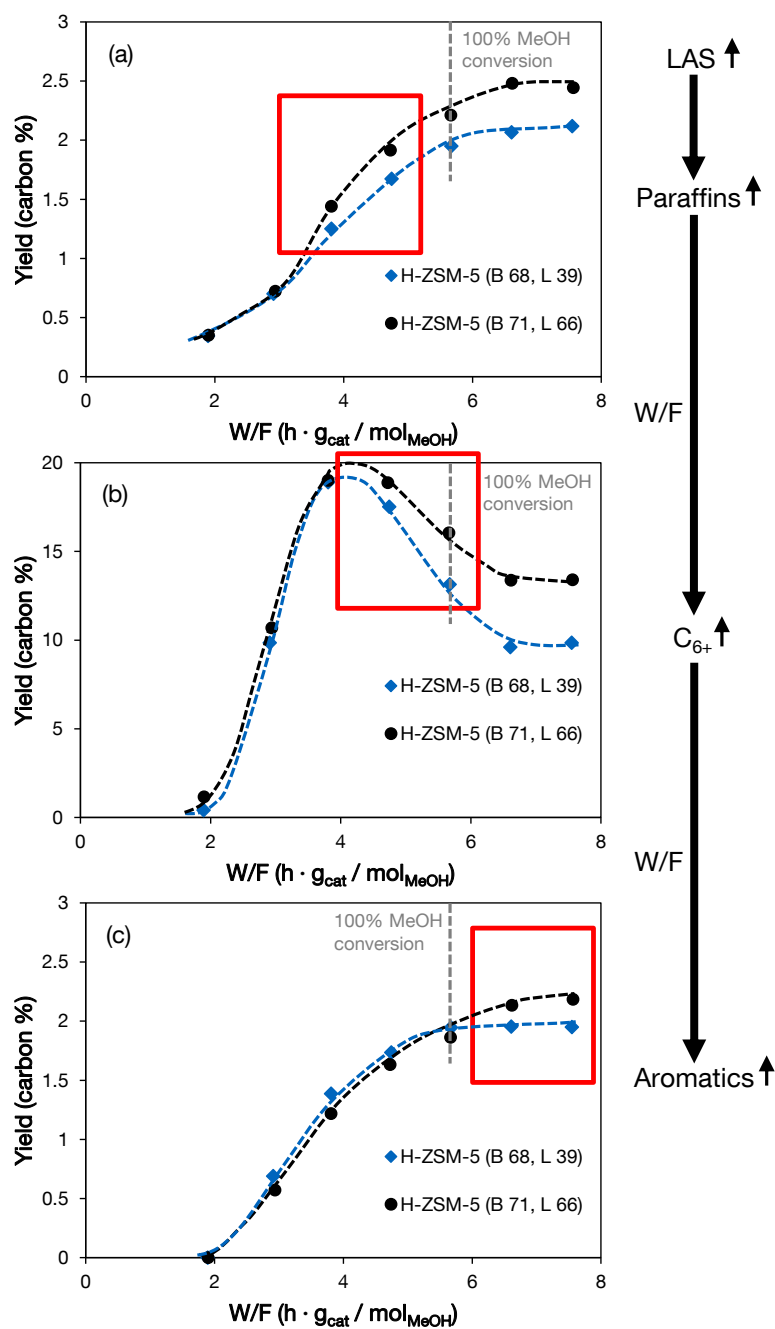
Figure 3.6. Paraffins (a), C_{6+} aliphatics (b) and aromatics (c) yield as a function of contact time obtained on H-ZSM-5 (B 68, L 39) and H-ZSM-5 (B 71, L 66) at p_{MeOH} = 178 mbar and T = 723 K.

3.3.1.2   Role of BAS

In exploring the specific role of BAS for hydrogen transfer in MTO conversion, it is focused on catalysts with similar low concentrations of LAS (ca. 20 µmol/g) and different BAS concentrations. As expected and in line with literature [37], the shortest initiation phase was observed for the catalyst with highest BAS concentration (Figure 3.7 (a)). If the aromatics yield

of these samples is compared at same conversion levels, it can be seen that less aromatics were formed with increasing BAS concentration (Figure 3.7 (b)). Interestingly, the selectivity difference was quite pronounced between the catalysts with BAS concentrations of 33 and 68 µmol/g. Conversely, only marginal differences in aromatics selectivity were observed between the catalysts with 68 and 113 µmol/g BAS.

Thus, it is concluded that the MeOH-induced hydrogen transfer, having a remarkably higher rate at partial conversion (Figure 3.3, [17]), was almost not affected by increasing the BAS concentration from 68 to 113 µmol/g. It is hypothesized that this is because the low concentration of LAS is rate-limiting for the MeOH-related hydrogen transfer. This statement is valid for H-ZSM-5 catalysts with BAS to LAS ratios in the range of 3-6, as those typically used in MTO conversion. Conversely, when decreasing the BAS to LAS ratio to values close to 1.5 (sample H-ZSM-5 (B 33, L 20)), the difference in aromatics selectivity, compared to the samples with 68 and 113 µmol/g, became evident. At such low BAS to LAS ratios, the rate of aromatics formation is observed to be higher than in samples with a higher BAS to LAS ratio, whereas the rates of olefin methylation and cracking are reduced.
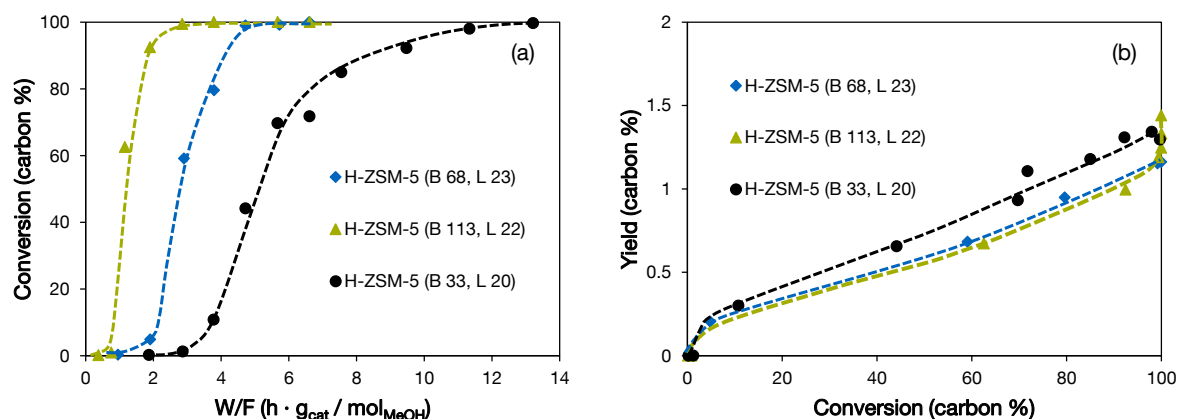
Figure 3.7. Change of conversion with contact time (a) and change of aromatics yield with conversion (b) at $p_{MeOH} = 178$ mbar and $T = 723$ K.

The aromatics selectivity, which is taken here as representative for hydrogen transfer (given the concomitant changes in the yields of aromatics and paraffins [4]), is shown in Figure 3.8 as a function of LAS concentration (at the same contact time of 6.6 h $\cdot$ $g_{cat.}$ / mol_{MeOH}) for all catalysts with a similar BAS concentration (68 µmol/g). It is important to note that at this contact time methanol and dimethyl ether were just fully converted by the samples with 68 µmol/g BAS (Figure 3.2 (a)). On the basis of the results shown in Figure 3.1, one can assume that HT products at this contact time mostly form via the methanol induced HT pathway. It is

clearly visible from Figure 3.8 that the hydrogen transfer ability increased linearly with LAS concentration for samples with same BAS concentration. An extrapolation of the line would intercept in the origin, which indicates that Lewis acid sites not only have a cooperative/supporting effect for hydrogen transfer, but are indeed necessary for the methanol-induced hydrogen transfer to happen. In order to understand HT products formation on catalysts under full conversion conditions, the sample H-ZSM-5 (B 113, L 22) was also included in Figure 3.8. The higher aromatics yield for the catalyst with a high BAS concentration can be explained by the fact that the catalyst with 113 µmol/g BAS had already reached full conversion at a contact time of 3.8 h · $g_{cat.}$ / mol$_{MeOH}$ and therefore not only the methanol-induced HT, but also the olefin-induced HT contributed to the overall aromatics formation for this sample at a contact time of 6.6 h · $g_{cat.}$ / mol$_{MeOH}$.
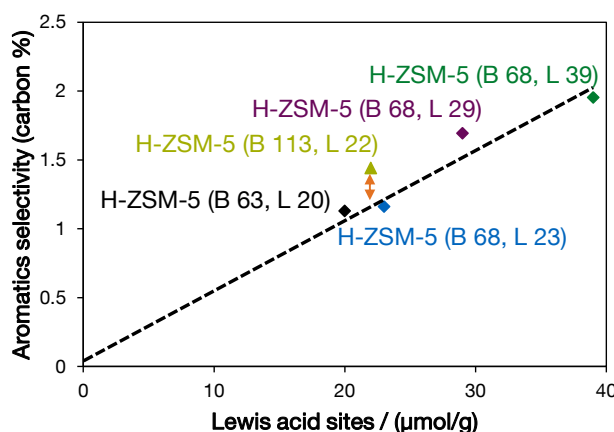
Figure 3.8. Correlation of aromatics selectivity with LAS concentration, including the samples H-ZSM-5 (B 68, L 39), H-ZSM-5 (B 68, L 29), H-ZSM-5 (B 68, L 23), H-ZSM-5 (B 63, L 20) and H-ZSM-5 (B 113, L 22). Reaction temperature was 723 K, methanol partial pressure 178 mbar, contact time 6.6 h · g_{cat} / mol$_{MeOH}$.

To prove this hypothesis, 1-hexene cracking experiments were conducted on the catalysts H-ZSM-5 (B 113, L 22) and H-ZSM-5 (B 68, L 23). The yield of HT products versus 1-hexene conversion is presented in Figure 3.9. It is clearly evident that the same yield of HT products was achieved for samples with varying BAS/LAS ratios, but same total LAS concentration. This proves that BAS are responsible for the rate of hydrogen transfer reaction between olefins, because the hydrogen transfer ability is linked with olefin conversion, which, in turn, correlates with BAS concentration. Thus, in MTO conversion, the contribution of olefin-induced HT increases with contact time after having reached full methanol conversion, in accordance with

Figure 3.1, while at partial conversions the presence of methanol inhibits olefin adsorption at BAS even at low concentrations [38], making this route negligible.
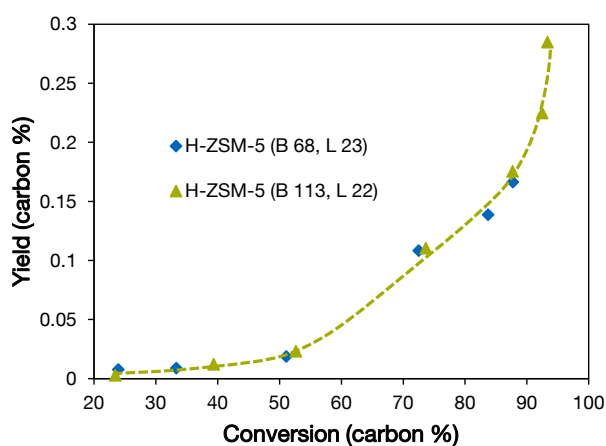
Figure 3.9. Change of HT products yield with 1-hexene conversion for two samples with different BAS concentration at $p_{1\text{-hexene}} = 29.7$ mbar and T = 723 K.

To summarize, hydrogen transfer in MTO comprised contributions of the MeOH-induced HT (involving LAS and BAS) and the olefin-induced HT (involving only BAS) upon reaching full conversion, while only the MeOH-related pathway is relevant at partial conversion.

3.3.2 Toward elucidating the MeOH-mediated hydrogen transfer pathway in MTO conversion

3.3.2.1 Detection of formaldehyde as reaction intermediate

In section 3.3.1, it has been shown that both BAS and LAS are involved in MIHT. Furthermore, the trend presented in Figure 3.8 indicates that LAS must be active sites where the methanol-induced hydrogen transfer pathway is initiated.

On the other hand, formaldehyde has been recently reported to form during MTO by hydrogen transfer [17], in line with an early proposal of Hutchings et al. [39]. Furthermore, it was reported to be involved in the formation of O-containing coke species in Chapter 2. Thus, it is proposed that the methanol-related hydrogen transfer takes place between methanol and alkenes on LAS of H-ZSM-5, yielding formaldehyde and alkanes as products.

In order to prove the participation of formaldehyde as reaction intermediate, experiments were performed pulsing the ether 1-methoxypropane ($CH_3OC_3H_7$), which would easily decompose into methanol and propene under reaction conditions. By this means, it is possible

to monitor the surface reaction of methanol with one olefin molecule at very low partial pressures, so that secondary reactions are avoided. Firstly, LAS catalyzed reactions can be tested by using a pure LAS-MFI. This material was prepared by $Al(OC_2H_5)_3$-treatment of a silicalite sample (see experimental section). It therefore exhibits the MFI-structure and contains only LAS due to EFAL, and no detectable amounts of BAS.

The gas phase products of the 1-methoxypropane pulse over the pure LAS-MFI were analyzed by IR spectroscopy. The IR spectrum after gas phase water subtraction (Figure 3.10, middle) shows the formation of propene and methanol, indicating that 1-methoxypropane decomposes into methanol/dimethyl ether and propene. In the IR spectrum taken 30 s after injection, formaldehyde was detected (Figure 3.10, top), suggesting that formaldehyde is strongly adsorbed on H-ZSM-5. As a consequence of formaldehyde formation, propene must act as hydrogen acceptor and therefore stoichiometric amounts of propane must have been formed. However, due to overlapping bands in the C-H region, IR spectroscopy could not provide unambiguous evidence of propane formation.
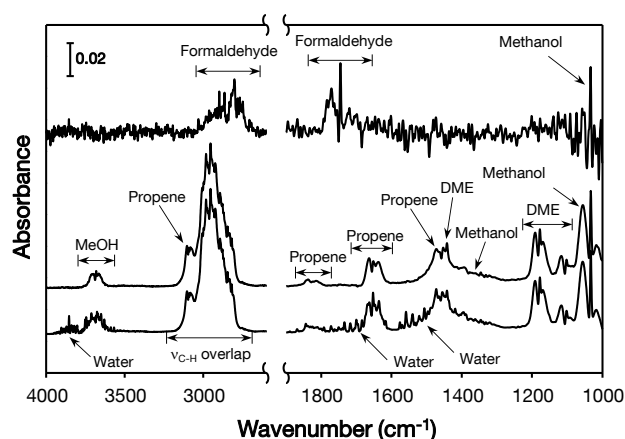
Figure 3.10. IR spectra of gas phase products after pulsing 0.5 µL 1-methoxypropane over pure LAS-MFI at 723 K: IR spectrum collected 10 s after injection (bottom), IR spectrum collected 10 s after injection with subtracted gas phase water (middle) and IR spectrum collected 30 s after injection with subtracted gas phase water (intensity x 100; top).

Next, 1-methoxypropane was reacted over LAS-MFI at 623 K in a plug-flow reactor ($p_{\text{1-methoxypropane}}$ = 178 mbar, W/F = 0.35 h · g_{cat} / $mol_{\text{1-methoxypropane}}$), and gas phase composition was analyzed by a GC connected with a FID. Aside from propene and methanol/dimethyl ether formation, propane could be detected in gas phase (Table 3.2). It should be noted that the FID response of formaldehyde is very low [40] and therefore no detection of formaldehyde was possible.

Table 3.2. Reaction of 1-methoxypropane on pure LAS-MFI at 623 K, $p_{1\text{-methoxypropane}}$ = 178 mbar and W/F ($h \cdot g_{cat}$ / $mol_{1\text{-Methoxypropane}}$) = 0.35.

Compound	Area (%)
Propene	4.02
Propane	0.02
DME	0.15
MeOH	0.81
1-Methoxypropane	94.43
Others	0.59

From the pulsing results and the results under continuous flow in a plug-flow reactor, it is deduced that [Al]-LAS catalyze the hydrogen transfer between methanol and light olefins to form formaldehyde and paraffins.

3.3.2.2   Impact of formaldehyde co-feeding

Inspired by the finding that formaldehyde can be generated at LAS, formaldehyde was co-fed over H-ZSM-5 (B 68, L 39) using dimethoxymethane (DMM). Under reaction conditions, DMM decomposed completely (Table 3.3) into mainly dimethyl ether, methanol and formaldehyde [41] and therefore co-feeding 3 C % dimethoxymethane on a methanol feed can be regarded as co-feeding 1 C % formaldehyde.

Table 3.3. Dimethoxymethane (DMM) conversion on H-ZSM-5 (B 68, L 39) at 723 K, p_{DMM} = 171 mbar and W/F ($h \cdot g_{cat}$ / mol_{DMM}) = 0.35.

Sample	DMM conversion (carbon %)
H-ZSM-5 (B 68, L 39)	99.6

Figure 3.11 shows the conversion, as a function of contact time, for the pure methanol feed and for the feed containing formaldehyde (1 C %) over H-ZSM-5 (B 68, L 39). Over the whole range of contact time, conversion was slightly lower when co-feeding formaldehyde. Furthermore, formaldehyde reduced the selectivity towards propene and butenes (Figure 3.12) at conversions above 60 C %. In contrast, the aromatics yield was higher at all conversions (Figure 3.13 (a)). Since the C_{6+} aliphatics yield increased with formaldehyde co-feeding (Figure

3.14), it is concluded that $C_{3-4}^=$ olefins reacted with formaldehyde and were transformed into aromatics via intermediate formation of C_{6+} aliphatics.
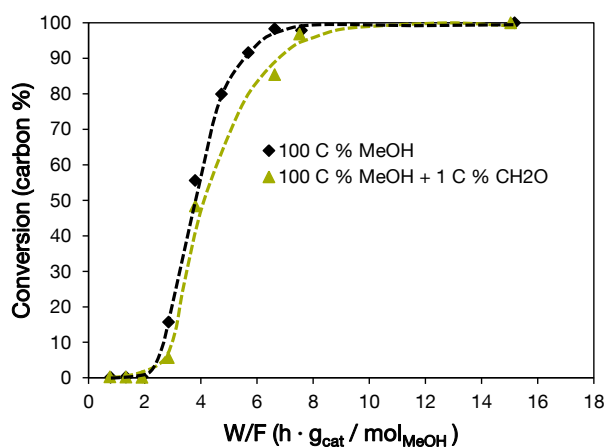
Figure 3.11. Change of conversion with contact time for the pure MeOH feed and the feed containing 1 C % formaldehyde (CH_2O) on H-ZSM-5 (B 68, L 39) at $p_{MeOH} = 100$ mbar and T = 723 K.
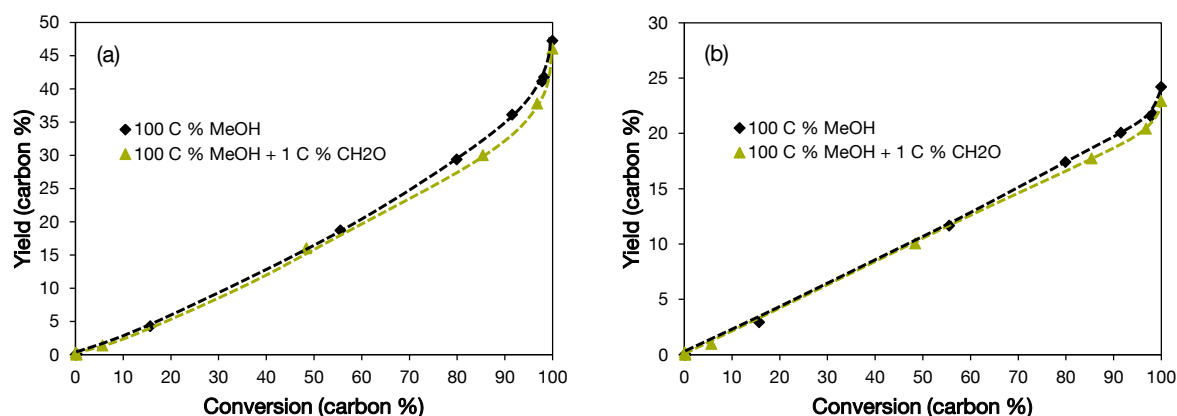
Figure 3.12. Yields of propene (a) and butenes (b) as a function of conversion for the feeds of methanol and methanol co-fed with 1 C % formaldehyde (CH_2O) on H-ZSM-5 (B 68, L 39) at $p_{MeOH} = 100$ mbar and T = 723 K.

Interestingly, the paraffins yield (Figure 3.13 (b)) was unaffected by formaldehyde co-feeding. According to the stoichiometry of the olefin based HT reaction, the same increment of paraffins and aromatics is typically verified. Therefore, this finding provides a first evidence of a reaction pathway in which paraffins are formed in the same step as formaldehyde, while the aromatics are formed in a subsequent reaction. However, it must be noted that the lower yield of paraffins with respect to aromatics is also partially related to the fact that formaldehyde favors in particular the formation of methane (Figure 3.15). As a consequence, a lower carbon-

based yield of paraffins is obtained than, for instance, when propane or butanes are formed by hydrogen transfer.

To sum up, these formaldehyde co-feeding experiments together with the results in section 3.3.2.1 have provided a link between high LAS to BAS ratios and high yields of HT products – namely aromatics and paraffins – as observed in Figures 3.2 and 3.3. High concentrations of LAS induce the formation of formaldehyde and a higher yield of paraffins. In a subsequent step, formaldehyde promotes aromatics formation leading to a higher yield of aromatics as well. The fact that the formation of aromatics depends on formaldehyde concentration in this proposed pathway explains well the deviations found at different contact times for paraffins and aromatics in Figure 3.6.
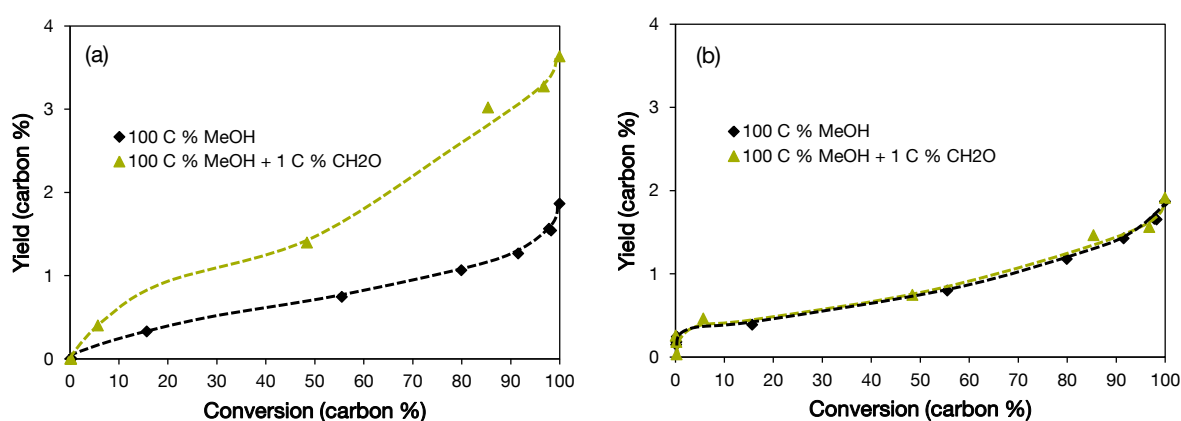
Figure 3.13. Change of aromatics (a) and C_{1-4} paraffins (b) yield with conversion for the pure MeOH feed and the feed containing 1 C % formaldehyde (CH_2O) on H-ZSM-5 (B 68, L 39) at $p_{MeOH} = 100$ mbar and T = 723 K.
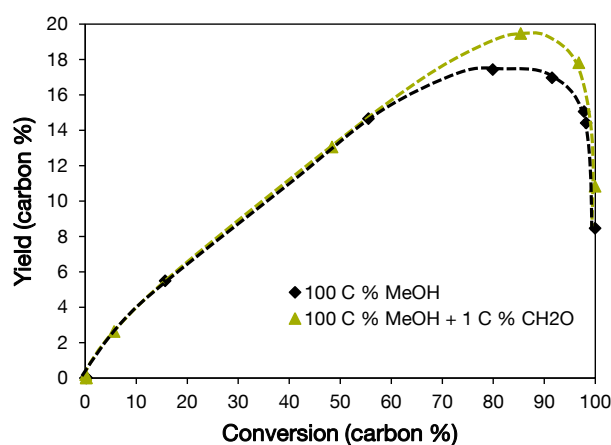
Figure 3.14. C_{6+} aliphatics yield as a function of conversion for the feeds of methanol and methanol co-fed with 1 C % formaldehyde (CH_2O) on H-ZSM-5 (B 68, L 39) at $p_{MeOH} = 100$ mbar and T = 723 K.
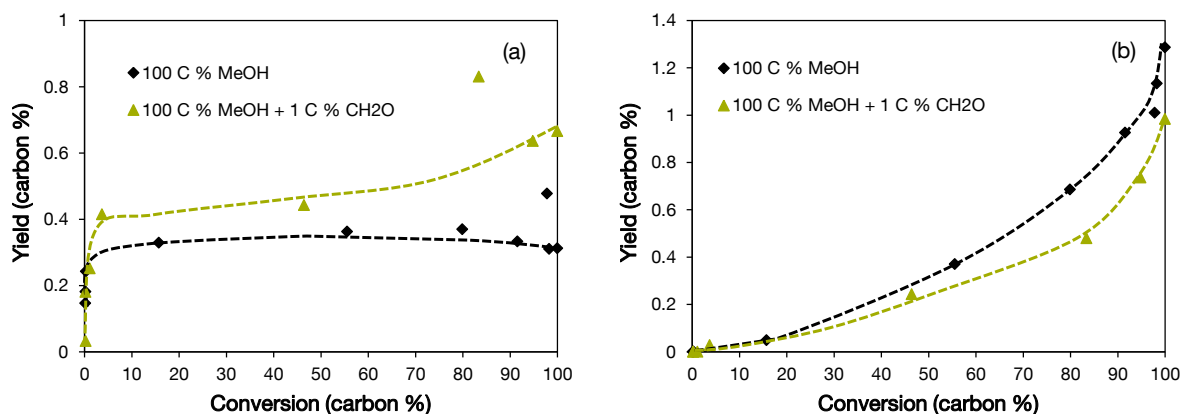
Figure 3.15. Methane (a) and C_4 paraffins (b) yield as a function of conversion for the feeds containing 100 C % MeOH and 100 C % MeOH/1 C % CH_2O.

3.3.2.3   Activation of formaldehyde

So far, it has been shown that LAS and BAS are involved in MIHT with formaldehyde as linking species. On the basis of the formaldehyde co-feeding experiments it was proposed that formaldehyde generated at LAS favors aromatics formation. Along with this proposal, the question arises which acid sites activate formaldehyde. Experiments with catalysts having varying BAS concentrations showed that the rate of aromatics formation is higher for samples with low BAS to LAS ratios compared to samples with high BAS to LAS ratios, while olefin methylation and cracking is suppressed. This suggests that formaldehyde chemisorbs to BAS, which is released by reaction to aromatics, and inhibits olefin adsorption at low BAS/LAS ratios. Dumitriu et al. [42], however, hypothesized that formaldehyde is activated at LAS for aldol condensation. To rule out activation of formaldehyde at LAS in MIHT and to support the proposal deduced from the results presented above, formaldehyde co-feeding experiments were carried out over two catalysts with varying LAS concentration. Both catalysts exhibited similar activity in MTO (Figure 3.16). Thus, the aromatics and C_{1-4} paraffins yields of both catalysts were compared as a function of contact time in Figure 3.17.

The lower paraffins yield obtained on H-ZSM-5 (B 63, L 20) compared to H-ZSM-5 (B 68, L 39) was the result of a lower LAS concentration, as shown and discussed in section 3.3.1.1. Typically, similar yields of paraffins and aromatics are obtained over an H-ZSM-5 catalyst for a pure MeOH feed. From Figure 3.17 it is evident that aromatics formation was promoted for both catalysts by formaldehyde co-feeding because the obtained yields are significantly higher than the corresponding yields of paraffins. If LAS could activate formaldehyde, a clearly visible

decline in aromatics yield should be induced by LAS removal (that is for H-ZSM-5 (B 63, L 20) in comparison to H-ZSM-5 (B 68, L 39)). Since the difference in aromatics yield (~0.7 C %) was close to 1 C %, which is the observed decline in paraffins yield, such pathway can be ruled out. Therefore, it is concluded that the aromatics formation via formaldehyde is catalyzed only by BAS.
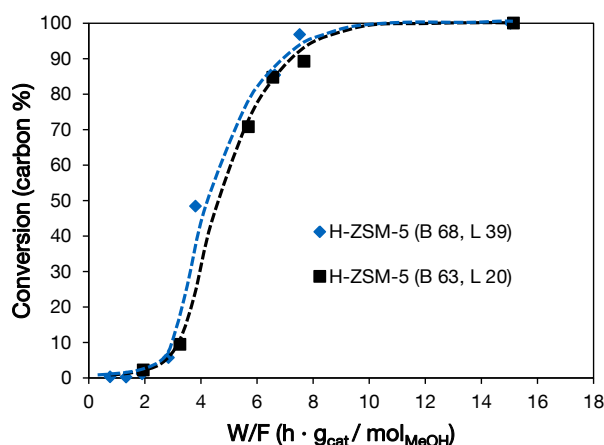
Figure 3.16. Conversion as a function of contact time on H-ZSM-5 (B 68, L 39) and H-ZSM-5 (B 63, L 20) for a feed containing methanol and 1 C % formaldehyde at p_{MeOH} = 100 mbar and T = 723 K.
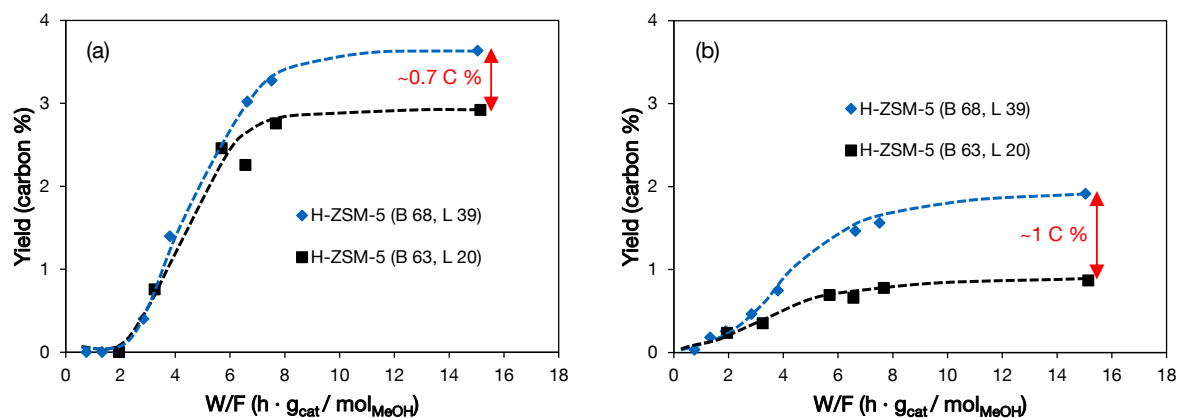
Figure 3.17. Aromatics (a) and C_{1-4} paraffins (b) yield as a function of contact time on H-ZSM-5 (B 68, L 39) and H-ZSM-5 (B 63, L 20) for a feed containing methanol and 1 C % formaldehyde (p_{MeOH} = 100 mbar and T = 723 K).

Further proof can be found when formaldehyde is co-processed with methanol over H-ZSM-5 catalysts with different BAS concentration and a similar low LAS concentration. Due to differences in catalyst activity (Figure 3.18 (a)), the aromatics yield is illustrated as a function of conversion (Figure 3.18 (b)). Aromatics formation was already correlated to the BAS concentration in Figure 3.7, where only a slight contribution of the BAS to LAS ratio was seen.

In good agreement with that, addition of formaldehyde – presumably formed on LAS and therefore equivalent to a decrease in BAS to LAS ratio – did not promote further the formation of aromatics. It is hypothesized that this is due to the fact that formaldehyde chemisorbs on BAS more strongly than methanol and hydrocarbons and therefore the coverage is relatively high. The reaction network must then continue by reaction of the adsorbed formaldehyde with an olefin from the gas phase, with the partial pressure of the latter determined by the total MTO conversion and related only to BAS concentration. In other words, the transformation of formaldehyde into aromatics is independent of the (relatively abundant) concentration of formaldehyde and, in extension, independent of the BAS to LAS ratio.

These results and the fact that high LAS concentrations did not promote formaldehyde-associated aromatics formation can be seen as a further indication for the reaction of formaldehyde with olefins on BAS.
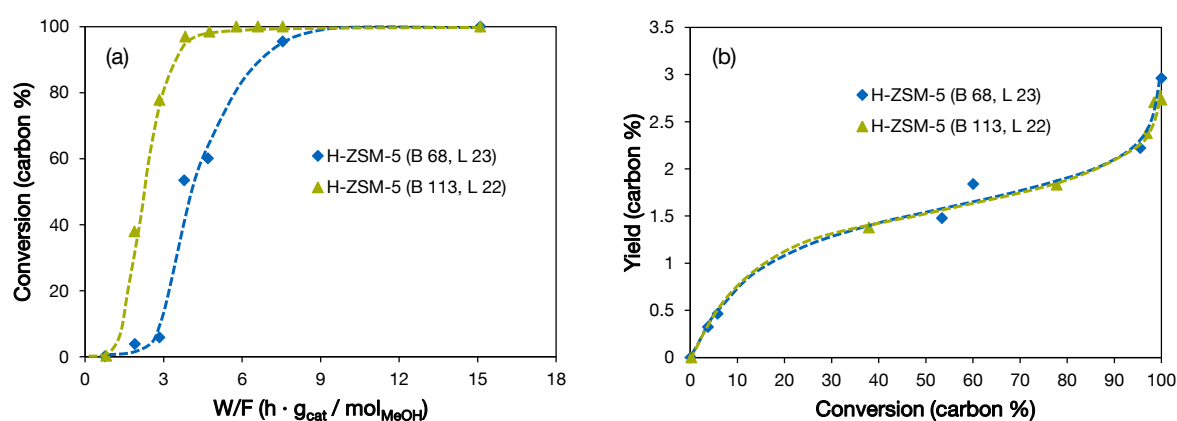
Figure 3.18. Conversion profiles as a function of contact time (a) and aromatics yield as function of conversion (b) for a feed of methanol with 1 C % formaldehyde over H-ZSM-5 (B 68, L 23) and H-ZSM-5 (B 113, L 22) at $p_{MeOH} = 100$ mbar at T = 723 K.

3.4   Discussion

Aromatics and C_{1-4} paraffins are undesirable products in MTO conversion [17]. Their formation is commonly associated with hydrogen transfer reactions between olefinic species [1]. This is indeed the type of reaction which would be responsible for aromatics and paraffins formation in the last region of the catalyst bed, when contact times are long enough to reach full methanol/dimethyl ether conversion. In the first zone, before full conversion of methanol, another hydrogen transfer pathway exists, which involves methanol or methanol-derived

species. The rate of formation of aromatics and paraffins via such pathway is faster than via the classical route between two olefinic species [17]. Thus, two zones develop along the catalyst bed, one in presence of methanol and the other in absence of it [43]. Here, the study of MTO conversion on a series of catalysts with controlled concentrations of BAS and LAS has provided mechanistic information on the methanol-related hydrogen transfer pathway.

It has been found that both BAS and LAS participate in the methanol-induced hydrogen transfer. Although a promoting effect of LAS on HT has often been described in literature, it has not been clear until today if LAS are catalytic sites for this type of reactions. Indeed, while no influence of the concentration of LAS on HT products selectivity in 1-hexene conversion was found, similar experiments in presence of methanol showed remarkable differences.

Having established the impact of LAS and BAS variation on aromatics and paraffins selectivity, the reactions occurring at LAS and BAS are addressed on a molecular level. Methanol reaction on a catalyst with relatively high LAS concentration (ratio of BAS to LAS close to one) showed consecutively important changes in paraffins, C_{6+} and aromatics yield with contact time (Figure 3.6). These consecutive changes in product distribution together with the results obtained by co-feeding formaldehyde (section 3.3.2.2), has enabled to identify the reaction network in the MIHT pathway and the role of BAS and LAS. It is hypothesized that in the first step paraffins are generated at LAS where hydrogen is transferred from methanol to an olefin molecule generating formaldehyde and the corresponding paraffin (Scheme 3.2). Then, reaction of formaldehyde on BAS with olefins would generate dienes, C_{6+} aliphatics and, ultimately, aromatics (Scheme 3.2). Therefore, it is proposed here that hydrogen transfer products formation is promoted rather due to a stepwise mechanism in which paraffins are formed on LAS and aromatics are subsequently formed on BAS than to a synergistic effect between BAS and LAS.
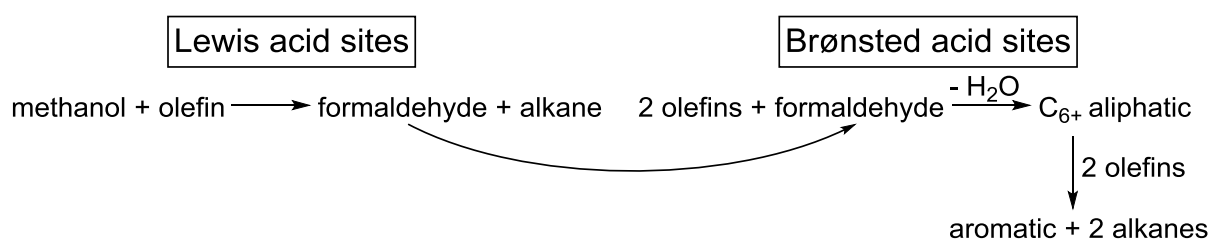
Scheme 3.2. Schematic reaction network of methanol-induced hydrogen transfer involving Lewis and Brønsted acid sites.

The reaction of methanol and propene – produced on the surface via decomposition of 1-methoxypropane – over pure Al-LAS MFI (section 3.3.2.1) unambiguously revealed that

paraffins and formaldehyde are generated at LAS. Formaldehyde then links the reaction steps at LAS and BAS in the overall MIHT reaction network (Scheme 3.2) as evidenced by co-feeding of formaldehyde. It can react with C_{3-4} olefins on BAS to form C_{6+} aliphatics, which are finally converted to aromatics (Scheme 3.2). Alternatively, formaldehyde can also promote the formation of larger aromatics by reaction with cyclohexene as shown in Scheme 3.3. However, only the route shown in Scheme 3.2 can explain the increase in C_{6+} aliphatics detected with increasing concentrations of LAS (Figure 3.6 (b)). The fact that co-feeding formaldehyde favored in particular the formation of methane (Figure 3.15), which results in a lower carbon-based yield of paraffins, argues additionally for latter mechanism and against the reaction with cyclohexene. It is important to note in passing that paraffins also form in the reaction step required for aromatics formation – in a one to two stoichiometry – and not only at LAS.
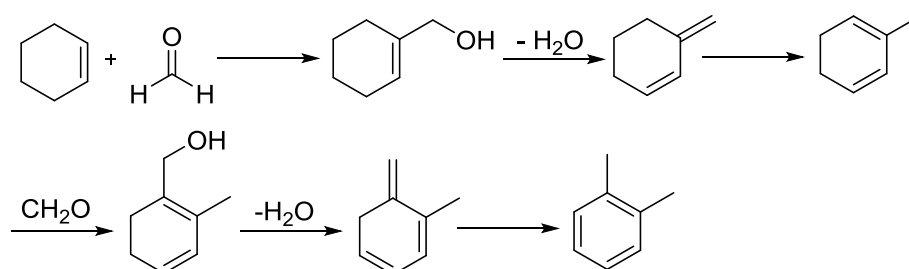
Scheme 3.3. Aromatics formation by reaction of cyclohexene with formaldehyde.

Furthermore, it was observed that co-feeding formaldehyde over catalysts with varying BAS concentration and a low LAS concentration (23 µmol/g) did not give rise to a higher aromatics yield. This is attributed to a relatively high formaldehyde coverage, due to preferential adsorption of formaldehyde on BAS in comparison to methanol and olefins adsorption [44]. In that case, the rate of formaldehyde reaction with olefins and cyclohexene depends on the availability of the other co-reactant and not on the formaldehyde. This strong adsorption is also observed in experiments on a catalyst with a BAS to LAS ratio close to one. Here an increase in aromatics yield at the expense of a decrease in olefins yield was observed (Figure 3.7 (b) and Figure 3.19), which is attributed to the competitive adsorption of formaldehyde on BAS, hindering olefin methylation and cracking reactions. In contrast, variation of BAS concentrations at high BAS to LAS ratios showed only minor differences (Figure 3.7 (b)). These results clearly show that LAS are the limiting sites for MIHT over typical MTO catalysts; that is, catalysts having a BAS to LAS ratio well above one.
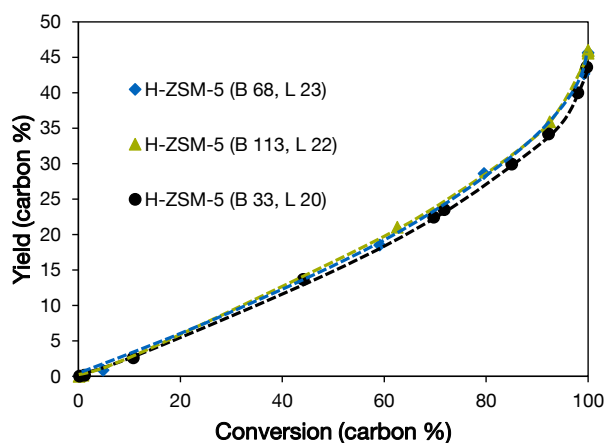
Figure 3.19. Change of propene yield with conversion at p_{MeOH} = 178 mbar and T = 723 K.

On the basis of the results discussed above, a mechanism for the MIHT with participation of both BAS and LAS is proposed (Scheme 3.4). The reaction follows a consecutive mechanism with MeOH activation to form formaldehyde and donate hydrogen as first step. For MeOH activation at LAS, two models can be invoked. The first option (Scheme 3.4 (ai)) is that MeOH shows a coordinative interaction with LAS, whereby the O-H bond is weakened. Adsorbed methanol may react with olefins in a concerted mechanism via a six-membered transition state to paraffins and formaldehyde. Such proposal, to the best of our knowledge, has not been made for MeOH reactions on zeolites so far. The proposal of MeOH and an olefin reacting via a six-membered transition state is based on the observations of Viola et al. [45]. The thermolysis of the olefinic benzyl alcohol $Ph-CHOH(CH_2)_3CH=CH_2$ at temperatures in the range of 713-723 K resulted in the formation of the respective phenone which was mechanistically explained by the simultaneous migration of two hydrogen atoms. On the other hand, MeOH could adsorb dissociatively on LAS (Scheme 3.4 (aii)), resulting in the formation of formaldehyde and surface hydrogen adatoms. An olefin is then hydrogenated to a paraffin. DeWilde et al. [46] reported an indirect hydrogen transfer mechanism to form acetaldehyde and ethane from ethanol on $\gamma-Al_2O_3$. They proposed the cleavage of the $C_\alpha-H$ of a surface ethoxy species on γ-Al_2O_3 leading to the formation of acetaldehyde and hydrogen adatoms as first step. Ethylene formed by ethanol dehydration was then hydrogenated by these surface adatoms.

Formaldehyde generated at LAS is subsequently protonated at BAS (Scheme 3.4 (b)) and reacts then with olefins in a nucleophilic addition to an allylic alcohol (Scheme 3.4 (c)). Dehydration of this allylic alcohol leads to the formation of a diene species (Scheme 3.4 (d)). The diene species may react to a carbenium ion at BAS. In the next step, a condensation reaction of this carbenium ion and an olefin occurs (Scheme 3.4 (e)), followed by a hydride shift

(Scheme 3.4 (f)), cyclization and dehydrogenation through hydrogen transfer reactions (Scheme 3.4 (g)).
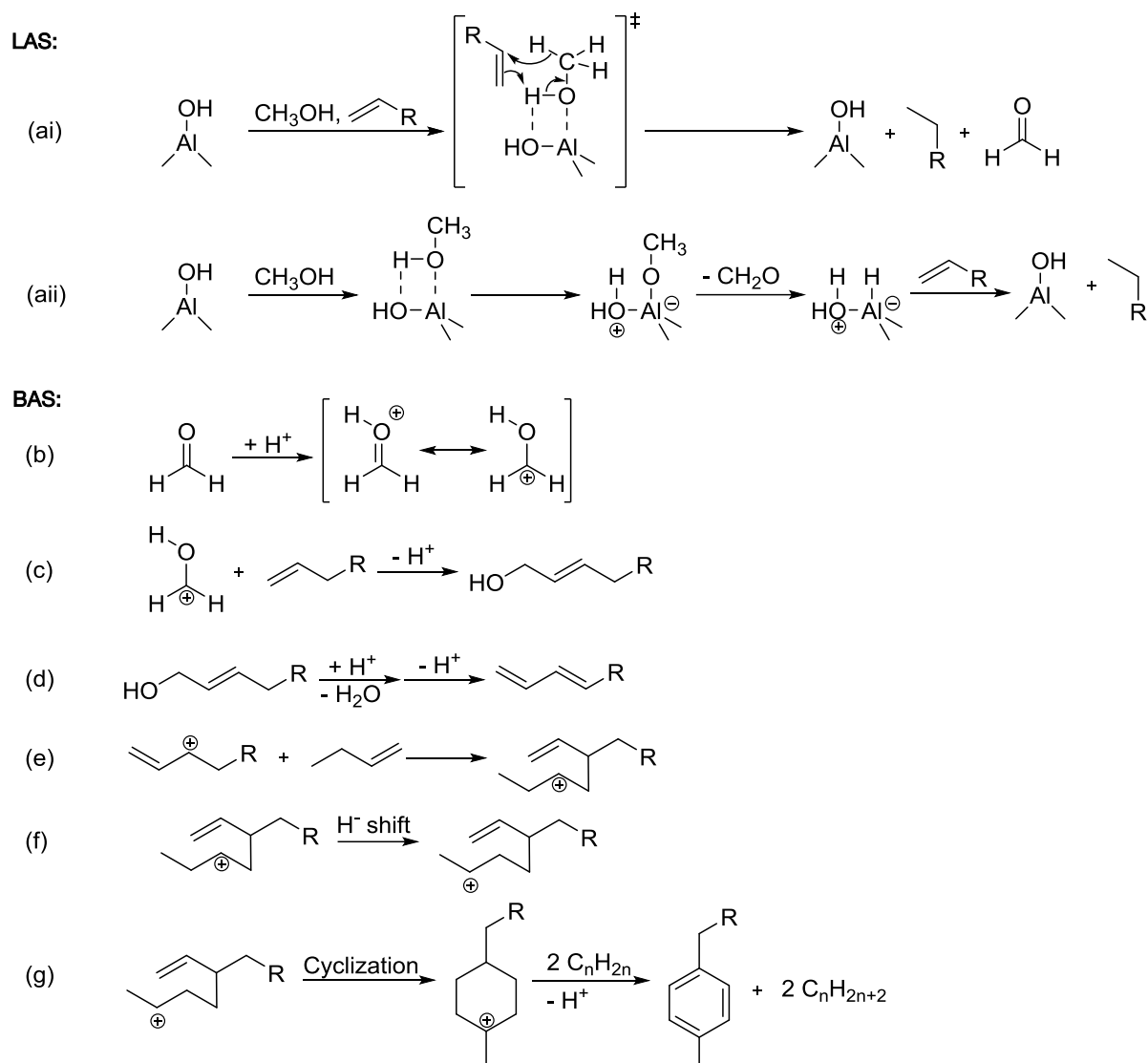
Scheme 3.4. Proposed reaction mechanism for the formation of aromatics and paraffins in the MeOH-mediated pathway. LAS are schematically represented with Al-OH end groups.

In the reaction mechanism presented in Scheme 3.4, dienes are proposed to react with olefins in a condensation reaction (Scheme 3.4 (e)). Due to the lower activation energy for cyclization of C_7 and C_8 dienes in comparison to C_6 diene cyclization [22] it is speculated that the cyclization described in Scheme 3.4 (g) occurs from C_7 and C_8 precursors which can also be expected assuming, for example, a condensation reaction of butadiene with propene or butenes.

The proposal of MIHT as dominant pathway for aromatics and paraffins formation contrasts the description of hydrogen transfer reported so far in the literature about methanol-to-

hydrocarbons conversion, where hydride transfer was typically described as a reaction between two olefins [32, 33]. Conversely, the impact of LAS was already noted by many authors, but until now no clear mechanistic explanation was provided. It is believed that the methanol induced pathway has been overlooked because most of the studies were performed at methanol full conversion and, under such conditions, it is not possible to distinguish between the contributions of MIHT or OIHT.

3.5   Conclusions

The study on the role of acid sites and hydrogen transfer pathways in MTO conversion on H-ZSM-5 has allowed elucidating the mechanism of a methanol-induced hydrogen transfer. This hydrogen transfer is the dominant pathway to undesirable aromatics and paraffins in the conversion of methanol on zeolites. It is proposed to consist of individual reactions occurring separately either on BAS or on LAS. The primary hydrogen transfer takes place between methanol and an olefin to form formaldehyde and a paraffin via a six-membered transition state which is stabilized by Lewis acid sites, or alternatively via dissociative adsorption of methanol on LAS. Formaldehyde reacts subsequently on BAS with olefins to form dienes, generating finally aromatics and paraffins.

In spite of the important role of BAS for some of the elementary steps involved in the reaction network, it is clear that this MIHT mechanism is initiated at Lewis acid sites. In good agreement with this, a decrease in the LAS concentration resulted in an important decrease of HT products yield, as a consequence of the suppression of this pathway. On the other hand, changes in BAS concentrations at constant LAS concentration only affected the selectivity to HT products when the BAS to LAS ratio was close to 1.5. Under such conditions, the intermediates of the MIHT pathway, initiated at the abundant LAS, started to compete for the Brønsted acid sites with methylation and cracking of olefins. It is hypothesized at present that the most probable cause of a decrease in olefins yield in favor of HT products at such low BAS to LAS ratio is a stronger adsorption of formaldehyde on BAS in comparison to olefins and methanol.

It is important to point out that a molecular-level understanding of the methanol-induced hydrogen transfer pathway, the main pathway to aromatics and paraffins in MTO conversion, has been achieved. The involved reactions could be classified in reactions at BAS and in

reactions at LAS. These results open new ways to design catalysts suppressing hydrogen transfer and, consequently, coke formation, without affecting the overall activity in MTO.

3.6   Acknowledgements

3.7   References

[1] S. Ilias, A. Bhan, ACS Catal. 3 (2013) 18.

[2] U. Olsbye, S. Svelle, M. Bjørgen, P. Beato, T.V.W. Janssens, F. Joensen, S. Bordiga, K.P. Lillerud, Angew. Chem. Int. Ed. 51 (2012) 5810.

[3] M. Stöcker, Microporous Mesoporous Mater. 29 (1999) 3.

[4] X. Sun, S. Mueller, H. Shi, G.L. Haller, M. Sanchez-Sanchez, A.C. van Veen, J.A. Lercher, J. Catal. 314 (2014) 21.

[5] V.B. Kazansky, M.V. Frash, R.A. van Santen, Quantum-chemical study of hydride transfer in catalytic transformation of paraffins on zeolites, in: S.-K.I. Hakze Chon, U. Young Sun (Eds.), Stud. Surf. Sci. Catal., Elsevier, Amsterdam, 1997, p. 2283.

[6] V.B. Kazansky, M.V. Frash, R.A. van Santen, Catal. Lett. 48 (1997) 61.

[7] M. Boronat, P. Viruela, A. Corma, J. Phys. Chem. B 103 (1999) 7809.

[8] M. Boronat, P. Viruela, A. Corma, Phys. Chem. Chem. Phys. 2 (2000) 3327.

[9] S. Ilias, A. Bhan, J. Catal. 290 (2012) 186.

[10] D.A. Simonetti, J.H. Ahn, E. Iglesia, J. Catal. 277 (2011) 173.

[11] D.A. Simonetti, J.H. Ahn, E. Iglesia, ChemCatChem 3 (2011) 704.

[12] J.E. Bercaw, P.L. Diaconescu, R.H. Grubbs, R.D. Kay, S. Kitching, J.A. Labinger, X. Li, P. Mehrkhodavandi, G.E. Morris, G.J. Sunley, P. Vagner, J. Org. Chem. 71 (2006) 8907.

[13] J.E. Bercaw, P.L. Diaconescu, R.H. Grubbs, N. Hazari, R.D. Kay, J.A. Labinger, P. Mehrkhodavandi, G.E. Morris, G.J. Sunley, P. Vagner, Inorg. Chem. 46 (2007) 11371.

[14] J.E. Bercaw, R.H. Grubbs, N. Hazari, J.A. Labinger, X. Li, Chem. Commun. (2007) 2974.

[15] J.E. Bercaw, N. Hazari, J.A. Labinger, V.J. Scott, G.J. Sunley, J. Am. Chem. Soc. 130 (2008) 11988.

[16] N. Hazari, J.A. Labinger, V.J. Scott, J. Catal. 263 (2009) 266.

[17] X. Sun, S. Mueller, Y. Liu, H. Shi, G.L. Haller, M. Sanchez-Sanchez, A.C. van Veen, J.A. Lercher, J. Catal. 317 (2014) 185.

[18] M. Bjørgen, S. Svelle, F. Joensen, J. Nerlov, S. Kolboe, F. Bonino, L. Palumbo, S. Bordiga, U. Olsbye, J. Catal. 249 (2007) 195.

[19] D.B. Lukyanov, J. Catal. 147 (1994) 494.

[20] M. Vandichel, D. Lesthaeghe, J. Van der Mynsbrugge, M. Waroquier, V. Van Speybroeck, J. Catal. 271 (2010) 67.

[21] Y.V. Joshi, K.T. Thomson, J. Catal. 230 (2005) 440.

[22] Y.V. Joshi, K.T. Thomson, J. Phys. Chem. C 112 (2008) 12825.

[23] S. Li, A. Zheng, Y. Su, H. Zhang, L. Chen, J. Yang, C. Ye, F. Deng, J. Am. Chem. Soc. 129 (2007) 11161.

[24] J. Kanellopoulos, A. Unger, W. Schwieger, D. Freude, J. Catal. 237 (2006) 416.

[25] S.M.T. Almutairi, B. Mezari, G.A. Filonenko, P.C.M.M. Magusin, M.S. Rigutto, E.A. Pidko, E.J.M. Hensen, ChemCatChem 5 (2013) 452.

[26] E.A. Pidko, S.M.T. Almutairi, B. Mezari, P.C.M.M. Magusin, E.J.M. Hensen, ACS Catal. 3 (2013) 1504.

[27] S. Schallmoser, T. Ikuno, M.F. Wagenhofer, R. Kolvenbach, G.L. Haller, M. Sanchez-Sanchez, J.A. Lercher, J. Catal. 316 (2014) 93.

[28] C. Mirodatos, D. Barthomeuf, J. Chem. Soc., Chem. Commun. (1981) 39.

[29] R. Gounder, A.J. Jones, R.T. Carr, E. Iglesia, J. Catal. 286 (2012) 214.

[30] O. Bortnovsky, P. Sazama, B. Wichterlova, Appl. Catal. A: Gen. 287 (2005) 203.

[31] B. Wichterlová, N. Žilková, E. Uvarova, J. Čejka, P. Sarv, C. Paganini, J.A. Lercher, Appl. Catal. A: Gen. 182 (1999) 297.

[32] J. Čejka, N. Žilková, Z. Tvarůžková, B. Wichterlová, Contribution of framework and extraframework Al and Fe cations in ZSM-5 to disproportionation and C_3 alkylation of toluene, in: B. Laurent, K. Serge (Eds.), Stud. Surf. Sci. Catal., Elsevier, Amsterdam, 1995, p. 401.

[33] P. Sazama, B. Wichterlova, J. Dedecek, Z. Tvaruzkova, Z. Musilova, L. Palumbo, S. Sklenak, O. Gonsiorova, Microporous Mesoporous Mater. 143 (2011) 87.

[34] W. Dai, X. Wang, G. Wu, N. Guan, M. Hunger, L. Li, ACS Catal. 1 (2011) 292.

[35] F. Schüßler, S. Schallmoser, H. Shi, G.L. Haller, E. Ember, J.A. Lercher, ACS Catal. 4 (2014) 1743.

[36] C. Sievers, A. Onda, R. Olindo, J.A. Lercher, J. Phys. Chem. C 111 (2007) 5454.

[37] J. Chen, J. Li, C. Yuan, S. Xu, Y. Wei, Q. Wang, Y. Zhou, J. Wang, M. Zhang, Y. He, S. Xu, Z. Liu, Catal. Sci. Technol. 4 (2014) 3268.

[38] W. Wu, W. Guo, W. Xiao, M. Luo, Chem. Eng. Sci. 66 (2011) 4722.

[39] G.J. Hutchings, F. Gottschalk, R. Hunter, Ind. Eng. Chem. Res. 26 (1987) 635.

[40] J.G. Dojahn, W.E. Wentworth, S.D. Stearns, J. Chromatogr. Sci. 39 (2001) 54.

[41] Y. Fu, H. Zhu, J. Shen, Thermochim. Acta 434 (2005) 88.

[42] E. Dumitriu, V. Hulea, I. Fechete, A. Auroux, J.-F. Lacaze, C. Guimon, Microporous Mesoporous Mater. 43 (2001) 341.

[43] M. Kaarsholm, F. Joensen, J. Nerlov, R. Cenni, J. Chaouki, G.S. Patience, Chem. Eng. Sci. 62 (2007) 5527.

[44] N.V. Pavlenko, Y.N. Kochkin, N.V. Vlasenko, K.N. Khomenko, V.V. Brei, Theor. Exp. Chem. 36 (2000) 103.

[45] A. Viola, S.A. Madison, Tetrahedron Lett. 18 (1977) 4495.

[46] J.F. DeWilde, C.J. Czopinski, A. Bhan, ACS Catal. 4 (2014) 4425.

Chapter 4

4. Formaldehyde chemistry in methanol conversion on H-ZSM-5

This chapter is based on:

S. Müller, Y. Liu, M. Sanchez-Sanchez, J.A. Lercher, "Formaldehyde chemistry in methanol conversion on H-ZSM-5", in preparation.

The role of formaldehyde in reaction and deactivation pathways of methanol-to-hydrocarbons (MTH) conversion has been elucidated applying H-ZSM-5 and methanol-to-olefin (MTO) conditions as examples. Temperature-programmed surface reactions showed that formaldehyde promoted first C-C bond and subsequent olefins formation. This has been unambiguously associated with the favoring of carbonylation reactions by decomposition of formaldehyde as well as with the participation of formaldehyde in following reaction steps. Addition of a low concentration of formaldehyde led to a higher deactivation rate compared to toluene cofeeding. This was linked to the presence of O-containing carbon deposits and to the partial transformation of latter coke into aromatic coke strongly chemisorbed onto Brønsted acid sites (BAS). This coke is different from the typical aromatic coke generated at long time on stream in MTO, which is trapped in the pores or deposited on the external surface with no or weak interaction with the BAS.

4.1 Introduction

The conversion of methanol to hydrocarbons (MTH) is considered a promising way of converting gas and coal to fuels and chemicals via methanol [1, 2]. By adjusting catalysts and reaction conditions, gasoline-range (methanol to gasoline; MTG) or olefin-range products (methanol to olefins; MTO) are selectively formed [1]. As a consequence of this versatility, methanol conversion has been commercialized in different variants [1, 3]. However, the single-pass selectivity in all these processes is low and recycling is required [3].

Understanding single steps within the complex reaction network of methanol conversion would allow tuning product selectivity in a certain direction. Thus, a lot of scientific efforts within the last 30 years have been devoted to understanding the reaction mechanism [1]. Early on, the MTH reaction was proposed to occur via an autocatalytic mechanism [4, 5]. However, no consensus existed on the issue whether olefins or aromatics are the critical species in MTH conversion. Dessau and co-workers suggested an olefin homologation/cracking route as the main reaction pathway at steady-state conditions [6, 7]. By co-processing olefins [8] and aromatics [9, 10] the co-catalytic effect on methanol conversion could be shown. Based on these observations, a "hydrocarbon pool" concept [11-13] was proposed in which products formation occurs by reaction of methanol with hydrocarbon fragments contained in the zeolite pores. This concept was refined by Svelle, Bjørgen and coworkers who proposed a dual-cycle mechanism. C_{3+} alkenes are involved in an alkene-based cycle while aromatics contribute predominantly to ethene formation in the so-called aromatics cycle [14, 15]. The relative contribution of each cycle depends on the local activities of specific hydrocarbon species and methanol conversion [16]. Recently, it has been proposed that the interaction of hydrocarbons and methanol is better described by an autocatalysis mechanism than by the original hydrocarbon pool mechanism. Accordingly, the acid site should predominantly be covered by methanol and attacked by mobile-phase hydrocarbons [16]. All these reports show unequivocally that the mechanistic pathways are still controversially discussed and a detailed understanding has not been achieved so far.

In Chapter 2, O-containing species were reported to cause fast deactivation during MTO conversion and it was hypothesized that the formation of these species requires the presence of formaldehyde. Furthermore, formaldehyde was found to be generated by the reaction of methanol and olefins at Lewis acid sites (LAS), promoting aromatics formation (see Chapter 3). Therefore, in light of these studies it is proposed that formaldehyde plays an important role during methanol conversion and that it must be included in the investigation of the mechanism.

Formaldehyde formation by disproportionation of methanol has been proposed in earlier reports. Kubelková et al. [17], for instance, reported formaldehyde and methane formation over H-ZSM-5 at 670 K and low methanol pressures (1-3 Pa). On the basis of these results a methane-formaldehyde mechanism was proposed, leading to first C-C bond and subsequent olefins formation. Hutchings et al. observed methane before C_2^+ hydrocarbons formation at low methanol coverage, supporting these results [18, 19]. According to theoretical calculations [20], the methanol-formaldehyde mechanism is feasible but difficult to occur due to a high energy barrier.

The present study aims to provide an overall picture of formaldehyde chemistry involved in MTO conversion. Accordingly, the formation of formaldehyde in MTO, the role of formaldehyde in the formation of the first olefinic product and its participation in the deactivation of an H-ZSM-5 catalyst were analyzed.

4.2   Experimental

4.2.1   Materials

The H-ZSM-5 catalyst with Si/Al = 90 used in this study was synthesized according to the procedure described by Ong et al. [21]. For some experiments, the catalyst was steamed at 753 K for 24 h with WHSV = 1 h^{-1} prior to usage. Accordingly, the samples are denoted as "H-ZSM-5 (90)" and "H-ZSM-5 (90, steamed)". For the TPSR/IR spectroscopy experiment an H-ZSM-5 with Si/Al = 15 was used (named as H-ZSM-5 (15)) which was purchased from Zeolyst.

Methanol (≥99.9%), toluene (99.9%) and dimethoxymethane (99%) were supplied by Sigma-Aldrich.

The BAS and LAS concentrations (determined by pyridine IR spectroscopy as described in chapter 2) of the H-ZSM-5 samples and the Na-ZSM-5 (90) are shown in Table 4.1.

Table 4.1. Concentrations of Brønsted acid sites (BAS) and Lewis acid sites (LAS) of the samples H-ZSM-5 and Na-ZSM-5 (determined by IR spectroscopy of adsorbed pyridine).

Sample	BAS (µmol / g)	LAS (µmol / g)
H-ZSM-5 (90)	150 ± 8	38 ± 2
H-ZSM-5 (90, steamed)	68 ± 3	39 ± 2
Na-ZSM-5 (90)	7 ± 1	181 ± 9
H-ZSM-5 (15)	920 ± 46	260 ± 13

4.2.2 TPSR/IR spectroscopy

Temperature-programmed surface reactions (TPSR) of methanol (MeOH) and dimethoxymethane (DMM) were performed in a home-made IR cell connected to a mass spectrometer. A self-supporting wafer of 25 mg H-ZSM-5 (15) was loaded in the cell center and perpendicular to the IR beam. The wafer was first activated at 723 K in vacuum for 1 h. After cooling down to 313 K, 3 mbar MeOH or 1 mbar DMM was introduced into the cell and kept for 15 min followed by desorption in vacuum for 30 min. Then, the wafer temperature was increased to 723 K with a rate of 3 K/min. Desorbed molecules were detected on line using mass spectrometry. *In-situ* IR spectra of the wafer were collected on a Bruker Vertex 70 FTIR spectrometer.

4.2.3 Temperature-programmed oxidation of spent catalysts

Thermogravimetric analysis (TGA) on a SETARAM Sensys Evo TGA-DSC was utilized to analyze coke deposition on deactivated catalysts. After treating 10-20 mg powdered sample (free of SiC) at 473 K in 16 mL/min He flow until weight stabilization, the temperature was raised to 923 K at 5 K/min in 16 mL/min O_2/He (1/9) flow and kept for 1 h. The coke amount was estimated from the total weight loss.

4.2.4 Catalytic testing

Catalytic measurements were performed in a fixed bed quartz reactor with an internal diameter of 6 mm at 723 K and ambient pressure. The H-ZSM-5 catalysts (200-280 μm) were homogeneously diluted with silicon carbide (ESK-SiC) in the range of 355-500 μm to ensure temperature uniformity. Catalysts were activated at 723 K for 1 h under N_2 atmosphere before reaction.

To investigate the deactivation with a pure methanol, a mixed methanol/dimethoxymethane and a mixed methanol/toluene feed, 105 mg H-ZSM-5 was deactivated for 18 h. The methanol partial pressure was maintained at 100 mbar. Methanol vapor was fed by passing N_2 through the methanol-containing saturator which was thermo-stated at 299 K. For toluene and dimethoxymethane (decomposition into dimethyl ether and formaldehyde under reaction

conditions) co-feeding, the vapor was introduced by passing dry N_2 flow through saturators containing the liquid reactants. The reactor effluents were transferred via a heated line into a gas chromatograph (HP 5890) equipped with a HP-PLOTQ capillary column. The concentration of co-feed is given as a molar ratio of its partial pressure to methanol partial pressure (100 mbar). The product distributions were given on a carbon basis, whereby the carbon in the methanol feed with a partial pressure of 100 mbar was defined as 100%.

For detecting species containing carbonyl groups, DMM was reacted on 5 mg H-ZSM-5 (90, steamed) at a partial pressure of 171 mbar, so that the yield of hydrocarbons was below 0.5 C %. Before the product stream was passed to the exhaust, it was condensed utilizing a mixture of isopropyl alcohol and dry ice. Subsequently, GC-MS analysis was conducted on a gas chromatograph–mass spectrometer (GCMS-QP2010S, Shimadzu) after diluting the condensed phase with methanol.

For investigating MeOH reaction on Na-ZSM-5 (90) (50 mg) and H-ZSM-5 (90) (2 mg) two reactors were connected in series as shown in Figure 4.1. The MeOH partial pressure was kept at 178 mbar. Products were analyzed using an IR detector.
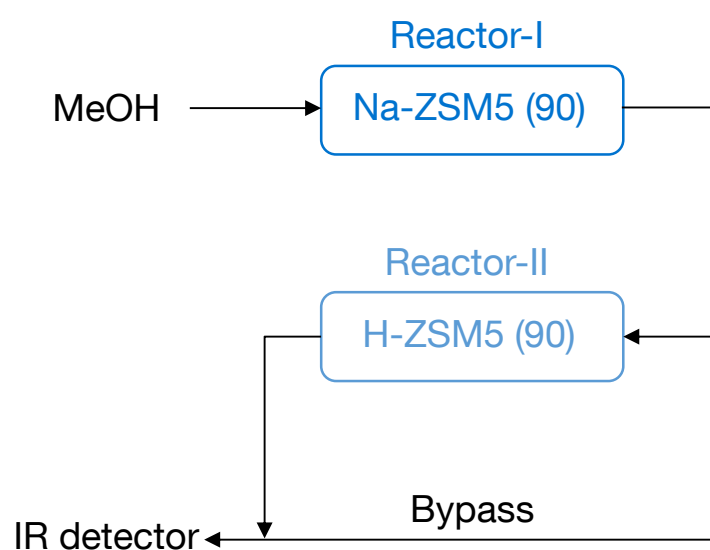
Figure 4.1. Experimental setup for MeOH reaction on Na-ZSM-5 (90) and H-ZSM-5 (90) in sequence (MeOH conversion <0.5 C %).

4.3 Results

4.3.1 Formaldehyde formation under MTO conditions

In exploring the role of formaldehyde in MTO conversion, the different pathways of formaldehyde formation are addressed first.

The disproportionation of methanol to methane and formaldehyde on H-ZSM-5 has been previously reported in literature on the basis of production distribution analysis [17-19], without, however, giving a detailed explanation on the mechanism. Here, the role of LAS and BAS of H-ZSM-5 for this disproportionation reaction is explored. Comas-Vives et al. [22] investigated MeOH disproportionation on γ-Al$_2$O$_3$ using combined IR- and solid-state NMR-spectroscopy and found this reaction to occur at LAS. To check whether this proposal is also valid for a MFI catalyst, where extra-framework Al is present providing LAS, the reaction of methanol over a Na-ZSM-5 (90) was studied. In the absence of BAS, conversions below 0.5 C % were reached and methane, formaldehyde and CO were detected (Figure 4.2). The formation of these compounds is assigned to the disproportionation reaction of methanol on LAS available in the Na-ZSM-5 (90). In order to determine whether formaldehyde can also be generated at BAS, the reactor filled with 50 mg Na-ZSM-5 (90) was connected with a second reactor filled with a small amount of H-ZSM-5 (90) (2 mg). Interestingly, more methane and less formaldehyde are initially detected compared to the pure Na-ZSM-5 experiment (Figure 4.2). This implies that formaldehyde is formed over Na-ZSM-5 and subsequently strongly adsorbed on H-ZSM-5. Since more methane was formed, it is proposed that two methanol molecules can react on BAS to form methane and formaldehyde via disproportionation through hydrogen transfer. In fact, with longer time on stream (TOS), methane formation declined and the amount of formaldehyde detected increased, finally reaching almost the levels of the Na-ZSM-5-only reaction. This indicates that the conversion of methanol to methane and formaldehyde at BAS was nearly suppressed, probably due to strong adsorption of formaldehyde on the BAS. Conversely, the CO amount detected after passing the H-ZSM-5 catalyst was lower in comparison to the Na-ZSM-5-only case and decreased continuously in the time range investigated. This suggests that CO was consumed on BAS by carbonylation reactions.
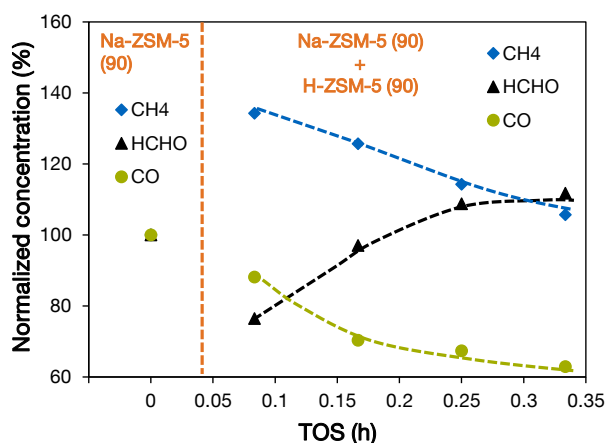
Figure 4.2. Formation of CH₄, HCHO and CO on Na-ZSM-5 (90); change of CH₄, HCHO and CO concentration formed over Na-ZSM-5 (90) by interaction with H-ZSM-5 (90). MeOH/DME conversion was <0.5 C %.

4.3.2   Role of formaldehyde in first C-C bond and first olefins formation

Having shown that formaldehyde can be formed from methanol under typical MTO conditions, the question arises in which steps of the complex reaction network of methanol conversion formaldehyde participates. In order to answer this, the impact of present formaldehyde on the activity and product distribution of MTO was studied. For this, DMM and MeOH TPSR experiments on an H-ZSM-5 were conducted. DMM was chosen because it decomposes on the zeolite into HCHO and DME, simulating the reaction of surface methyl groups with formaldehyde. In this way, a comparison of a MeOH TPSR experiment (only surface methyl groups present) with a TPSR in presence of a known amount of formaldehyde is possible.

In the MeOH TPSR experiment on H-ZSM-5 (15) (Figure 4.3 (b)), MeOH desorbed with a maximum at approximately 360 K. At this temperature, DME appeared due to the equilibration of MeOH and DME, reaching the maximum desorption at 440 K. The MeOH-DME equilibration was not observed for DMM as reactant (Figure 4.3 (a)) because DMM decomposes into HCHO and DME. Surface methyl groups are then directly generated and equilibrated without going through the MeOH to DME step which was monitored for the pure MeOH feed. Since surface methyl species are generated from MeOH and DME, the reaction should not be affected by the MeOH-DME equilibration. Both ethene and propene (lumped together as olefins) started to form and desorb at 470 K in the DMM TPSR experiment with the maximum of desorption at 560 K (Figure 4.3 (a)), while aromatics formation started at 520 K

with the maximum of desorption at 620 K. Conversely, in the MeOH TPSR experiment olefins appeared at approximately 570 K and aromatics started to be produced at 600 K (Figure 4.3 (b)). In both cases, the compounds desorbed with maxima at 633 K. Since olefins were detected at lower temperature for DMM, it is proposed that the presence of formaldehyde favors olefins formation. Aromatics appeared after olefins for MeOH and DMM, indicating that olefins are the first hydrocarbons formed. Interestingly, olefins were detected over a broader temperature range in the DMM experiment in comparison to the MeOH experiment. Furthermore, the temperatures of the maximum desorption for olefins and aromatics were similar under pure MeOH feed. Conversely, the rate of aromatics desorption for the DMM feed reached the maximum at higher temperatures than olefins desorption and was almost constant from 580 to 650 K, in the range of the declining olefin peak. Thus, it is speculated that the presence of formaldehyde promotes an additional pathway to aromatics.
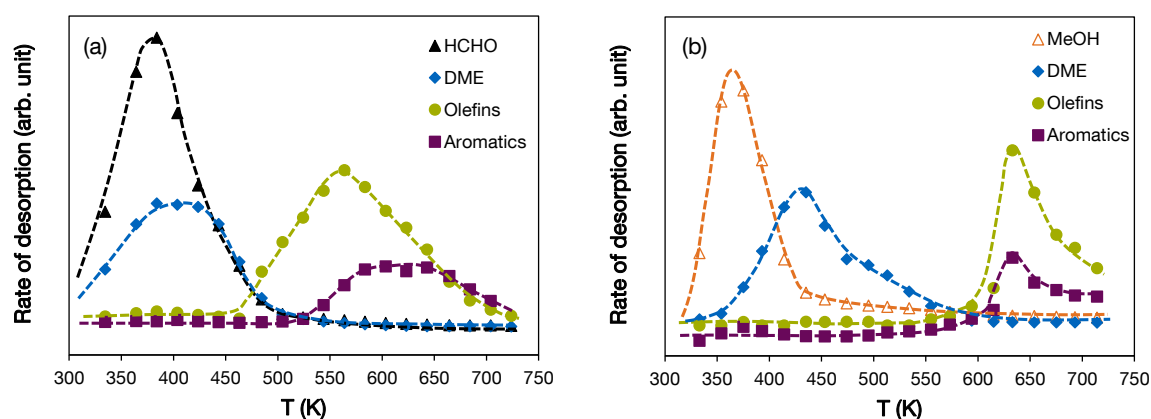
Figure 4.3. Temperature-programmed surface reactions of dimethoxymethane (a) and methanol (b) on H-ZSM-5 (15). Desorbed molecules were detected on line using mass spectrometry.

Further information can be derived from *in-situ* IR spectra of the surface species generated after MeOH and DMM was adsorbed on H-ZSM-5 (15) at 313 K and subsequent temperature ramp. At 473 K, olefins readily desorbed in the DMM TPSR experiment, but not in the MeOH TPSR experiment (Figure 4.4 (a)). *In-situ* IR spectra of H-ZSM-5 (15) at 473 K showed a series of vibrations from 1670 to 1770 cm^{-1} and bands at 1620, 1469 and 1450 cm^{-1} when DMM had been adsorbed at 313 K, while no vibrations between 1670 and 1770 cm^{-1} were detected at this temperature in the case of methanol (Figure 4.4 (b)). The overlapping bands between 1670 and 1770 cm^{-1} which cannot be clearly separated are assigned to stretching vibrations of different carbonyl groups [23] while the band at 1620 cm^{-1} is attributed to the deformation vibration of adsorbed water [24] and the bands at 1469 and 1450 cm^{-1} originate from CH deformation

vibrations [25] of surface methyl groups. Due to the absence of C=O stretching bands for MeOH, the higher reactivity of DMM is tentatively attributed to the existence of surface carbonyl groups. In order to test this, it must be probed if the surface carbonyl groups are consumed during olefin formation.
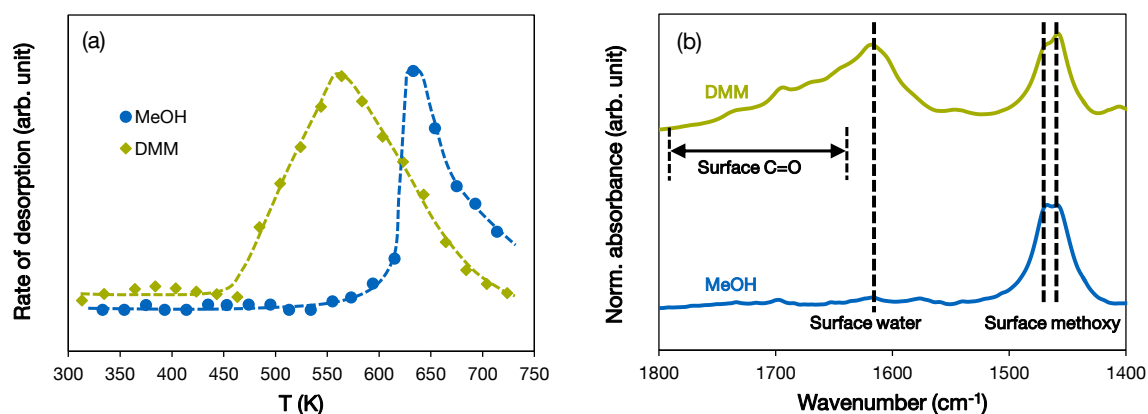
Figure 4.4. Olefin desorption profiles for MeOH and DMM in TPSR experiments (a); *in-situ* IR spectra of H-ZSM-5 (15) at 473 K. MeOH and DMM were adsorbed at 313 K, followed by desorption in vacuum. Wafer temperature was increased to 723 K at 3 K/min (b).

Figure 4.5 shows *in-situ* IR spectra of H-ZSM-5 (15) at temperatures of 473 K, 523 K, 573 K and 623 K after DMM adsorption at 313 K, followed by evacuation and temperature increase of the wafer. From 473 to 623 K, the vibration bands of surface carbonyl groups in the range of 1670 to 1770 cm^{-1} decreased remarkably. In turn, the olefin desorption profile reached a maximum at 560 K and decreased afterwards (Figure 4.4 (a)). This indicates that surface carbonyl groups generated from formaldehyde were consumed along with the formation of olefins. The participation of formaldehyde in the formation of olefins is further supported by the fact that surface carbonyl groups appeared only at 573 K in the MeOH TPSR (Figure 4.6), which is coincident with the onset of olefin formation in this experiment.

With the aim of identifying the species containing carbonyl groups, DMM was reacted on H-ZSM-5 (90, steamed) at 723 K and the exhaust gas stream was condensed utilizing a mixture of dry ice and isopropyl alcohol. GC-MS analysis of the condensed phase revealed the presence of methyl methoxyacetate with a mass pattern of 31 Da (CH_3O^+), 45 Da ($CH_3OCH_2^+$) and 74 Da ($CH_3OCH_2CO^+$) (Figure 4.7). The formation of this species is assigned to the carbonylation of dimethoxymethane. Thus, it is proposed that MeOH and DME undergo carbonylation in a similar way.
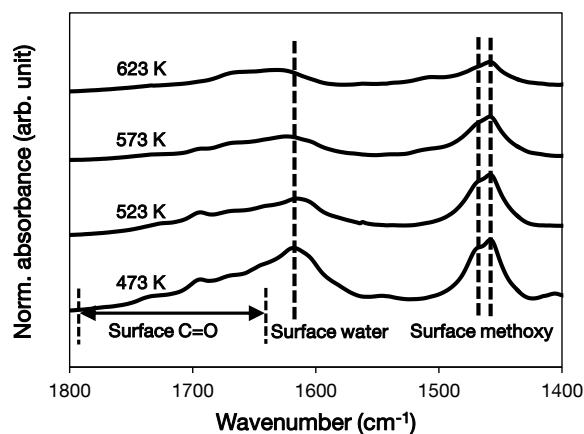
Figure 4.5. *In-situ* IR spectra of H-ZSM-5 (15) in TPSR of DMM (adsorbed at 313 K) at 473 K, 523 K, 573 K and 623 K.
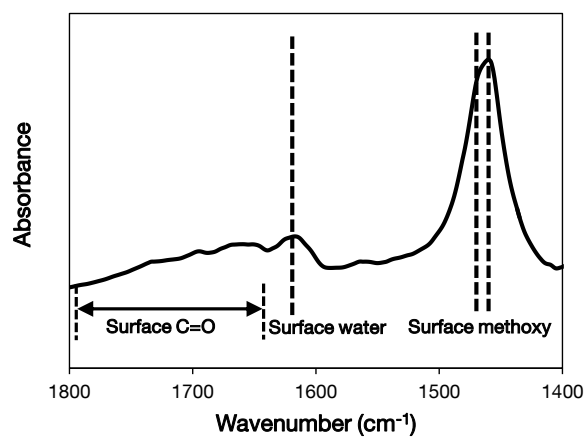
Figure 4.6. *In-situ* IR spectrum of H-ZSM-5 (15) in TPSR of MeOH (adsorbed at 313 K) at 573 K.
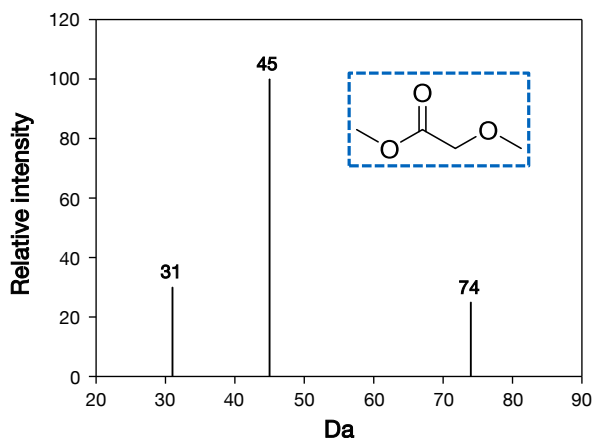
Figure 4.7. MS fragmentation pattern of methyl methoxyacetate which was found in the condensed exhaust gas stream of DMM reaction on H-ZSM-5 (90, steamed) at 723 K and p_{DMM} = 171 mbar.

4.3.3   Role of formaldehyde in deactivation

So far, it has been shown that formaldehyde is formed in different ways under MTO conditions and that formaldehyde favors the formation of olefins as the first hydrocarbon species. In Chapter 2, it was shown that O-containing species cause fast deactivation during MTO conversion and it was hypothesized that the formation of these species requires the presence of formaldehyde. Thus, the role of formaldehyde in deactivation was addressed as a next step, comparing the deactivation under a pure methanol feed with a mixed methanol/DMM feed. To support the hypothesis that formaldehyde induces stronger deactivation than aromatics, the impact of co-feeding toluene on deactivation was examined as well.

Figure 4.8 shows the MeOH/DME conversion as a function of TOS for the pure methanol feed and for the feeds containing 3 C % DMM and 1 C % toluene. For the pure MeOH feed, the rate of deactivation was slightly higher within the first 2 h TOS in comparison to longer TOS. Co-feeding 1 C % toluene resulted in higher initial conversion because the initiation phase was shortened by the co-fed aromatics [3], which act as initiators of the hydrocarbon pool and propagate the aromatics-based cycle [16]. However, the rate of deactivation was higher than for the pure MeOH feed and remained constant throughout the reaction. On the other hand, co-feeding 1 C % DMM led to lower initial conversion in comparison to the pure MeOH feed, suggesting that formaldehyde deactivated the catalyst rapidly at very short TOS (before the first data point could be taken). The conversion decreased faster in the first 2 h than at longer TOS. With longer TOS the rate of deactivation was apparently similar to cofeeding toluene. It is important to point out that the initial conversion levels in all three experiments were different, even though the MeOH-related contact times are approximately the same. Thus, the rate of deactivation was normalized to the respective MeOH/DME conversions for gaining further insights. From Figure 4.9, it is clearly evident that the normalized rate of deactivation was highest with DMM cofeeding at all TOS. In the toluene cofeeding experiment, the rate of deactivation was about half of that when cofeeding DMM. This suggests that high concentrations of formaldehyde promote faster deactivation pathways than toluene. Interestingly, the normalized rate of deactivation was initially higher for a pure MeOH feed than for a mixed MeOH/toluene feed, suggesting that toluene cofeeding counteracts fast initial deactivation by promoting the aromatics-based cycle, whereas initially a large amount of highly deactivating species formed for a pure MeOH feed. These species are proposed to form under involvement of formaldehyde which is deduced from the empirical observation that deactivation rates are higher for pure MeOH and mixed MeOH/DMM feeds at short TOS. After

4-h TOS, the deactivation rate was clearly lower under pure MeOH than under a MeOH/toluene feed. Thus, it is hypothesized that the formation rate of these highly deactivating species for the pure MeOH feed declines and that deactivation by toluene-derived species gains in importance.
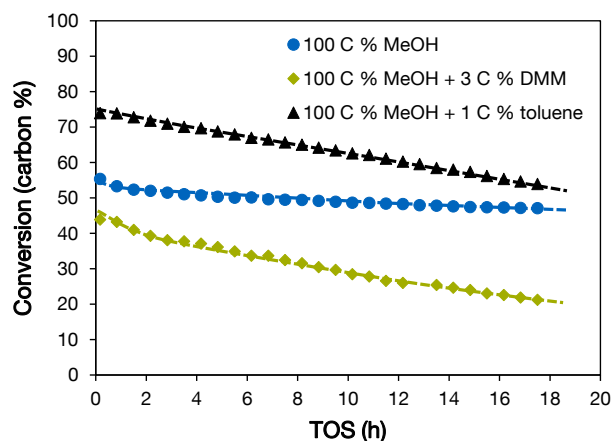
Figure 4.8. Change of MeOH/DME conversion during MTO reaction of 105 mg H-ZSM-5 (90, steamed) for a pure MeOH feed and feeds containing either 3 C % dimethoxymethane (DMM) or 1 C % toluene at p_{MeOH} = 100 mbar and T = 723 K.
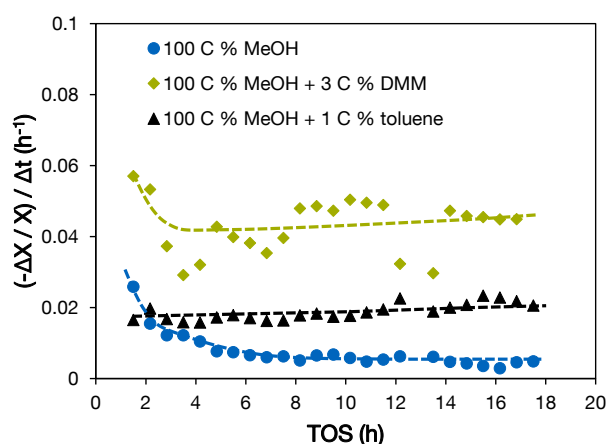
Figure 4.9. Normalized rate of deactivation as a function of TOS for the pure MeOH feed, for the feed containing 3 C % DMM and for the feed containing 1 C % toluene over 105 mg H-ZSM-5 (90, steamed) at p_{MeOH} = 100 mbar and T = 723 K.

Inspired by the fact that the rate of deactivation is associated with the composition of the feed, TPO experiments were designed to analyze the amount and type of coke formed in each case. In Chapter 2, it was reported that two types of carbon deposits form on an H-ZSM-5 during MTO reaction. These two types of coke can be differentiated by their heat of combustion and therefore their different temperature of the maximum in the TPO profiles, and are named

coke-I and coke-II. Coke-I represents O-containing carbon deposits. The average composition of coke-II corresponds to an aromatic hydrocarbon. Accordingly, Table 4.2 depicts the results obtained by TGA analysis.

Table 4.2. Total coke deposition, amounts of coke-I and coke-II, normalized to consumed MeOH after 17.5 h reaction over H-ZSM-5 (90, steamed) at p_{MeOH} = 100 mbar and T = 723 K.

Feed	Coke wt.% / mol_{MeOH} converted	Coke-I wt.% / mol_{MeOH} converted	Coke-II wt.% / mol_{MeOH} converted
100 C % MeOH	2.8	0.31	2.5
100 C % MeOH + 3 C % DMM	11.0	0.21	10.7
100 C % MeOH + 1 C % toluene	6.0	0.20	5.8

Both cofeeding DMM and toluene resulted in higher overall coke selectivity after 17.5 h TOS in comparison to a pure MeOH feed. The differences in coke selectivity (Table 4.2) can be well correlated with the observed differences in deactivation rates (Figure 4.9). For the MeOH/DMM (MeOH/formaldehyde) feed, the selectivity towards coke-II was almost twice than when cofeeding toluene, whereas comparable coke-I selectivities were observed. Under a pure MeOH feed, higher coke-I selectivity was obtained in comparison to the mixed feeds.

From Figure 4.9 it is clearly evident that the catalyst deactivates initially faster for both the pure MeOH feed and the mixed MeOH/DMM feed, despite different coke distribution after 17.5 h TOS (Table 4.2). Since O-containing coke-I is expected to be more deactivating (Chapter 2) and to be favored by higher concentrations of formaldehyde as further oxidized species of methanol, it is hypothesized that initially high amounts of coke-I are formed for the MeOH/DMM feed which are, however, transformed by reaction with additional formaldehyde at longer TOS.

4.4 Discussion

It is commonly accepted that unravelling the reaction mechanism of MTO conversion is required for controlling product selectivity and retarding catalyst deactivation. This is, however, a demanding task due to the complex reaction network [1, 2, 26]. The formation of the first C-C bond has been under debate [20, 27, 28] since the first report about methanol conversion on zeolites by Chang and Silvestri [4], including our recent proposal of carbonylation reactions as a key step [29]. Despite discrepancies in explaining the formation of the first C-C bond, the

formation of C_{2-4} olefins under steady-state operation is nowadays mostly explained by a dual olefin and aromatic methylation catalytic cycle [2]. As a refinement of the early dual cycle concept in which propene solely formed in the olefin cycle, it has been discussed recently that propene was also generated in the aromatics cycle and might compete with aromatics, propagating the olefins cycle [16]. On the basis of these results, a modified dual-cycle mechanism was proposed (Scheme 4.1).
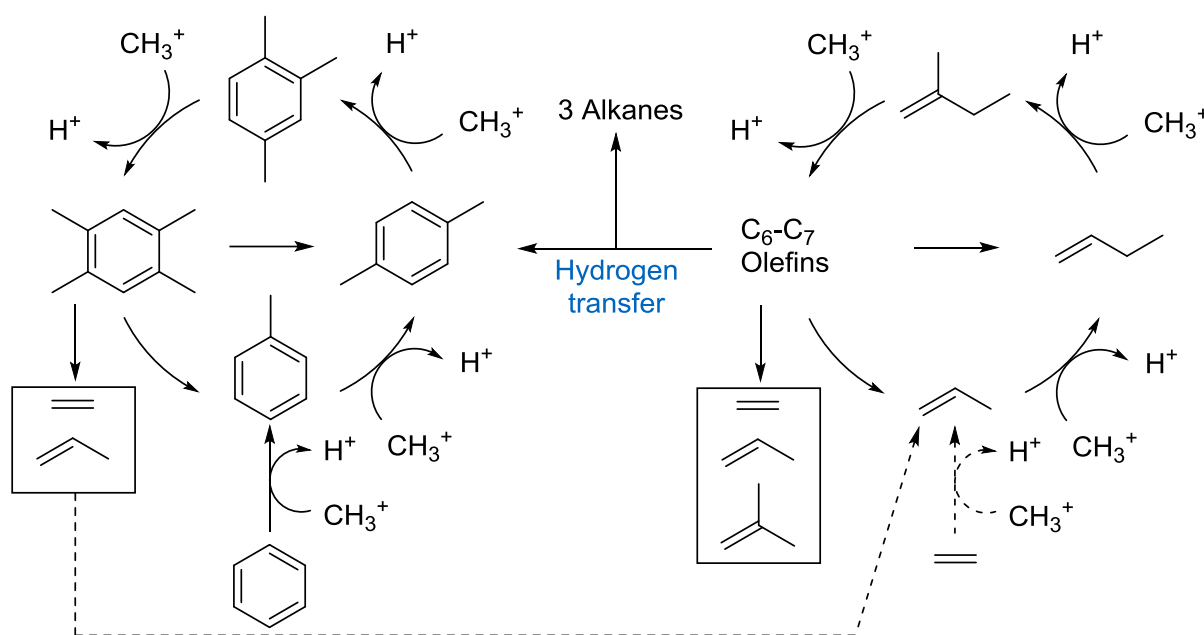
Scheme 4.1. Modified dual-cycle mechanism in operation during MTH catalysis on H-ZSM-5 under MTO conditions [16].

In Chapter 2, O-containing species were reported to cause fast deactivation and it was hypothesized that these species are formed via intermediates derived from formaldehyde. Furthermore, it was shown in Chapter 3 that a MeOH-induced hydrogen transfer pathway exists, leading to formaldehyde formation and favoring aromatics. Thus, it is believed that most of the former investigations that consider only hydrocarbons as key species give inevitably an incomplete picture on the chemistries involved in MTO conversion. In light of these observations, formaldehyde chemistry must be included in the reaction network, especially when addressing the primary steps initiating methanol conversion and coke formation.

At first, it is important to examine the formation of formaldehyde during MTO conversion. Very recently, Comas-Vives et al. [22] reported dimethyl ether activation on the 110 facet of γ-Al_2O_3, yielding methane, alkenes and surface formate species. This was explained by the disproportionation reaction to methane and formaldehyde as well as first carbon-carbon bond formation on extra-framework Al. The reaction of methanol on Na-ZSM-5 (Figure 4.2)

demonstrated that formaldehyde is also formed at LAS of a MFI catalyst by disproportionation. The connection of two reactors, the first one filled with Na-ZSM-5, the second one with only a small amount of H-ZSM-5, enabled to identify another pathway for formaldehyde formation. Since the methane yield was higher after the reactor sequence Na-ZSM-5/H-ZSM-5 in comparison to Na-ZSM-5 (Figure 4.2), methane and formaldehyde are proposed to form at BAS via a reaction sequence illustrated in Scheme 4.2, in accordance with an early suggestion of Hutchings et al. [18]. In such mechanism, a methyl group is reduced by hydride transfer from methanol. This may be relevant during the initiation phase of MTO conversion when no or little olefin species exist [16]. Because the initial formaldehyde concentration over Na-ZSM-5/H-ZSM-5 was lower compared to the Na-ZSM-5 reaction (Figure 4.2), it was concluded that formaldehyde formed on the available LAS of Na-ZSM-5 as well as by the HT reaction between two methanol molecules on BAS (Scheme 4.2) adsorbs competitively on BAS with respect to methanol and may cause deactivation of the site. If olefins are present, strongly adsorbed formaldehyde further reacts with olefins to an allylic alcohol (Scheme 4.3) releasing the BAS. The allylic alcohol can then dehydrate to a diene. It should be noted that a certain amount of methanol decomposes on inert materials such as SiC under MTO conditions [29].
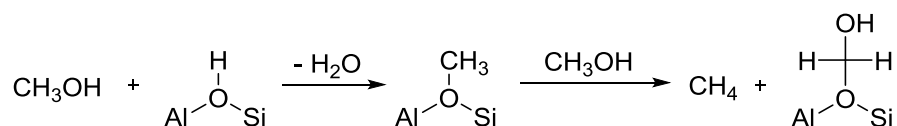
Scheme 4.2. Proposed reaction mechanism for methane and formaldehyde (BAS adsorbed CH_2O) formation via hydrogen transfer between two methanol molecules on BAS.
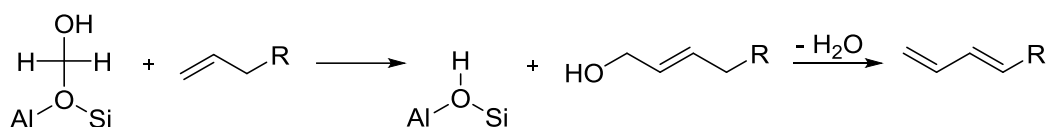
Scheme 4.3. Release of surface adsorbed formaldehyde by reaction with an olefin to an allylic alcohol, thereby recovering the BAS. In the following step, a diene species forms.

Having established the different ways of formaldehyde formation under MTO conditions, the importance of formaldehyde in the reaction pathway is discussed. In the TPSR experiment conducted under a DMM feed (that is, under a methanol feed with higher concentrations of formaldehyde), olefins are formed at lower temperature than for pure MeOH (Figure 4.4 (a)). This is indicative of the participation of formaldehyde in first C-C bond formation and suggests that olefins are the first gas phase products formed. IR bands originating from surface carbonyl

groups were only observed at 473 K when DMM was used as reactant (Figure 4.4 (b). At this temperature, olefins were already detected in the gas phase in this experiment, while for the TPSR under pure MeOH both surface carbonyl species and gas phase olefins were detected at 573 K. Thus, the presence of formaldehyde promotes CO formation and in consequence the formation of surface carbonyl groups. These carbonyl species are consumed during reaction (Figure 4.5) indicating that they are important for the formation of olefins. Methyl methoxyacetate was detected for the DMM reaction on H-ZSM-5 (Figure 4.7), which is the carbonylation product of DMM [30]. Therefore, it is proposed that surface methyl groups generated from MeOH or DME can undergo carbonylation in a similar manner (Scheme 4.4). The formed surface acetyl group reacts with methanol (Scheme 4.4 (a)) or water (Scheme 4.4 (b)), restoring the Brønsted acid site. Because of the remarkable impact of formaldehyde, it is hypothesized that surface acetyl groups react with formaldehyde, leading to 3-hydroxypropionyl groups (Scheme 4.4 (c)).
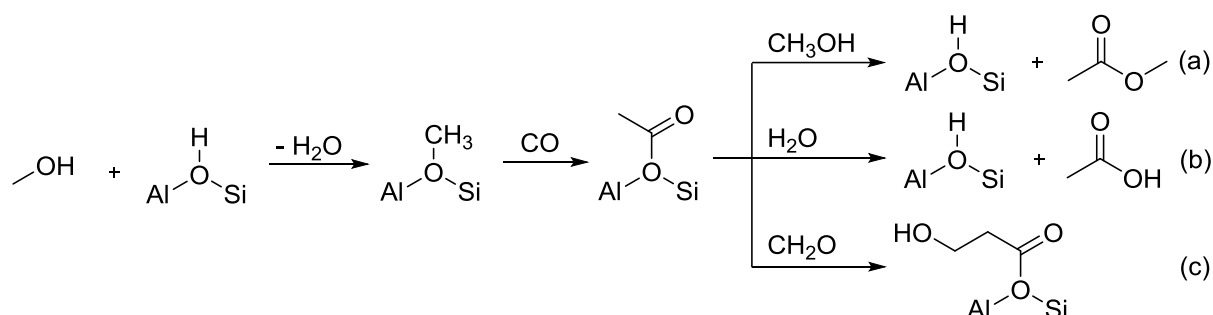
Scheme 4.4. Mechanistic proposal for the formation of the first C-C bond by carbonylation of surface-adsorbed methanol, followed by reaction with methanol (a), water (b) or formaldehyde (c).

Due to the favored olefin formation observed in presence of formaldehyde (Figure 4.4), it is proposed that the 3-hydroxypropionyl group (generated as shown in Scheme 4.4 (c)) dissociates into 3-hydroxypropionic acid (Scheme 4.5 (b)). Subsequent dehydration results in the formation of acrylic acid which can react to ethene by decarboxylation (Scheme 4.5 (b)). In addition, acrylic acid may react to propene via methylation and decarboxylation reactions (Scheme 4.5 (c)). Alternatively, propene can also be formed by ketonic decarboxylation of acetic acid, followed by Meerwein-Ponndorf-Verley reduction and dehydration (Scheme 4.5 (a)). With regard to the reactions illustrated in Scheme 4.4, it is important to point out that formaldehyde has, according to this proposal, a dual function in the mechanism of olefins formation from methanol. On one hand, it decomposes into CO which takes part in

carbonylation reactions (Scheme 4.4). On the other hand, formaldehyde itself takes part in an aldol reaction (Scheme 4.4 (c)).

In light of the remarkable enhancement of olefins formation by formaldehyde cofeeding, also an alternative to the mechanism depicted in Schemes 4.4 and 4.5 should be put forward. The mechanism (Scheme 4.6 (a)) assumes that a surface hydroxymethyl group, which is generated due to strong chemisorption of formaldehyde on BAS, is carbonylated to form a surface glycolate. Due to keto-enol tautomerism, methylation can subsequently occur, followed by reaction with water and restoration of the BAS. Acrylic acid is formed by dehydration of 2-hydroxypropionic acid (Scheme 4.6 (a)). It can then either decarboxylate and react to ethene as shown in Scheme 4.6 (b) or further react by methylation and decarboxylation to finally form propene (Scheme 4.6 (c)).
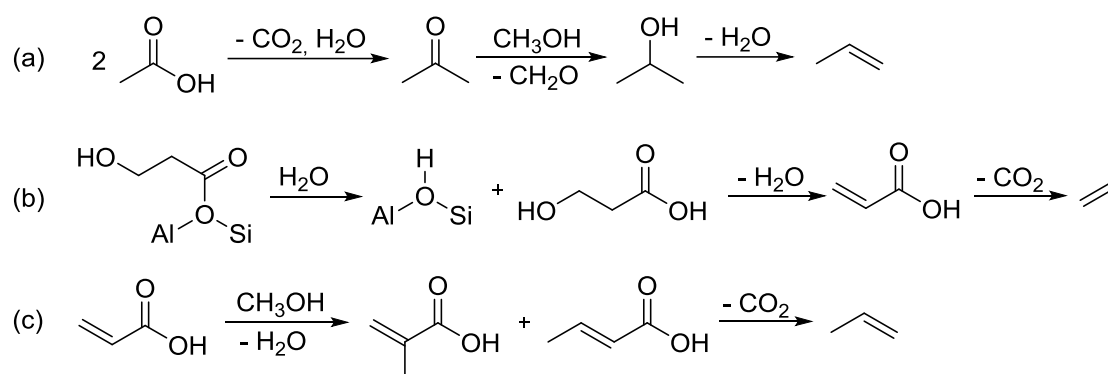
Scheme 4.5. Possible mechanism for propene formation from acetic acid (a). Mechanistic proposal for ethene formation from a 3-hydroxypropionyl group via intermediate formation of acrylic acid (b). Proposed mechanistic pathway for the formation of propene from acrylic acid via methylation and decarboxylation (c).

Formaldehyde is, however, not only involved in the formation of the first C-C bond and of first olefins, but also in aromatics formation. DMM TPSR (Figure 4.3 (a)) showed that aromatics formation was constant in the temperature range of 580-650 K, while olefins formation and desorption declined. Such stabilization in aromatics formation and desorption could, however, not be observed in the MeOH TPSR experiment and therefore it is concluded that another aromatics formation pathway must exist that involves formaldehyde. This pathway is related to the formation of a diene species as first step, starting from a surface hydroxymethyl group (Scheme 4.3). Such diene species would be protonated forming a carbenium ion at BAS, followed by condensation reaction with an olefin (Scheme 4.7 (a)). After a hydride shift

(Scheme 4.7 (b)), aromatics and paraffins can be formed by cyclization and dehydrogenation through hydrogen transfer reactions (Scheme 4.7 (c))
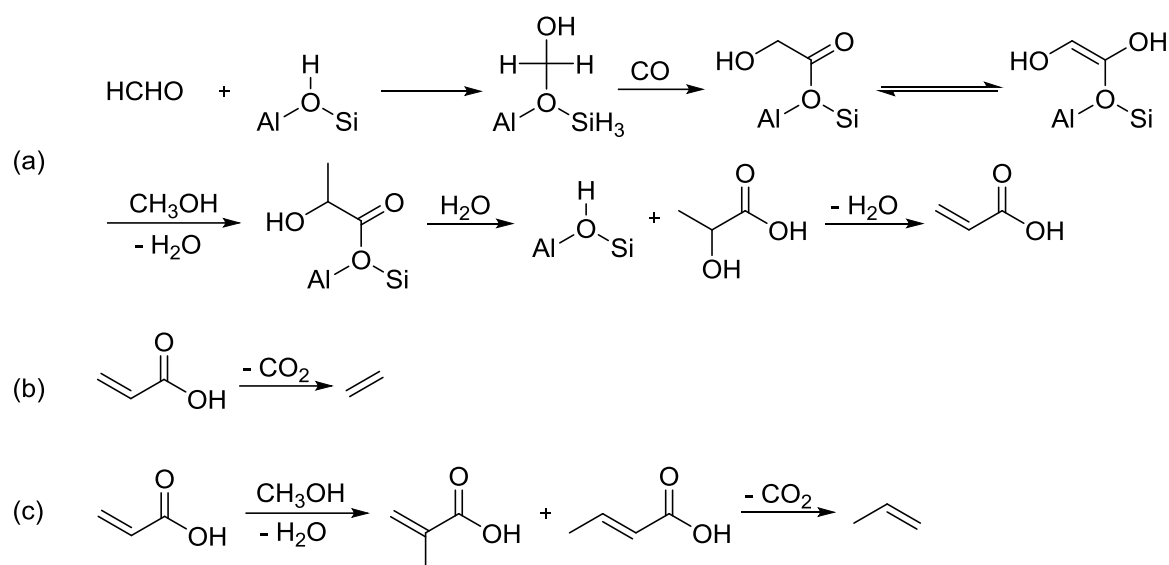
Scheme 4.6. Proposed mechanism for acrylic acid formation via several steps, starting from a surface hydroxymethyl group (generated by formaldehyde adsorption on BAS) (a). Possible mechanisms for ethene (b) and propene (c) formation from acrylic acid.
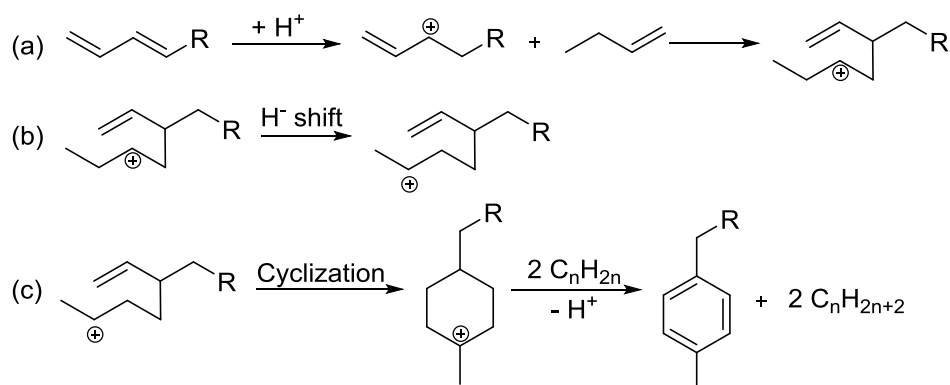
Scheme 4.7. Mechanistic proposal for the reaction of a diene species, which formed by reaction of formaldehyde and olefins at BAS (as exemplarily depicted in Scheme 4.3), to aromatics.

So far, it has been shown that formaldehyde favors olefins formation at short contact time and can also promote aromatics formation in secondary reaction steps. A higher selectivity towards aromatics is often associated with the promotion of deactivation because aromatics are precursors of coke [2, 3]. Furthermore, it was hypothesized in Chapter 2 that formaldehyde triggers the formation of highly deactivating O-containing carbon deposits and increases the amount of aromatic-type coke species. Therefore, the role of formaldehyde in the deactivation of an H-ZSM-5 catalyst was studied in detail by comparing the deactivation rate under a pure

MeOH feed with mixed MeOH/DMM and MeOH/toluene feeds (Figures 4.8 and 4.9). Despite the promoting effect of formaldehyde on the formation of olefins and aromatics observed in the TPSR experiment (Figure 4.3), the conversion decreased rapidly under a MeOH/DMM feed (Figure 4.8) and the normalized deactivation rate was the highest at all TOS (Figure 4.9), in comparison to the pure MeOH and mixed MeOH/toluene feeds. This is a first indication that formaldehyde is responsible for the formation of strongly deactivating species throughout the reaction. Because the conversion was remarkably lower at 10 min TOS (first data point which was taken) under a MeOH/DMM feed compared to the pure MeOH and mixed MeOH/toluene feeds (Figure 4.8), it is proposed that a large fraction of these species is formed in particular in the first stages, that is, when the fresh catalyst is in contact with high methanol concentrations. Considering the results of methanol conversion over Na-ZSM-5/H-ZSM-5 (Figure 4.2), formaldehyde adsorption forming a hydroxymethyl group might cause strong deactivation by BAS coverage at the beginning of the reaction, inhibiting the development of the MTO reaction network. However, the hydroxymethyl group can be eventually converted by reaction with CO, available due to methanol disproportionation and following decomposition, to form a surface glycolate. This species can participate subsequently in olefins formation (Scheme 4.6). Alternatively, the surface hydroxymethyl group can react with olefinic products present in the zeolite pores to dienes (Scheme 4.3).

The proposal on the formation of strongly deactivating species driven by formaldehyde is further supported by the observations regarding coke deposits and deactivation of the catalyst under different feeds. The deactivation rates obtained for feeds composed by MeOH, MeOH/DMM and MeOH/toluene correlated with the overall coke selectivities, and, in particular with the selectivities towards coke-II (Figure 4.9 and Table 4.2). Interestingly, the quantification of coke deposits (Table 4.2) showed that at 17.5 h TOS the selectivity towards O-containing coke-I was lower for the mixed methanol/dimethoxymethane feed compared to the pure methanol feed, while coke-II selectivity was four times higher. This clearly shows that formaldehyde promotes the formation of aromatic-type coke-II. On the other hand, it is evident that fast deactivation occurs in the first hours on stream under a MeOH/DMM feed (Figure 4.8). As discussed above, the chemistry involving hydroxymethyl groups and the presumed deactivation of BAS by strong adsorption of formaldehyde is only relevant at the first stages because surface hydroxymethyl groups can be converted to dienes (Scheme 4.3) or acrylic acid (Scheme 4.6 (a)), thereby recovering BAS. In light of the high deactivation rate throughout the reaction and the high coke-II selectivity observed at longer TOS, another mechanism for formation of O-containing species and their successive conversion into aromatics is

hypothesized to exist. Such mechanism is proposed to start from surface methoxy groups. It should be noted that this mechanism might also be operative at short TOS because the amount of formaldehyde generated from methanol at the beginning of the reaction is low in comparison to the availability of methoxy groups [16]. In this mechanistic proposal shown in Scheme 4.8 and proposed in Chapter 2, surface acetyl groups are generated by carbonylation reactions which can then react with formaldehyde to a surface furan species (Scheme 4.8 (a) and (b)). The furan species can be transformed into aromatics (Scheme 4.8 (c)) which are covalently bonded to the framework O that was originating the BAS, and therefore causes site blocking. These aromatic species are quantified as coke-II by TPO/TGA analysis, which has been explained in detail in Chapter 2, and cannot be distinguished by common techniques from typically adsorbed aromatic coke that is generated by hydrogen transfer pathways and by methylation of aromatic intermediates. The proposed reaction pathway would explain the high selectivity towards aromatic-type coke-II under DMM co-feeding, which is even higher than for the experiment under a mixed MeOH/toluene feed.

Having discussed the impact of formaldehyde co-feeding on deactivation, it is turned now to the comparison of a pure MeOH feed with a mixed MeOH/toluene feed. The normalized deactivation rate was higher for the methanol feed in comparison to a mixed methanol/toluene feed at the beginning of the reaction and decreased within the first hours TOS (Figure 4.9). As presented in Chapter 2, a larger fraction of formaldehyde-related strongly deactivating species (coke-I) forms initially on the fresh catalyst under pure MeOH, causing a higher deactivation rate. Conversely, when MeOH and toluene are fed, the aromatics cycle is directly propagated [31]. This explains the higher conversion obtained under a MeOH/toluene feed (Figure 4.8). Furthermore, the fast rate of aromatics methylation and development of the hydrocarbon pool competes with the formation of highly deactivating coke-I. Therefore, the amount of coke-I formed under presence of toluene was lower than for pure methanol. However, with longer TOS, the normalized deactivation rate was higher with toluene co-feeding than for a pure methanol feed (Figure 4.9) which can be correlated with the higher production of coke-II (Table 4.2). The deactivating effect of aromatics co-feeding overcame then the effect of promoting the active aromatics cycle.
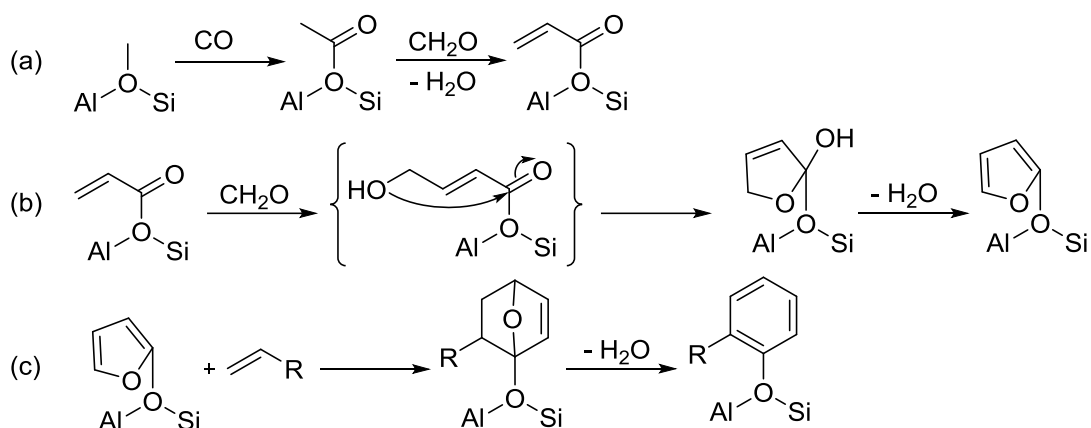
Scheme 4.8. Mechanistic proposal for the formation of O-containing coke-I ((a) and (b)) and localized aromatics (c), as presented in Chapter 2.

4.5   Conclusions

The study on the impact of formaldehyde in MTO conversion revealed its importance during the first stages of the conversion of methanol to olefins and aromatics, as well as its role in the deactivation of an H-ZSM-5 catalyst.

This investigation showed unequivocally that formaldehyde is generated under MTO conditions. Several pathways are available for the formation of formaldehyde from methanol: Formaldehyde formed by thermal decomposition or by disproportionation/reaction at LAS and formaldehyde generated by hydrogen transfer at BAS. It was found that formaldehyde strongly chemisorbed on BAS and might cause strong deactivation in the first stages of the catalyst bed. If MTO products like olefins are present, it is, however, released from the surface via several steps. Thus, the carbon deposits formed in subsequent steps are found to be more important for deactivation than surface adsorbed formaldehyde.

It is important to emphasize that clear evidence could be given that aromatic-type coke causing site blocking cannot only form via pathways typically discussed in literature, but also by a pathway involving formaldehyde.

The formaldehyde-related mechanisms discussed here shed light on the first elementary steps involved in methanol conversion to hydrocarbons, which have been only marginally studied in the literature to date. The knowledge gained here opens new pathways for the design of catalysts and the control of deactivation.

4.6 Acknowledgements

4.7 References

[1] U. Olsbye, S. Svelle, M. Bjørgen, P. Beato, T.V.W. Janssens, F. Joensen, S. Bordiga, K.P. Lillerud, Angew. Chem. Int. Ed. 51 (2012) 5810.

[2] S. Ilias, A. Bhan, ACS Catal. 3 (2013) 18.

[3] X. Sun, S. Mueller, H. Shi, G.L. Haller, M. Sanchez-Sanchez, A.C. van Veen, J.A. Lercher, J. Catal. 314 (2014) 21.

[4] C.D. Chang, A.J. Silvestri, J. Catal. 47 (1977) 249.

[5] N.Y. Chen, W.J. Reagan, J. Catal. 59 (1979) 123.

[6] R.M. Dessau, R.B. LaPierre, J. Catal. 78 (1982) 136.

[7] R.M. Dessau, J. Catal. 99 (1986) 111.

[8] Y. Ono, T. Mori, J. Chem. Soc., Faraday Trans. 1 77 (1981) 2209.

[9] T. Mole, J.A. Whiteside, D. Seddon, J. Catal. 82 (1983) 261.

[10] T. Mole, G. Bett, D. Seddon, J. Catal. 84 (1983) 435.

[11] I.M. Dahl, S. Kolboe, Catal. Lett. 20 (1993) 329.

[12] I.M. Dahl, S. Kolboe, J. Catal. 149 (1994) 458.

[13] I.M. Dahl, S. Kolboe, J. Catal. 161 (1996) 304.

[14] M. Bjørgen, S. Svelle, F. Joensen, J. Nerlov, S. Kolboe, F. Bonino, L. Palumbo, S. Bordiga, U. Olsbye, J. Catal. 249 (2007) 195.

[15] S. Svelle, F. Joensen, J. Nerlov, U. Olsbye, K.-P. Lillerud, S. Kolboe, M. Bjørgen, J. Am. Chem. Soc. 128 (2006) 14770.

[16] X. Sun, S. Mueller, Y. Liu, H. Shi, G.L. Haller, M. Sanchez-Sanchez, A.C. van Veen, J.A. Lercher, J. Catal. 317 (2014) 185.

[17] L. Kubelková, J. Nováková, P. Jírů, Reaction of Small Amounts of Methanol on Hzsm-5, Hy and Modified Y Zeolites, in: P.A. Jacobs, N.I. Jaeger, P. Jírů, V.B. Kazansky, G. Schulz-Ekloff (Eds.), Stud. Surf. Sci. Catal., Elsevier, Amsterdam, 1984, p. 217.

[18] G.J. Hutchings, F. Gottschalk, R. Hunter, Ind. Eng. Chem. Res. 26 (1987) 635.

[19] G.J. Hutchings, F. Gottschalk, M.V.M. Hall, R. Hunter, J. Chem. Soc., Faraday Trans. 1 83 (1987) 571.

[20] D. Lesthaeghe, V. Van Speybroeck, G.B. Marin, M. Waroquier, Angew. Chem. 118 (2006) 1746.

[21] L.H. Ong, M. Dömök, R. Olindo, A.C. van Veen, J.A. Lercher, Microporous Mesoporous Mater. 164 (2012) 9.

[22] A. Comas-Vives, M. Valla, C. Copéret, P. Sautet, ACS Cent. Sci. 1 (2015) 313.

[23] O. Kresnawahjuesa, R.J. Gorte, D. White, J. Mol. Catal. A: Chem. 208 (2004) 175.

[24] R. Kefirov, E. Ivanova, K. Hadjiivanov, S. Dzwigaj, M. Che, Catal. Lett. 125 (2008) 209.

[25] G. Mirth, J.A. Lercher, M.W. Anderson, J. Klinowski, J. Chem. Soc., Faraday Trans. 86 (1990) 3039.

[26] J.F. Haw, W. Song, D.M. Marcus, J.B. Nicholas, Acc. Chem. Res. 36 (2003) 317.

[27] M. Stöcker, Microporous Mesoporous Mater. 29 (1999) 3.

[28] D. Lesthaeghe, V. Van Speybroeck, G.B. Marin, M. Waroquier, Ind. Eng. Chem. Res. 46 (2007) 8832.

[29] Y. Liu, S. Müller, D. Berger, J. Jelic, K. Reuter, M. Tonigold, M. Sanchez-Sanchez, J.A. Lercher, First C-C bond and first olefin formation in methanol conversion to hydrocarbons, unpublished results.

[30] F.E. Celik, T.-J. Kim, A.T. Bell, J. Catal. 270 (2010) 185.

[31] S. Ilias, A. Bhan, J. Catal. 290 (2012) 186.

Chapter 5

5.   Conclusions

Methanol-to-olefins (MTO) conversion is controlled by a complex, interconnected network of parallel and sequential reactions. Its understanding allows tuning catalysts as well as reaction conditions. This thesis therefore aims to gain a better understanding of elementary reaction steps of MTO conversion, including deactivation, aromatics and paraffins formation and the formation of the first C-C bond and first olefins.

By comparing the catalysis in plug-flow (PFR) and fully back-mixed reactors (CSTR) under identical reaction conditions, coke formation and deactivation pathways on H-ZSM-5 were elucidated. The study under homogeneous gas phase in the CSTR revealed that deactivation starts by site blocking, well before external pore blocking. Fast deactivation was linked to oxygen-containing species which are strongly chemisorbed to Brønsted acid sites (BAS). They form under high local methanol concentrations, involving carbonylation of methoxy groups as a first step. These oxygenates may be transformed by reaction with hydrocarbon species into aromatic coke that remains attached to BAS causing deactivation. On the other hand, aromatics formed by hydrogen transfer exhibit weaker interaction with the zeolite and therefore cause slower deactivation.

For the industrial implementation of methanol conversion technologies for olefins production, it is also of vital importance to diminish the further reaction of olefins to undesired aromatics and paraffins. By studying catalysts with varying concentrations of BAS and Lewis acid sites (LAS) and examining the evolution of the product distribution under the presence of proposed MTO reaction intermediates such as formaldehyde, the mechanisms of hydrogen transfer pathways were elucidated. A methanol-mediated pathway was identified as the major hydrogen transfer pathway. It involves the reaction of methanol and an olefin to formaldehyde

and a paraffin at LAS. Formaldehyde reacts subsequently with olefins to dienes at BAS and finally to aromatics and paraffins. Decreasing selectively the concentration of LAS allows a reduction of the hydrogen transfer ability of catalysts.

Formaldehyde which is formed by thermal decomposition or by disproportionation/reaction at Lewis acid sites under typical MTO conditions does not only play a role for the formation of aromatics and paraffins. It is also involved in the formation of the first C-C bond and the first olefins. This is associated with the favoring of carbonylation reactions by decomposition of formaldehyde to CO and the participation of formaldehyde in the following reaction steps to olefins. A comparison of the deactivation rate for mixed methanol/toluene and mixed methanol/formaldehyde feeds showed that formaldehyde promotes the formation of oxygen-containing coke and aromatic coke which is strongly chemisorbed to BAS. From these results it can be concluded that the formaldehyde concentration in the reactor is a critical factor which needs to be considered precisely when running methanol conversion reactions on zeolites or zeotype materials.

Chapter 6

6.   Zusammenfassung

Die Umsetzung von Methanol zu Olefinen (MTO) wird durch ein komplexes, untereinander verbundenes Netzwerk an parallelen und sequentiellen Reaktionen kontrolliert. Ein Verständnis dieses Netzwerks ermöglicht es, Katalysatoren sowie Reaktionsbedingungen zu optimieren. Ziel dieser Arbeit ist es deshalb, ein besseres Verständnis der elementaren Reaktionsschritte der MTO Umsetzung, darunter der Deaktivierung, der Aromaten- und Paraffinbildung sowie der Bildung der ersten C-C-Bindung und der ersten Olefine, zu erzielen.

Durch den Vergleich der Katalyse in einem Rohrreaktor (PFR) und in einem vollständig rückvermischten Reaktor (CSTR) unter identischen Reaktionsbedingungen wurden Koksbildungs- und Deaktivierungspfade an H-ZSM-5 aufgeklärt. Die Studie unter homogener Gasphase in einem CSTR zeigte, dass die Deaktivierung durch das Blockieren aktiver Zentren beginnt, deutlich vor dem Blockieren von Poren. Eine schnelle Deaktivierung wurde mit sauerstoffhaltigen Spezies, die stark an Brønsted-Säurezentren (BAS) chemisorbiert sind, in Verbindung gebracht. Sie bilden sich unter hohen lokalen Methanolkonzentrationen, wobei die Carbonylierung von Methoxygruppen den ersten Schritt darstellt. Diese sauerstoffhaltigen Verbindungen können durch die Reaktion mit Kohlenwasserstoffen in Aromaten umgewandelt werden, die an BAS adsorbiert bleiben und Deaktivierung hervorrufen. Andererseits zeigen Aromaten, die sich durch Hydrogentransfer bilden, eine schwächere Wechselwirkung mit dem Zeolithen und bewirken deshalb eine langsamere Deaktivierung.

Für die industrielle Anwendung der Methanolumsetzung zur Herstellung von Olefinen ist es außerdem von entscheidender Bedeutung, die Weiterreaktion von Olefinen zu unerwünschten Aromaten und Paraffinen zu reduzieren. Durch die Studie von Katalysatoren mit unterschiedlichen Konzentrationen an BAS und Lewis-Säurezentren (LAS) und durch die

Untersuchung der Entwicklung der Produktverteilung in Gegenwart vorgeschlagener MTO-Reaktionsintermediate wie Formaldehyd wurden die Hydrogentransfermechanismen aufgeklärt. Ein Methanol-vermittelter Pfad wurde als der wesentliche Hydrogentransferpfad identifiziert. Methanol reagiert dabei an LAS mit einem Olefin zu Formaldehyd und einem Paraffin. Formaldehyd reagiert anschließend an BAS mit Olefinen zu Dienen, und schließlich zu Aromaten und Paraffinen. Durch selektives Verringern der Konzentration an LAS lässt sich die Fähigkeit von Katalysatoren zum Hydrogentransfer herabsetzen.

Formaldehyd, welches sich unter typischen MTO-Bedingungen durch thermischen Zerfall oder durch Disproportionierung/Reaktion an LAS bildet, spielt nicht nur bei der Bildung von Aromaten und Paraffinen eine Rolle. Es ist auch an der Bildung der ersten C-C-Bindung und der ersten Olefine beteiligt. Dies hängt damit zusammen, dass durch den Zerfall von Formaldehyd zu CO Carbonylierungsreaktionen begünstigt werden und dass Formaldehyd an den nachfolgenden Reaktionsschritten zu Olefinen beteiligt ist. Ein Vergleich der Deaktivierungsrate für Methanol/Toluol und Methanol/Formaldehyd Eduktmischungen zeigte, dass Formaldehyd die Bildung von sauerstoffhaltigen Kohlenstoffablagerungen und aromatischem Koks, welcher stark an BAS adsorbiert ist, fördert. Aufgrund dieser Resultate kann geschlussfolgert werden, dass die Konzentration an Formaldehyd im Reaktor ein kritischer Faktor ist, der genau bedacht werden muss, wenn Methanol an Zeolithen oder zeolithähnlichen Materialien umgesetzt wird.

7. List of Figures, Tables and Schemes

7.1 List of Figures

7.2　　List of Tables

7.3 List of Schemes

Curriculum Vitae

Persönliche Daten

Name	Sebastian Müller
Geburtsdatum/-ort	21.02.1986 in Wasserburg am Inn
Familienstand	Ledig
Staatsangehörigkeit	Deutsch

Berufserfahrung

10/2011 – 08/2015	**Technische Universität München** **Promotion am Lehrstuhl für Technische Chemie II in Kooperation mit der Clariant Produkte (Deutschland) GmbH**
08/2010 – 09/2010	**Industriepraktikum bei der Reactana Katalysatoren und Chemikalien GmbH, Biebesheim am Rhein**

Studium/Schule

10/2009 – 08/2011	**Technische Universität München** **Masterstudium Chemie** (Note: 1,2) • Schwerpunkte: Anorganische und Metallorganische Chemie, Katalyse und Reaktionstechnik • Masterarbeit: Activation of ethane over supported alkali-chloride catalysts (Note: 1,0)
10/2006 – 08/2009	**Technische Universität München** **Bachelorstudium Chemie** (Note: 1,8) • Bachelorarbeit: Alkanaktivierung an verschiedenen LaY-Zeolithen bei der Isobutan/2-Buten Alkylierung (Note: 1,0)
09/1996 – 06/2005	**Gymnasium Dorfen** • Allgemeine Hochschulreife (Note: 1,4)

Auslandserfahrung

08/2014	Vortrag und Posterpräsentation auf dem 248. ACS Meeting in San Francisco, USA

List of publications

Journal contributions

2015 <u>S. Müller</u>, Y. Liu, M. Sanchez-Sanchez, J. A. Lercher, *"Formaldehyde chemistry in methanol conversion on H-ZSM-5"*, in preparation.

<u>S. Müller</u>, Y. Liu, M. Sanchez-Sanchez, J. A. Lercher, *"On understanding active sites and mechanism of hydrogen transfer during methanol-to-olefins conversion on H-ZSM-5"*, in preparation.

<u>S. Müller</u>, Y. Liu, M. Vishnuvarthan, X. Sun, G. L. Haller, A. C. van Veen, M. Sanchez-Sanchez, J. A. Lercher, *"Coke formation and deactivation pathways on H-ZSM-5 in the conversion of methanol to olefins"*, J. Catal. 325 (2015) 48-59.

2014 X. Sun, <u>S. Müller</u>, H. Shi, G. L. Haller, M. Sanchez-Sanchez, A. C. van Veen, J. A. Lercher, *"On reaction pathways in the conversion of methanol to hydrocarbons on HZSM-5"*, J. Catal. 317 (2014) 185-197.

X. Sun, <u>S. Müller</u>, H. Shi, G. L. Haller, M. Sanchez-Sanchez, A. C. van Veen, J. A. Lercher, *"On the impact of co-feeding aromatics and olefins for the methanol-to-olefins reaction on HZSM-5"*, J. Catal. 314 (2014) 21-31.

M. Deriwinski, P. Sarv, X. Sun, <u>S. Müller</u>, A. C. van Veen, J. A. Lercher, *"Reversibility of the Modification of HZSM-5 with Phosphate Anions"*, J. Phys. Chem. C 118 (2014) 6122-6131.

Oral presentations

2015 X. Sun, <u>S. Müller</u>, Y. Liu, H. Shi, G. L. Haller, M. Sanchez-Sanchez, A. C. van Veen, J. A. Lercher, *"Methanol to Gasoline/Olefins revisited"*, 24th North American meeting (NAM) of the Catalysis Society, Pittsburgh, USA.

J. A. Lercher, <u>S. Müller</u>, Y. Liu, M. Sanchez-Sanchez, *"New insight into hydrocarbon formation routes in the methanol to olefin process"*, QAFCO-Texas A&M at Qatar Conference 2015, Doha, Qatar.

2014 <u>S. Müller</u>, Y. Liu, X. Sun, M. Sanchez-Sanchez, J. A. Lercher, *"Deactivation pathways during methanol to propylene (MTP) conversion over ZSM-5 catalysts"*, 248th ACS National Meeting, San Francisco, USA.

2013   X. Sun, <u>S. Müller</u>, A. C. van Veen, J. A. Lercher, *"Impact of co-feeding aromatics and olefins in the methanol-to-olefins conversion over HZSM-5 catalysts"*, IDECAT Konferenz, Brixen, Italy.

2012   X. Sun, <u>S. Müller</u>, A. C. van Veen, J. A. Lercher, *"On the impact of co-feeding aromatics and olefins in the methanol-to-olefins conversion over H-ZSM-5 catalysts"*, DGMK Konferenz, Berlin, Germany.

Poster presentations

2015   <u>S. Müller</u>, Y. Liu, M. Vishnuvarthan, M. Sanchez-Sanchez, J. A. Lercher, *"Hydrogen transfer pathways in the methanol to propylene (MTP$^{©}$) conversion over H-ZSM-5 catalysts"*, 48. Jahrestreffen Deutscher Katalytiker, Weimar, Germany.

             <u>S. Müller</u>, Y. Liu, M. Vishnuvarthan, M. Sanchez-Sanchez, P. Hintermeier, J. A. Lercher, *"Role of acidity of H-ZSM-5 catalysts in hydrogen transfer pathways of methanol to propylene (MTP$^{©}$) conversion"*, 27. Deutsche Zeolith-Tagung, Oldenburg, Germany.

2014   <u>S. Müller</u>, Y. Liu, X. Sun, M. Sanchez-Sanchez, J. A. Lercher, *"Deactivation pathways during methanol to propylene (MTP) conversion over ZSM-5 catalysts"*, Sci-Mix, 248th ACS National Meeting, San Francisco, USA.

             <u>S. Müller</u>, M. Vishnuvarthan, M. Sanchez-Sanchez, J. A. Lercher, *"Coke formation and deactivation rate of ZSM-5 catalysts during methanol-to-olefins conversion"*, 47. Jahrestreffen Deutscher Katalytiker, Weimar, Germany.

2013   X. Sun, <u>S. Müller</u>, A. C. van Veen, J. A. Lercher, *"Impact of co-feeding olefins or aromatics in the methanol-to-hydrocarbons conversion over H-ZSM-5 catalysts"*, 46. Jahrestreffen Deutscher Katalytiker, Weimar, Germany.

2012   C. A. Gärtner, <u>S. Müller</u>, A. C. van Veen, J. A. Lercher, *"Mechanistic understanding of the oxidative dehydrogenation of ethane over supported molten alkali chloride catalysts"*, 15th International Congress on Catalysis, Munich, Germany.

             C. A. Gärtner, M. F. Wagenhofer, <u>S. Müller</u>, A. C. van Veen, J. A. Lercher, *"Kinetic and mechanistic aspects of the oxidative dehydrogenation of ethane over supported eutectic alkali-chloride catalysts"*, 45. Jahrestreffen Deutscher Katalytiker, Weimar, Deutschland.